Title
A STUDY OF K+p AND K+d INTERACTIONS AT 1.585 GeV/c

Author
Seeger, Victor Harrison.

Publication Date
1971

UCRL-20628

c 2

A STUDY OF K^+p AND K^+d INTERACTIONS AT 1.585 GeV/c

Victor Harrison Seeger
(Ph. D. Thesis)

January 4, 1971

AEC Contract No. W-7405-eng-48

LAWRENCE RADIATION LABORATORY
UNIVERSITY of CALIFORNIA BERKELEY

UCRL-20628

34 a

DISCLAIMER

DEDICATION

To the memory of my father

and to my mother and sister.

A STUDY OF K^+p AND K^+d INTERACTIONS AT 1.585 GeV/c

Contents

A STUDY OF K^+p AND K^+d INTERACTIONS AT 1.585 GeV/c

Victor Harrison Seeger

Lawrence Radiation Laboratory
University of California
Berkeley, California 94720

January 4, 1971

ABSTRACT

The Lawrence Radiation Laboratory's 25-inch bubble chamber filled first with hydrogen and then with deuterium was exposed to incident K^+'s at 860, 970, 1210, 1365, and 1585 MeV/c. This thesis covers the analysis of the data taken at 1585 MeV/c. Single and double pion production reactions and the charge exchange reaction were studied.

Single pion and double pion production cross sections were obtained. Relations derived from isospin conservation were used to obtain some cross sections not accessible to direct observation. Single pion production is dominated by $K\Delta$ and K^*N production. K^*-Δ interference was observed and measured by fitting the Dalitz plots. K^*-background and Δ-background interference also was observed. Double pion production reactions were seen to be dominated by $K^*\Delta$ production even below the nominal $K^*\Delta$ threshold.

The cross section for K^* production in the $I = 0$ channel in single pion production was obtained and its production and decay angular distributions were studied in terms of t channel analysis. Its production was seen to proceed almost entirely via pseudoscalar exchange. This is in contrast with K^* production in the $I = 1$ channel which proceeds largely through vector exchange but the behavior of the cross section as a function of beam momentum is very similar to that of the K^* in the $I = 1$ channel. A rough model involving π, ρ, and ω exchange is seen to account for the general features of K^{*o} and K^{*+} production. More detailed features were

seen, in particular correlations between decay angles, which are not accounted for by OME models.

The differential cross section for the charge exchange reaction was measured and compared with predictions of a model based on Regge theory. The absolute value of the ratio of the real part of the scattering amplitude in the forward direction to the imaginary part was measured and found to be in good agreement with another Regge theory prediction.

I. INTRODUCTION

The K25 experiment was proposed in November 1962 to study K^+p and K^+d interactions over the momentum range from 800 to 1200 MeV/c. The reasons for interest in this region were:

1) the known rapid rise in the K^+p total cross section from approximately 12 mb at 800 MeV/c to a leveling off at about 18 mb above 1200 MeV/c due apparently to the very rapid rise in the inelastic one pion production cross section known to increase by about a factor of eight in this interval,[1]
2) the study of production and decay angular distributions of the established resonances $K^*(890)$ and $\Delta(1236)$ below, at and above their thresholds,
3) a previously reported enhancement in the $K\pi$ system at a mass of about 720 MeV, the so-called κ meson and
4) a previously reported enhancement in the Kp system at a mass of about 1480 MeV. Seen in the same reaction in the same low statistics experiment,[2] it was an open question whether these enhancement were real resonances, kinematic effects or statistical fluctuations. The κ is now generally thought to have been a statistical fluctuation. The Kp enhancement was seen in the K25 experiment to be a kinematic reflection of $K\Delta$ production.

The proposal was approved by the Bevatron Scheduling Committee in 1963. The beam, a variable momentum separated $K^\pm$ beam, was built in late 1963 and early 1964 and the experiment was run with the newly constructed 25-inch bubble chamber at the Bevatron in mid-1964. During the run it was decided to push the beam somewhat beyond its design limits to 1360

and then to almost 1600 MeV/c. One of the reasons for this decision was the idea that the κ might be seen in double pion production below the $K^*\Delta$ threshold since it was known that double pion production was dominated by double resonance production at higher momenta. The subject of this report is the data at the highest momentum of this run, 1585 MeV/c.

During the time the K25 data was being processed, Cool et al.[3] and Bugg et al.[4] published very accurate measurements of K^+p and K^+d total cross sections. These measurements revealed a distinct peak or bump at the top of the above mentioned rise in cross section at about 1200 MeV/c with the cross sections dropping about 1 mb in hydrogen and 1.5 mb in deuterium before leveling off at about 1500 MeV/c. This structure suggests the possibility of an s-channel positive strangeness baryon resonance. The exploration of this important possibility has been reported on often and at length elsewhere.[5-12] The data at 1585 MeV/c is beyond this region of structure and represents the lowest region of unambiguously non s-channel resonance. It thus provides a check on the t-channel analysis at lower momenta and a tie-in point to higher momenta besides being itself a valid region of interest in t-channel analysis.

This report is organized as follows: in Section II we describe the experimental set-up and the beam, list the number of pictures taken in hydrogen and deuterium, describe the data reduction procedures and programs and give the final event count. This section also contains a description of how the serious problem of pion contamination was handled. Section III lists the cross sections for the stable final states and describes the procedures and corrections used in obtaining them. Included also is an outline of the isospin relations used in analyzing the deuterium data. This procedure is covered in greater detail in Appendix I. Section

IV contains the analysis of the resonant states, Dalitz plots, cross sections and angular distributions. The combination of reactions which yields the cross section and angular distributions for K^* production in the $I = 0$ channel is discussed. The energy dependence of the cross section for this state is compared with that of the K^* in the $I = 1$ channel. They are seen to be remarkably similar. This section also contains correlation plots for the decay angles for these K^*'s and for the individual reactions comprising the $K^*(I = 0)$ state. The analysis of double pion production is discussed. Section V contains the analysis of the charge exchange data.

II. DESCRIPTION OF THE EXPERIMENT

A. The Beam

The K25 beam was a variable momentum separated $K^{\pm}$ beam[13] and was designed for this experiment and a K^- experiment in the same momentum range. It made use of the newly available external proton beam facility at the Bevatron. By targeting in the EPB outside the magnetic field and the physical structure of the Bevatron it was possible to take both positive and negative kaons from the target at 0^o and to place the initial beam elements relatively close to the target thus subtending a larger solid angle and providing a shorter path length from target to bubble chamber than would otherwise have been possible. These considerations were critical in obtaining a sufficient K^- flux but they were useful also in improving the quality of the K^+ beam. An additional benefit from being entirely outside the Bevatron's magnetic field is of course that the beam optics were identical for K^+'s and K^-'s and all that was necessary to go from one operation to the other was to reverse the polarity of the beam magnets. The K^- experiment was done by the Powell-Birge group at LRL which had collaborated in the design and construction of the beam with the Trilling-Goldhaber group.

Figure 1 shows the layout of the beam. Separation was accomplished in two stages, two electrostatic separators each followed by a quadrupole doublet to focus the image vertically at the mass slits. There was also a horizontal focus at the first slit which was cocked at 20^o from the beam direction to accommodate chromatic aberration in the first stage. There was no horizontal focus at the second mass slit. Bending magnet M3 was shimmed to include a sextupole moment to cancel chromatic aberration in the vertical plane from both stages and the second mass slit was then set perpendicular to the beam direction.

Unfortunately the jaws of the slits were not massive enough at the edges to absorb or sufficiently degrade grazing pions and at the relatively high momentum of 1585 MeV/c the spatial separation afforded by the spectrometers was not great enough to bury all the pions in the slits. Thus there was considerable pion contamination at this momentum. A lead collimator placed at the entrance to the bubble chamber eliminated most of the background coming in above, below or to either side of the beam position and made the pictures scannable. The K's occupied a rather well defined band within the window defined by the collimator while the pion contamination was much more diffuse. This made it possible to reduce pion contamination in the final data sample to an acceptable level by imposing beam entrance criteria based on reliable identification of events. Details of this procedure are presented in Part D of this Section.

B. The Data

In the K25 experiment approximately 600,000 pictures were taken, 428,000 in hydrogen, 172,000 in deuterium. Of these there were approximately 51,000 scannable pictures in hydrogen and 32,000 in deuterium of K^+'s at 1585 MeV/c. In Table I we list the numbers of events in each topology analyzed at this momentum. Two-prong events with no vee were not analyzed because of the high pion contamination. The two-prong cross section for $\pi^+ p$ at this momentum is 35.6 mb of which 16.7 mb is elastic scattering.[14] The two-prong cross section for $K^+ p$ at this momentum is 15.4 mb of which about 8 mb is elastic scattering. Pion and kaon elastic scatters at this momentum are difficult to resolve either by kinematic fitting or by ionization.

All the film at 1585 MeV/c was scanned twice for three- or four-prong events and for vee events. Each scan was found to have an efficiency

greater than 90% for all topologies. Thus the overall scanning efficiency can be taken as 100%. All measuring was done on Franckensteins. All fitted events were output scanned for ionization. All non-fitting events were output scanned for additional information as to why they failed.

C. Data Reduction -- Hydrogen

Hydrogen events were processed through the PACKAGE kinematic fitting program. In this part of the data pion contamination was found not to present a serious problem in three- or four-prong events or in V^o events. Three-prong events had to be taus. No four-prong events kinematically fit both $\pi^+ p \rightarrow \pi^+ p\pi^+\pi^-$ and $K^+ p \rightarrow K^+ p\pi^+\pi^-$. No four-prong events found in a roll of pion film taken at this momentum for contamination studies kinematically fit $K^+ p \rightarrow K^+ p\pi^+\pi^-$. About 12% of the final data sample for this four-constraint reaction are kinematically ambiguous with one-constraint pion fits but in view of the pion film result just quoted were all assumed to come from kaons. Pion-produced K^o events would have to come from the associated production reactions $\pi^+ p \rightarrow \overline{K^o} K^+ p$ or $\pi^+ p \rightarrow K^o \Lambda \pi^+ \pi^+$. The cross sections for these reactions are very low, 30 μb and 5 μb respectively at 1.76 BeV/c,[15] and would be even lower at 1585 MeV/c due to severe phase space limitations. A number of Λ's were seen in the experiment but these came almost entirely from the reaction $\pi^+ p \rightarrow K^+ \Lambda \pi^+$ which has a larger cross section at 1.76 BeV/c, 190 μb, and less severe phase space limitations at 1585 MeV/c than the $K^o \Lambda \pi^+ \pi^+$ final state. The fitting program distinguished Λ's from K^o's quite well and at the low momenta involved ionization judgments were reliable.

After measuring and fitting and inspection of ionization, all events were either accepted, rejected as one of a number of distinct reject types or remeasured. For an event to be accepted it was required that it be

well measured as indicated by the spread of measured points from the fitted curve. After several remeasurements this criterion was relaxed and some events, less than 5% of the final data, were accepted only on the basis of χ^2 and ionization fits. The χ^2 cutoff was made at the 1% confidence level. Less than 5% of the total data remain unresolved.

The reject types are defined as follows:

False Event - duplicate events, phony "events" due to crossing background tracks in the chamber, background V^o's and real two-prong events with Dalitz pairs.

Immeasurable - obscured by passing tracks, chamber distortion due to turbulence (the chamber was double pulsed), or film damage.

Non-Beam Track - events produced by either grossly non-beam tracks as seen on the scan table or by tracks failing to meet PACKAGE beam criteria. These criteria were that the measured beam track momentum be within three standard errors of the central beam momentum and that the dip and azimuthal angles be within 1.25^o of the average of a sample of taus.

No Fit - apparently well measured but fitting no hypothesis with incident K^+, π^+, or proton. Hypotheses assuming an incident K^+ used beam averaging, that is the measured beam track values for each event were averaged in with appropriately weighted errors with those from the tau sample before attempting a fit. Pion or proton hypotheses used the individually measured beam track values each with its own errors. Thus the No Fit category includes off momentum K^+'s with poorly measured beam tracks and events with more than one missing neutral.

Zero Constraint - well measured but with a secondary scatter or

decay so near the primary vertex that the momentum of the secondary cannot be measured. Such events with one missing neutral will be under-constrained.

Outside Fiducial Volume or Outside Decay Fiducial Volume - fiducial volumes were imposed so as not to require identification of events near the edges of the chamber. The escape correction required for reactions producing a K^o is discussed in Part B of Section III.

The distribution of rejected events by topology and by reject type for the hydrogen data is given in Table II. The distribution of accepted events by reaction is given in Table III.

D. Data Reduction -- Deuterium

Deuterium data were processed originally through PACKAGE but later were reprocessed through SIOUX when that system became available. SIOUX has the feature of incorporating unseen spectator protons into the fit by assuming zero momentum for them with large errors, ± 30 MeV/c for Δp_x and Δp_y and ± 40 MeV/c for Δp_z. This feature picks up three constraints which would otherwise be lost in half the events off the neutron and in particular makes such events with one missing neutral fittable. Pion contamination presented no difficulties in V^o events as before but did present a serious problem in three- and four-prong events. Resolution of K-π ambiguities was first attempted only by fitting and visual estimation of ionization. No beam track acceptance criteria were imposed at this stage. K hypotheses used beam averaging, π and p hypotheses did not. Visual K-π resolution was not attempted when the ionization of the track in question was less than 1.3 times minimum. Resolution could be made in most cases where the ionization of the track was greater than

1.5 times minimum. Reject categories were the same as for the hydrogen data except for the "non-beam track" category and for the "no fit" category for V^o events where missing mass fits were accepted. The distribution of rejected events by topology and by reject type for the deuterium data is also given in Table II. For an event to be accepted it had to be well measured, have a χ^2 less than five times the number of constraints for the hypothesis in question and fit the ionization called for by the hypothesis.

Missing mass hypotheses were accepted for K^o events when there was no other fit at the interaction vertex and the calculated missing mass was greater than the lowest sum of possible missing neutrals. The distribution of accepted events by reaction, including unresolved ambiguities, is given in Table IV. It is apparent that resolution by fitting and by ionization is not sufficient for three- and four-prong events.

Figure 2 compares the spatial distribution of beam tracks at the entrance to the chamber[16] for four different classes of events. Class 1) consists of taus and K^o events, definitely K^+ produced. Class 2) consists of events which unambiguously fit the four-constraint reaction $K^+d \to K^+\pi^-pp$, thought to be almost entirely K^+ produced. Class 3) consists of events which fit both $K^+d \to K^+\pi^-pp$ and $\pi^+d \to \pi^+\pi^-pp$ kinematically and by ionization. Class 4) consists of events which unambiguously fit $\pi^+d \to \pi^+\pi^-pp$. It is clear that incoming π's are more broadly distributed than the K^+ beam, that ambiguous events for this reaction are mostly K^+ produced, and that entrance criteria can be established which will reduce the percentage of pion contamination in the final data sample. Figure 3 shows correlation plots of dip angle vs azimuthal angle for the same classes of events. Clearly the same observations apply.

Beam entrance criteria were established from these plots consisting of sharp cutoffs in x, z, λ, and φ. This effective beam "window" was then used to select the final data sample for this reaction. Table V shows the numbers of events in each class before and after this cut. The in window/out window ratio is seen to be nearly the same for classes 1) and 2) confirming that class 2 events are almost all K^+ produced. The final data sample is taken to be the unambiguous events in the window plus the ambiguous fits in the window. Unambiguous K fits outside the window are excluded to avoid possible biases. Figure 4 compares the measured beam momentum for the same four classes of events in and out of the window. The pion beam momentum is seen to be degraded with respect to the kaon momentum but attempts to take advantage of this fact by including a momentum cutoff in the definition of the beam window did not succeed due to large errors in the beam track momentum measurement for many events. It is not meaningful to make a sharp cutoff when measurement errors are large and incorporating these errors into the window criteria resulted in too great an overlap of K's and π's.

The useful feature of the momentum distributions is that they are not significantly different in or out of the window. This enables one to estimate the pion contamination in the final data in the following simple manner. Let the number of events in classes 2) and 4) in and out of the window be represented by K_i, K_o, π_i, and π_o. For every event unambiguously identified as $K^+d \rightarrow K^+\pi^-pp$ there will be some number of K produced ambiguous events, say a_K. Similarly one defines a_π. Then class 3) events in and out of the window, A_i and A_o, are

$$A_i = a_K K_i + a_\pi \pi_i$$

$$A_o = a_K K_o + a_\pi \pi_o \quad .$$

Solving for the a's gives the pion contamination in this reaction

$$\frac{a_{\pi} \pi_i}{K_i + A_i} = 0.04 \pm 0.007 \quad .$$

The pion contamination in this reaction without using the beam window is

$$\frac{a_{\pi}(\pi_i + \pi_o)}{(K_i + K_o) + (A_i + A_o)} = 0.13 \pm 0.02 \quad .$$

The overall pion contamination in the beam can be calculated using the a's and the cross sections for the reactions $\pi^+ d \rightarrow \pi^+ \pi^- pp$ at this momentum[17] and $K^+ d \rightarrow K^+ \pi^- pp$ from this experiment. We have

$$\frac{\text{number of } \pi^+ d \rightarrow \pi^+ \pi^- pp \text{ events}}{\text{number of } K^+ d \rightarrow K^+ \pi^- pp \text{ events}} = \frac{\text{pion flux} \times \text{cross section}}{\text{kaon flux} \times \text{cross section}}$$

or

$$\frac{N_{\pi}}{N_K} = \frac{\varphi_{\pi} \sigma_{\pi}}{\varphi_K \sigma_K}$$

from which

$$\frac{\varphi_{\pi}}{\varphi_K} = \frac{\sigma_K}{\sigma_{\pi}} \frac{N_{\pi}}{N_K}$$

$$= \frac{\sigma_K}{\sigma_{\pi}} \frac{(\pi_i + \pi_o)(1 + a_{\pi})}{(K_i + K_o)(1 + a_K)}$$

$$\approx 0.6 \quad .$$

The in window/out window ratio for unambiguous fits to one-constraint reactions was not compatible with those for the 4C reactions just discussed. Apparently the large number of π produced 1C reactions swamped the corresponding K produced events so that errors in ionization judgment coupled with the relatively loose 1C fits were enough to make even the so-called unambiguous identifications unreliable. In the case of the reaction $K^+ d \rightarrow \pi^+ \pi^- pp K^o$ all fits were rescanned for V^o's. These V^o events were

then the final data sample used in calculating the cross section. In the case of the reaction $K^+d \rightarrow K^+\pi^-pp\pi^o$, events fitting only that reaction or only $\pi^+d \rightarrow \pi^+\pi^-pp\pi^o$ were apportioned according to the in/out ratio of the 4C reactions. If we call α the fraction of "unambiguous" 1C K events which are really K produced and ρ the fraction of "unambiguous" 1C π identifications which are really K produced, we have

$$\frac{\alpha K_i + \beta\pi_i}{\alpha K_o + \beta\pi_o} = R_K$$

and

$$\frac{(1 - \alpha)K_i + (1 - \beta)\pi_i}{(1 - \alpha)K_o + (1 - \beta)\pi_o} = R_\pi$$

where R_K and R_π are the in/out ratios for K's and π's from the 4C reactions. Knowing the K's and π's and R's, one then solves for α and β. We here once again make use of the fact that the K beam momentum distribution is nearly the same in or out of the window and similarly for the π's. The relatively small number of ambiguous events were also apportioned according to these ratios using the relations

$$\frac{A_{K_i}}{A_{K_o}} = R_K$$

and

$$\frac{A_{\pi_i}}{A_{\pi_o}} = \frac{A_i - A_{K_i}}{A_o - A_{K_o}} = R_\pi \quad .$$

Knowing A_i and A_o and R_K and R_π one then solves for A_{K_i} and A_{K_o}. The final data sample is then

$$\text{no. of } K^+d \rightarrow K^+\pi^-pp\pi^o \text{ events} = \alpha(K_i + K_o) + \beta(\pi_i + \pi_o) + A_{K_i} + A_{K_o} \quad .$$

The same procedure was followed in the case of the reaction

$K^+d \rightarrow K^+\pi^+\pi^-pn$ after separating proton and neutron reactions according to which final state nucleon had the greater momentum. An internal check on the entire procedure was to compare the $K^+d \rightarrow K^+\pi^+\pi^-p(n)$ cross section with that of $K^+p \rightarrow K^+\pi^+\pi^-p$ from the hydrogen data. The agreement was very good, 0.38±0.05 mb in hydrogen, 0.35±0.07 mb in deuterium.

III. CROSS SECTIONS FOR STABLE FINAL STATES

A. The Formula and the Results

Cross sections for stable final states were calculated from the final corrected event count and the number of tau decays using the standard formula

$$\sigma = \frac{N_{interaction}}{N_{decay}} \times \frac{B}{\eta c \tau} \times \frac{A}{\rho N_A}$$

where

$B = K^+$ branching ratio into the τ decay mode

$= 0.056 \pm 0.0004$,

$\eta = P_{beam}/m_{K^+}$,

$c = 2.998 \times 10^{10}$ cm/sec,

$\tau = K^+$ lifetime $= 1.235 \times 10^{-8}$ sec,[18]

A = atomic weight = 1.008 for hydrogen, 2.015 for deuterium,

ρ = density in the bubble chamber

$= 0.0608$ gm/cm^3 for hydrogen,

$= 0.1352$ gm/cm^3 for deuterium,[19]

and N_A = Avogadro's Number $= 6.0225 \times 10^{23}$ mole^{-1}.

Corrections to $N_{interaction}$ and N_{decay} are described in Part B of this Section. The final results for the hydrogen data are included in Table III. The final results for the deuterium data are listed in Table VI where the reactions are arranged according to the number of pions produced and the charge states of these pions. The reason for this arrangement has to do with the analysis of the deuterium data and is explained in detail in Part C of this Section. The errors given in Table VI are statistical.

B. Corrections to the Data

The actual numbers of accepted events in the hydrogen data were corrected by distributing unresolved events within each topology according to the number of accepted events in each reaction and, in the case of K^o events, by applying an escape correction factor. Both corrections are small, about 2.5% each. Zero length K^o events in hydrogen were fitted as additional hypotheses and were accepted only if one of the $\pi^+\pi^-$ pairs had the K^o mass $\pm$ 25 MeV. Zero length K^o events in deuterium were not fitted as such due to a problem in SIOUX and are assumed to be misidentified as pion events. The decay fiducial volume for K^o events in deuterium was defined to include a minimum distance cutoff. The resultant loss of events was then made up by the escape correction factor. This factor also contained the branching ratio for the unseen decay modes of the K^o. The number of unresolved events in deuterium is small, less than 5% of the total, and was not distributed among the accepted events. As mentioned before, scanning loss was negligible because the film was completely scanned twice. Pion contamination was discussed at length in the previous Section and was seen to involve not merely a correction factor but a revised procedure in certain reactions. In the case of $K^+d \rightarrow K^+\pi^-pp$ where the data sample was restricted to the beam window the tau sample used in calculating the cross section was of course similarly restricted. One further small effect of the pion contamination is shown in Fig. 5 where the $\pi^+d \rightarrow \pi^+\pi^+\pi^-pn$ fits are plotted as a function of the target nucleon momentum. The events of interest are in the peak in the next-to-lowest momentum bin. The proton was an unseen spectator in 14 of these events. The masses of the three pion systems for these events are listed in Table Vb. Apparently 12 of these events are misidentified taus and were added to the tau sample.

C. Deuterium σ's: KNN, KNNπ, KNNππ

The deuterium reactions are listed in Table VI in the same order as that presented by C. G. Wohl and A. A. Hirata in their analysis of the deuterium data at the four lower momenta of the K25 experiment.[11] Directly measured cross sections are those with the reactions not enclosed by brackets. Comments to the right of the cross sections indicate the procedures involved in obtaining them. The ingenious method of analysis developed and used by Wohl and Hirata was followed very closely here. The method enables one to obtain the KNNπ and KNNππ cross sections even though not all the individual cross sections were measured. The procedure utilizes isospin relations among the cross sections for KNNπ reactions and for KNNππ reactions. These relations are[20]

$$\sigma_c = 2\sigma_o \tag{1}$$

and

$$2\sigma_{cc} = 4\sigma_{oo} + \sigma_{co} \tag{2}$$

where σ_c is the sum of cross sections for all $K^+d \rightarrow KNN\pi$ reactions where the π is charged and σ_o is the sum of all $K^+d \rightarrow KNN\pi^o$ cross sections. Similarly σ_{cc} is the sum of all $K^+d \rightarrow KNN\pi\pi$ cross sections for reactions in which both pions are charged, σ_{co} is the sum of cross sections for all $K^+d \rightarrow KNN\pi\pi$ reactions with one charged and one neutral pion and σ_{oo} is the sum of cross sections for all $K^+d \rightarrow KNN\pi^o\pi^o$ reactions.

From (1)

$$\sigma(KNN\pi) = \sigma_c + \sigma_o \tag{3a}$$

$$= 3\sigma_o \tag{3b}$$

$$= \frac{3}{2}\sigma_c \quad . \tag{3c}$$

Not all of either σ_c or σ_o was measured in this experiment but it is still possible to obtain $\sigma(KNN\pi)$. At the lower momenta this was done by using the measured cross section for $K^+p \rightarrow K^+n\pi^+$ for the unmeasured

reaction $K^+d \to K^+nn\pi^+$. This procedure could not be used at 1585 MeV/c because the two-prong events were not analyzed due to excessive pion contamination. Instead, an interpolated value was used for $K^+p \to K^+n\pi^+$.[21] This is satisfactory because this cross section is small, less than one tenth of the total $KNN\pi$ cross section. Similarly, not all of either σ_{co} or σ_{oo} was measured but it is still possible to obtain $\sigma(KNN\pi\pi)$ from the ispin relations. From (2),

$$\sigma(KNN\pi\pi) = \sigma_{cc} + \sigma_{co} + \sigma_{oo} \qquad (4a)$$

$$= 3(\sigma_{cc} - \sigma_{oo}) \qquad (4b)$$

$$= \frac{3}{2}(\sigma_{co} + 2\sigma_{oo}) \qquad (4c)$$

$$= \frac{3}{4}(\sigma_{co} + 2\sigma_{cc}) \quad . \qquad (4d)$$

These equations become inequalities if just the measured cross sections are put in. Since all of σ_{cc} is measured, (4b) gives an upper limit to $\sigma(KNN\pi\pi)$. The other three equations give lower limits from which the most restrictive was selected, (4d) in this experiment. The value for $\sigma(KNN\pi\pi)$ was then taken as midway between the upper and lower limits and the error was obtained by folding in half the difference between upper and lower limits with the statistical errors on them.

The cross section for $K^+d \to KNN$ was obtained next by subtracting the $KNN\pi$ and $KNN\pi\pi$ cross sections from the total K^+d cross section. The cross section for $K^+d \to K^+pn$ was obtained in turn by subtracting the measured $K^+d \to K^0pp$ cross section from the $K^+d \to KNN$ cross section. The K^+pn cross section includes the $K^+d \to K^+d$ cross section. The $K^+d \to K^0\pi^+d$ fits were separated from the ambiguous $K^+d \to K^0\pi^+pn$ fits by ionization, range of the "p", and the mass of the pn system. The reaction $K^+d \to K^0\pi^+d\pi^0$ is a one-constraint fit; the corresponding $K^+d \to K^0\pi^+pn\pi^0$ reaction is a missing mass fit. Figure 6 is a plot of the cross

sections for the stable final states measured in deuterium as described above as a function of beam momentum. Figure 7 is a plot of the total K^+d cross section and 0-pion, 1-pion, and 2-pion production cross sections for K^+d interactions as a function of beam momentum.

D. Effective K^+n Cross Sections

Neutron cross sections were obtained from deuterium reactions with two protons in the final state by applying an empirical Glauber, or shielding, correction to the K^+d cross sections. This correction factor was simply the ratio of the cross section for the reaction $K^+p \rightarrow K^o\pi^+p$ from the hydrogen data to the cross section for the reaction $K^+p(n) \rightarrow K^o\pi^+p(n)$ from the deuterium data. This latter was obtained from the reaction $K^+d \rightarrow K^o\pi^+pn$ by considering the final state nucleon momenta. Figure 8 is a correlation plot of the proton momentum vs the neutron momentum for this reaction. Most of the events are seen to be clearly $K^o\pi^+p(n)$ or $K^o\pi^+n(p)$. Spectator cutoffs at 150 MeV/c were used to determine the data samples used for Dalitz plots and angular distributions. Events in the intermediate region between the spectator cutoffs (both nucleon momenta greater than 150 MeV/c) were apportioned for calculation of the cross sections according to the ratio of events in the "pure" regions. This is the same procedure as that used at the lower momenta. Figure 9 shows the cross sections for $K^+d \rightarrow K^o\pi^+pn$ separated into $K^+d \rightarrow K^o\pi^+p(n)$, $K^o\pi^+n(p)$ and $K^o\pi^+d$ as described and compares the $K^+d \rightarrow K^o\pi^+p(n)$ reaction cross section with that for $K^+p \rightarrow K^o\pi^+p$ as a function of beam momentum. The empirical Glauber correction at 1585 MeV/c is 1.14±0.12. Table VII is a list of the neutron cross sections.

E. Cross Section for the I = 0 KN Channel

The isospin relations (1) and (2) apply also to the reactions considered as occurring off free protons or neutrons. The symbols still refer to the sums of cross sections for the indicated pion charge states taken over both proton and neutron reactions. The one-pion reactions are

$$\begin{aligned} K^+p &\to K^o\pi^+p \\ &\to K^+\pi^+n \\ &\to K^+\pi^op \\ K^+n &\to K^o\pi^+n \\ &\to K^+\pi^-p \\ &\to K^o\pi^op \\ &\to K^+\pi^on \end{aligned}$$

The isospin 0 and 1 channel cross sections expressed in terms of the sums of the above reaction cross sections are

$$\sigma_1(KN\pi) = \sigma_p \qquad (5a)$$

and

$$\sigma_o(KN\pi) = 2\sigma_n - \sigma_p \ . \qquad (5b)$$

Combining (5b) and (1) one gets directly

$$\sigma_o(KN\pi) = 3[\sigma(K^+n \to K^+\pi^-p) + \sigma(K^+n \to K^o\pi^+n) - \sigma(K^+p \to K^+\pi^op)] \ . \quad (6)$$

The last reaction in (6) has a two prong-no "V" topology, not analyzed at this momentum and so again interpolation was used.[21] All contributions from the I = 1 state have been subtracted out in (6). This includes the Δ, K^* from the I = 1 state, $K^*\Delta$ interference, and I = 1 background. What is left is K^* from the I = 0 state and nonresonant I = 0 background. By considering the K^* cross section in the reactions in (6) we can get the cross section for K^* in the I = 0 channel. Thus

$$\sigma_o(K^*) = 3[\sigma(K^+n \rightarrow K^{*o}p) + \sigma(K^+n \rightarrow K^{*+}n) - \sigma(K^+p \rightarrow K^{*+}p)] \quad (7)$$
$$\hookrightarrow K^+\pi^- \qquad \hookrightarrow K^o\pi^+ \qquad \hookrightarrow K^+\pi^o$$

Again, a substitution was necessary for the last reaction. We used the reaction $K^+p \rightarrow K^{*+}p$ ($\hookrightarrow K^o\pi^+$) which was analyzed at this momentum and included the appropriate Clebsch-Gordan factor of 1/2. The $I = 0$ channel total cross section, $KN \rightarrow KN$ cross section and $KN \rightarrow KN\pi$ cross section are shown in Fig. 10 as a function of beam momentum. The cross section for the K^* produced in the $I = 0$ channel is shown in Fig. 38 as a function of beam momentum. The procedures for obtaining the individual resonance cross sections are described in the next Section.

IV. RESONANCE PRODUCTION

A. Cross Sections and Mass Distributions

The single pion production reactions observed in this experiment are

$$K^+p \rightarrow K^o\pi^+p$$
$$K^+d \rightarrow K^o\pi^+p(n)$$
$$K^+d \rightarrow K^o\pi^+n(p)$$
$$K^+d \rightarrow K^+\pi^-p(p)$$
$$K^+d \rightarrow K^o\pi^op(p) \quad .$$

Figures 11 and 12 contain the Dalitz plots for these reactions. The data plotted for the $K^+d \rightarrow K^o\pi^+p(n)$ and $K^+d \rightarrow K^o\pi^+n(p)$ reactions come from the well separated "pure" regions of Fig. 6 where the spectator nucleon has a momentum less than 150 MeV/c. The very well known fact that single pion production is dominated by quasi-two-body production is quite clear in all these Dalitz plots. Reactions off the neutron are seen to be mainly K^*N; reactions off the proton also show strong $K\Delta$ production. K^*-Δ interference shows up particularly clearly in the $K^+d \rightarrow K^o\pi^+p(n)$ plot.

The Dalitz plots were fitted with an empirical interference model in which the K^* and Δ intensities were each a product of a p-wave Breit-Wigner,[24,25] a factor giving the distribution of one diparticle mass along a line of fixed mass for the other diparticle pair, and a P-wave production angular momentum barrier. The interference term contains a relative phase factor and a numerical factor allowing for less-than-maximal interference between the K^*N and $K\Delta$ amplitudes. In this model then the Dalitz plot density is given by

$$\frac{d^2\sigma}{dm^2_{K\pi}dm^2_{N\pi}} = a + bI_{K^*} + cI_\Delta + 2d(bcI_{K^*}I_\Delta)^{1/2}\cos(\varphi_\Delta - \varphi_{K^*} + \varphi_o) \qquad (8)$$

where a = nonresonant, non-interfering background (phase space),

$$I_{K^*} = BW_{K^*}(1 + A_{K^*} \cos^2 \lambda_{K\pi}) \frac{q_{K^*}^2}{q_{K^*}^2 + m_\omega^2/2} ,$$

$$I_\Delta = BW_\Delta(1 + A_\Delta \cos^2 \lambda_{N\pi}) \frac{q_\Delta^2}{q_\Delta^2 + m_\rho^2/2} ,$$

$$BW = \frac{1}{\pi} \frac{\Gamma \frac{p_o}{p} m_o}{(m^2 - m_o^2)^2 + (\Gamma m_o)^2} ,$$

and $$\Gamma = \Gamma_o \left(\frac{p^2}{p^2 + m_\pi^2} \Big/ \frac{p_o^2}{p_o^2 + m_\pi^2} \right) \frac{p}{p_o} ,$$

where m_o and Γ_o are the nominal resonance mass and width, taken as 1236 MeV and 116 MeV for the Δ and 891 MeV and 50 MeV for the K^*, m is the appropriate diparticle mass, p_o and p are the two-body c.m. decay momenta corresponding to m_o and m, and q_{K^*} and q_Δ are the K^* and Δ momenta in the overall c.m. The angle $\lambda_{K\pi}$ is defined as shown in Fig. 13 as the pion decay angle in the $K\pi$ c.m. with respect to the nucleon direction. The angle $\lambda_{N\pi}$ is similarly defined as the pion decay angle in the $N\pi$ c.m. with respect to the kaon direction. Along a line of constant $m_{K\pi}^2$, $m_{N\pi}^2$ varies linearly with $\cos \lambda_{K\pi}$, where $\cos \lambda_{K\pi} = \pm 1$ corresponds to the edges of the Dalitz plot. Because both K^* and Δ decay in p waves their decay distributions in λ are of the form

$$W(\cos \lambda) \propto 1 + A \cos^2 \lambda \quad .$$

The values of A for the two resonances are left as free parameters to be varied in the fit.

The P wave production angular momentum barrier is important only near the resonance thresholds; its effect is small at this momentum. It affects the mass distributions, that is the shape and position of the resonances, by suppressing high mass production but to an extent

that is significant only when the resonance bands occupy much of the Dalitz plots as they do at the lower momenta of this experiment. The fitting program was written by R. W. Bland as part of his exhaustive study of Δ and K^* production in K^+p reactions at the lower momenta.[6] The P wave factor was appropriate there because the Δ is produced largely via P waves down to threshold and because K^*-Δ interference indicates a strong P wave component in K^* production. By 1585 MeV/c, however, higher waves than P have become strongly present in Δ production and pseudoscalar exchange as well as vector exchange has shown up strongly in the decay angular distributions of the K^*, indicating a strong S wave component in K^* production. The P wave factor is therefore no longer really appropriate. Moreover, K^* production in reactions off the neutron indicates mostly pseudoscalar exchange and is highly peripheral by 1585 MeV/c, involving many partial waves. So the P wave factor is not really appropriate for K^+n reactions. However because the effect is unimportant at this momentum due to the much greater size of the Dalitz plots and because including the factor is probably as correct as omitting it in lieu of the unknown correct and probably much more elaborate barrier factor, the fitting program was applied "as is." Results of the fits are listed in Table VIII. The Δ cross sections in the fits to the deuterium data were constrained to agree with the hydrogen data scaled with the empirical shielding correction and Clebsch-Gordan coefficients. The use of these results to obtain the cross section for the K^* produced in the $I = 0$ channel was described in Part E of the previous Section.

One more point to be mentioned is that this fitting model assumes that the background does not interfere with the resonances. This is not really true either. Dalitz plots below the K^* threshold show an asymmetry

in the $K\pi$ mass distribution in the Δ band indicating interference between the Δ and background.[26] Variation with $N\pi$ mass of the coefficients in the Legendre polynomial expansion of the Δ production angular distribution also indicates interference between the Δ and background. Finally, correlation plots in the decay angles of the K^* show strong correlation effects which may be due to K^*-background interference. However, the complexities involved in trying to incorporate all these secondary features into the fit are probably not justified in a statistics-limited experiment. Uncertainty in the model was reflected by doubling the statistical errors to obtain those quoted in Table VIII.

Double pion production reactions in deuterium were swamped by the beam pion contamination as described earlier. The reactions observed in the hydrogen data are

$$K^+p \rightarrow K^+\pi^+\pi^-p \qquad (9)$$

$$K^+p \rightarrow K^o\pi^+\pi^op \qquad (10)$$

and

$$K^+p \rightarrow K^o\pi^+\pi^+n \ . \qquad (11)$$

Of these, only the first was observed with sufficient statistics to warrant some analysis. Figure 14 is a triangle plot for this reaction in which $M_{p\pi^+}$ is plotted vs $M_{K^+\pi^-}$. The cluster of points near the high mass kinematical limit is indicative of double resonance production, Δ^{++} and K^{*o}, which apparently dominates this reaction even below the nominal $K^*\Delta$ threshold which occurs at 1750 MeV/c for the central values of the resonance masses. Thus at 1585 MeV/c double resonance production occurs on the low mass tails of the resonances. This is further illustrated in Fig. 15 where the events are projected onto the axes of the triangle plot. The K^* and Δ peaks are seen to be shifted well below their nominal values.

The triangle plot was fitted with a program which assumed the incoherent superposition of the 4 main processes: a) double resonance production, b) $\Delta^{++}K^{+}\pi^{-}$, c) $K^{*o}p\pi^{+}$, and d) $p\pi^{+}K^{+}\pi^{-}$. The distribution function is then

$$P(M_{K^+\pi^-},M_{p\pi^+}) = \{\alpha(BW(\Delta)BW(K^*)) + \beta BW(\Delta) + \gamma BW(K^*) + \delta\}q_{cm}p_{\Delta}p_{K^*}$$

where BW is the p-wave Breit-Wigner described above, q_{cm} is the Δ or K^* momentum in the overall c.m. and p_{Δ} and p_{K^*} are the Δ and K^* decay momenta in their respective c.m.'s. The factor $q_{cm}p_{\Delta}p_{K^*}$ is nonresonant phase space. The parameters α, β, and γ were varied in the fit with δ determined by the overall normalization. The triangle plot was divided into 13 bins and the best χ^2 was 13.4 for 9 degrees of freedom. The conclusion was that $K^*\Delta$ production comprises 65±15% of the reaction with a cross section of 0.25±0.07 mb. The remainder of the reaction is divided between $\Delta K^{+}\pi^{-}$ and background in a ratio not well determined by the fit. The solid curves in Fig. 15 correspond to the fit; the dashed curves correspond to the $K^*\Delta$ component.

The other two double pion reactions are also apparently dominated by double resonance production. This is suggested by the fact that the cross sections for the three reactions are consistent with the ratios dictated by isospin conservation in $K^*\Delta$ decay, 18:13:2.

B. Δ Production and Decay

Because the Δ ($I = 3/2$) can be produced only in the $I = 1$ channel and not in the $I = 0$ channel, it is seen more strongly in $K^{+}p$ reactions than in $K^{+}n$ reactions and more clearly in hydrogen than in deuterium. In hydrogen, it is produced at threshold through the three single pion production reactions

$$K^+p \rightarrow K^0\pi^+p \qquad (12)$$

$$K^+p \rightarrow K^+\pi^0p \qquad (13)$$

and $$K^+p \rightarrow K^+\pi^+n \ . \qquad (14)$$

Clebsch-Gordan coefficients for the isospin states involved show that the Δ is produced in these three reactions in the ratios 9:2:1. Thus the first reaction is the appropriate one for study, fortunately, since at 1585 MeV/c it was the only one available.

The features of Δ production and decay near threshold in this reaction were studied in detail by R. W. Bland and reported in his thesis[6] and in a later report, UCRL-19357.[8] The final data at 1585 MeV/c were analyzed in collaboration with Bland in the same way as the data at the lower momenta and included in the later report. The main conclusions are outlined here and the figures repeated. Because the figures contain the data from the lower momenta, the results at 1585 MeV/c are seen in their proper context.

In selecting the data sample for the study of angular distributions there is the problem of the K^*-Δ overlap region. As seen in the Dalitz plot, Fig. 11, this occurs at 1585 MeV/c in the center of the Δ band and in the lower portion of the K^* band. The mass conjugation technique of Eberhard and Pripstein[27] was used to simulate K^* production in the overlap region. The mass conjugated distributions were subtracted out of the distributions in the overlap region in order to purify the Δ sample. (In the study of the K^*, the upper half of the Dalitz plot ($\cos \lambda_{K\pi} < 0$) was used.) This approximation neglects K^*-Δ interference and background, both shown in the Dalitz plot fits to be relatively small components of the reaction cross section. The Δ band was taken to be 1160-1280 MeV.

Figure 16 shows the cross section for Δ production in reaction (12)

as a function of beam momentum. The cross sections have all been multiplied by a factor of 4/3 to include Δ production in reactions (13) and (14) as well. The solid curve (b) is the prediction of the Stodolski-Sakurai ρ exchange model for Δ production[28] using the value for the product of the coupling constants suggested by Jackson.[29] The solid curve (a) differs from (b) only in that the suggested value for the product of the squares of the coupling constants has been multiplied by a factor of five so as to achieve a fit near threshold. The fit is seen to be quite good up to about 1.1 BeV/c where other channels, notably K^*N, open up and the unitarity limit requires the cross section to fall below the prediction of the model. The good fit near threshold is due to the predominance of P-wave production of the Δ, called for by the theory and seen in the production cross sections, in the shape of the Nπ mass distributions (the P-wave angular momentum barrier discussed earlier) and in the production and decay angular distributions.

Figure 17 shows the production angular distribution in the overall c.m. for Δ production in reaction (12) as a function of incident beam momentum. The distribution is mostly $\sin^2\theta$ near threshold, indicating P-wave, and becomes more forward peaked as the beam momentum increases, indicating the strong presence of other, probably higher waves. The curves in Fig. 17 are the predictions of the Stodolski-Sakurai model. The experimental data were fitted with Legendre polynomials up to the fourth order in the expression

$$W(\cos\theta) \propto 1 + \sum_{\ell=1}^{4} A_\ell P_\ell(\cos\theta) \quad .$$

The results are shown in Fig. 18. Pure $\sin^2\theta$ would have $A_2 = -1$. The data at 1585 continue the trend away from that value. That fact plus the increasing magnitudes of A_1, A_3, and A_4 all reflect the increasing

presence of other partial waves in Δ production with increasing beam momentum. The coefficient A_4 represents higher waves than P and the odd Legendre coefficients represent interference between waves of opposite parity.

The second kind of Δ-background interference mentioned in Part A shows up in the plot of the first two Legendre coefficients, A_1 and A_2, vs Nπ mass, Fig. 19. The variation of these coefficients apparently results from the changing relative phase between background and Δ according to the Breit-Wigner dependence of the Δ. As seen here in the production angular distribution, the decay angles have been integrated out so the part of the background responsible for this interference must have the Nπ system in a $p_{3/2}$ state as other ℓ_j states are orthogonal to the $p_{3/2}$ Δ.

The decay angular distributions of the Δ were studied using the coordinate systems shown in Fig. 20. The angles are measured with respect to the outgoing nucleon in the Δ c.m. The Stodolski-Sakurai model makes simple predictions for the distributions in γ and δ, namely

$$W(\cos\gamma) \propto 1 + 3\cos^2\gamma$$

and

$$W(\delta) = \text{isotropic} \quad .$$

The experimental distributions are shown in Figs. 21 and 22, folded in accordance with the parity-imposed symmetry of the decay. The solid curves are the normalized predictions of the model. The fits in cos γ are seen to be very good; the fits in δ may not be so good, especially near threshold, but the error bars are large and it is not clear what significance to give to the deviations from isotropy. Another way of presenting the same information is to look at the density matrix elements. When these are defined in terms of the angles α and φ of Fig. 20, the model makes the following predictions:

$$\rho_{33} = 0.375 \ , \quad \text{Re}\ \rho_{3-1} = 0.218 \ , \quad \text{Re}\ \rho_{31} = 0 \ .$$

Figure 23 shows the comparison between these predictions and the results of a maximum likelihood fit of the data. Again, agreement is quite good at 1585, not so good near threshold. These observations give more support to the model and its assumption of magnetic dipole (M1) coupling to the p-Δ vertex than simply the P-wave production feature of the Δ. The exchanged particle must have $I = 1$ and normal spin-parity. Stodolski-Sakurai suggested ρ exchange. Bland et al. were led to suggest that heavier particles than the ρ, notably the A_2, probably are exchanged and that this might account for the higher values of the coupling constants.

C. K^* Production in the $I = 1$ Channel

Since K^+p is pure $I = 1$ and K^+n is half $I = 1$ and half $I = 0$ it is best to study K^* production in the $I = 1$ channel in hydrogen rather than deuterium. The Clebsch-Gordan coefficients give the ratio for K^* production in reactions (12) and (13) as 2:1. Thus reaction (12) is the appropriate one for study here as in the case of Δ production. As was the case in the discussion of the Δ, the figures here were taken from the UCRL report, UCRL-19357, and contain the data near the K^* threshold as analyzed by Bland.

The problem of the overlap of the K^* and Δ bands in the Dalitz plot at 1585 MeV/c was handled by using only data in the upper half of the Dalitz plot, i.e., $\cos \lambda_{K\pi} < 0$. The K^* band was taken to be 840-940 MeV.

The production angular distribution for $K^+p \rightarrow K^{*+}p$ is given in Fig. 24. The reaction is seen to become more peripheral with increasing beam momentum. The "bump" in the distribution just below $\cos \theta = 0$ is very clear at 1585 MeV/c but is also noticeable at all momenta in

this experiment and suggests the presence of D waves or higher even down to threshold. Figure 25 shows the Legendre polynomial coefficients to fourth order for these distributions.

The decay angular distributions are described in a coordinate system similar to that used to describe the decay of the Δ, Fig. 20; the z axis is along the normal to the production plane and the x axis is along the direction of the incoming K^+ meson as seen in the $K\pi$ c.m. The angles measured are those of the outgoing K^o. The decay angular distribution is given in terms of the density matrix elements as[30]

$$W(\cos\alpha,\varphi) = \frac{3}{4\pi}\{\rho_{oo}\cos^2\alpha + \rho_{11}\sin^2\alpha - \rho_{1-1}\sin^2\alpha\cos 2\varphi - \sqrt{2}\,\mathrm{Re}\,\rho_{10}\sin 2\alpha\cos\varphi\}$$

where $\rho_{11} = \frac{1}{2}(1 - \rho_{oo})$. The density matrix elements are shown in Fig. 26. The distributions in $\cos\alpha$ and φ corresponding to these density matrix elements are shown in Fig. 27, folded in accordance with the symmetry imposed by parity conservation.

In a peripheral OME model, pseudoscalar exchange leads to pure $\cos^2\alpha$, corresponding to $\rho_{oo} = 1$; exchange of normal spin parity leads to pure $\sin^2\alpha$, corresponding to $\rho_{oo} = 0$. Figures 26 and 27 indicate dominance by normal spin parity exchange near threshold, presumably vector, with pseudoscalar exchange also coming in as the momentum increases to 1585 MeV/c. At higher momenta previously reported,[32] the reaction is again dominated by natural parity exchange, apparently isoscalar since the reaction $K^+n \to K^{*o}p$ which requires a charge exchange is dominated by pseudoscalar exchange. The usual assumption is that the ω is the isoscalar natural parity system important in $K^+p \to K^{*+}p$. The data at 1585 MeV/c suggest an intermediate region where pseudoscalar exchange is also important.

D. $K^*\Delta$ Production

As discussed in Part A of this Section, K^+p double pion production is dominated by $K^*\Delta$ production even below the nominal $K^*\Delta$ threshold. The major decay modes are produced in reaction (9) for which we have a barely analyzable amount of data at 1585 MeV/c. Fortunately there is no ambiguity in this final state in pairing the particles.

Figure 28 shows the production angular distributions for $K^*\Delta$ production at a lower momentum at which it is seen in Bland's data, at 1585 MeV/c and at one higher momentum, 1.96 GeV/c, from another experiment.[33] At 1367 MeV/c, Bland found that resonance production could not be separated from background. At 1585 MeV/c, double resonance production comprises 65±15% of reaction (9) but all the events are plotted in Fig. 28. A cut on $M_{K\pi}$ at 800 MeV, considering only events with $M_{K\pi} > 800$ MeV was tried. It reduced the background from 35% to about 10% but no significant differences in the production or decay angular distributions were seen. The production is seen to be highly peripheral even below threshold. The apparently sharper forward peaking at 1585 MeV/c is largely an illusion, the result of the binning.

The density matrix elements for this reaction are presented in Table X along with the predictions of the OPE model. Data from an experiment at 3.0 GeV/c are included.[35] The results at 1585 MeV/c are far from satisfying the pion exchange predictions for ρ_{oo} and ρ_{33} but the trend of the data with increasing beam momentum is seen to be toward the OPE values.

E. K^* Production in K^+n Reactions

The single pion production reactions off the deuterium neutron are

$$K^+n(p) \rightarrow K^+\pi^-p(p) \qquad (15)$$

$$\rightarrow K^o\pi^op(p) \qquad (16)$$

$$\rightarrow K^o\pi^+n(p) \qquad (17)$$

$$\rightarrow K^+\pi^on(p) \qquad (18)$$

the parentheses indicating the spectator proton. Reaction (18) has a two-prong no "V" topology in the bubble chamber and could not be analyzed at 1585 MeV/c because of the pion contamination.

The first three reactions are dominated by K^* production as is seen by inspection of the Dalitz plots, Fig. 12. The relative absence of Δ in these reactions is entirely expected since the K^+n state is half $I = 0$ and the $I = 3/2$ Δ cannot be formed from this state in single pion production and because of the Clebsch-Gordan coefficients for Δ decay.

The cross sections for K^{*o} production in reactions (15) and (16) and for K^{*+} production in reaction (17) are given in Table VIII. Their calculation, involving a Dalitz plot fitting program was discussed in Part A of this Section. Cross sections for K^* production off a free neutron were obtained from the deuterium cross sections by multiplying the latter by the empirical Glauber correction factor described in Part D of Section III and are given in Table IX. Clebsch-Gordan coefficients for the decay of the $I = 1/2$ K^* into $K^+\pi^-$ and $K^o\pi^o$ predict cross sections for K^* production in reactions (15) and (16) in the ratio 2:1. The values from Table IX are seen to be in good agreement with this expectation.

The $K\pi$ mass squared distributions for reactions (15)-(17) are shown in Fig. 29. The curves are the results of the Dalitz plot fitting program. The $N\pi$ mass squared plots are given in Fig. 30.

The K^* production and decay angular distributions for reactions (15)-(17) are shown in Fig. 31. The data for all studies of angular distributions consists of those events where the spectator proton momentum

is less than 150 MeV/c, the cut being made to avoid final state interactions. The K^* band was taken to be 840-940 MeV. K^{*o} production is seen to be highly peripheral at 1585 MeV/c.

The density matrix elements, calculated by the method of moments,[36] are given in Table XI along with OME model predictions for pseudoscalar and vector exchange. It is seen that, at this momentum, K^{*o} production is dominated by pion exchange but there is certainly vector exchange present also. The same observations apply to the K^{*+} but with much poorer statistics.

Figure 32 contains exchange diagrams for the reactions $K^+n \to K^{*o}p$, $K^+p \to K^{*+}p$, and $K^+n \to K^{*+}n$. Included in these diagrams are the lowest mass particles on the trajectories allowed in the exchanges, i.e., those particles expected to dominate the exchanges. In earlier work at a higher momentum,[32] the K^{*o} was seen as produced entirely via pseudoscalar exchange with no ρ exchange contributing. From charge independence in the t channel, K^{*+} production in K^+p interactions has been thought also not to involve ρ exchange but to be mainly ω exchange along with some pion exchange. We can adduce two arguments against this conclusion:

1) We do see some vector exchange in K^{*o} production. This becomes particularly evident when we obtain the decay angular distributions for the K^* produced in the $I = 0$ channel (in the next Part). This is seen to be very nearly pure pion exchange, much more so than the K^{*o}, and is obtained by subtraction from the K^{*o} decay angular distributions. Thus there was some vector exchange in the K^{*o} decay angular distributions.

2) The experimental ratio of the cross sections for the reactions

$$K^+p \to K^{*+}p \quad \text{and} \quad K^+n \to K^{*+}n$$
$$\hookrightarrow K^o\pi^+ \qquad\qquad \hookrightarrow K^o\pi^+$$

is about 2:1. The ω and ρ amplitudes have the same sign in the K^+p reaction, the opposite sign in the K^+n reaction. Hence if both amplitudes are present they can interfere constructively in the first case and destructively in the latter.

One more very interesting feature in K^* production, called to my attention by C. Fu,[37] is shown in the correlation plots of $\cos\alpha$ vs φ, the decay angular parameters, for the K^{*o} produced in reactions (15) and (16) and for the K^{*+} produced in reaction (17) and off the proton. These plots are shown in Figs. 33 and 34. The plots in Fig. 33 have been folded in φ according to parity conservation in the decay of the K^*, i.e.,

$$\varphi \rightarrow \varphi + 180^o$$

$$\cos\alpha \rightarrow -\cos\alpha \ .$$

The plots in Fig. 34 have been folded in φ according to overall parity conservation,

$$\varphi \rightarrow -\varphi$$

$$\cos\alpha \rightarrow \cos\alpha \ .$$

No correlations are seen in Fig. 33 as is expected in the strong decay of a definite parity state. The origins of the marked correlations seen in Fig. 34 are not well understood. Multiperipheral Regge models have been suggested to account for this effect in $K^{*o}(890)\Delta^{++}(1236)$ production at 4.6 and 9 GeV/c.[38] Interference with background has also been suggested as a possible source especially at this low momentum. We note only that a simple OME model does not account for this effect.[39]

F. K^* Production in the $I = 0$ Channel

K^+n reactions contain the information on $I = 0$ channel amplitudes and exchange mechanisms but they also contain $I = 1$ information which has to be separated out. The means for doing so is a simple subtraction,

Eqs. (6) and (7), derived and discussed in Part E of Section IV. Eq. (7) was used to obtain the cross section for K^* production in the $I = 0$ channel using the individual reaction K^* cross sections obtained by fitting the Dalitz plots. Equation (6) was used to study the production and decay angular distributions.

A mass cut of 840-940 MeV in the $K\pi$ system was used to determine the K^* sample. No correction was made for background. The last reaction in Eq. (6) was replaced by

$$K^+p \rightarrow K^{*+}p$$
$$\hookrightarrow K^o\pi^+$$

weighted with the appropriate Clebsch-Gordan factor of 1/2 as in the calculation of the cross section. Each reaction distribution was normalized to its free nucleon cross section.

Figure 35 shows the differential cross section and decay angular distributions for the component reactions and for the $I = 0$ channel K^*. The reaction

$$K^+n \rightarrow K^{*o}p$$
$$\hookrightarrow K^+\pi^-$$

dominates the data but the composite production angular distribution is seen to be even more sharply forward peaked than in that individual reaction distribution and the decay angular distributions indicate more nearly pure pion exchange than in K^{*o} production. Figure 36 shows $\frac{d\sigma}{|dt|}$ for the $I = 0$ channel K^* and density matrix elements for three intervals in $|t|$.

In his thesis,[12] A. A. Hirata develops a model for $K^+N \rightarrow K^*N$ reactions by considering s and t channel isospin amplitudes. We describe the origins of the model in Appendix B. It ascribes K^* production to a

combination of π, ρ, and ω exchange with the ρ amplitude being about 1/3 as large as the ω amplitude and opposite in phase. It also leads to certain predictions for the relative sizes of the various cross sections observed. These predictions and the experimental results at 1585 MeV/c are presented in Table XII. There is reasonable agreement considering the large statistical errors in the experimental results.

From the correlation plots in Fig. 34 it is evident that the subtraction procedure will produce even stronger correlations between $\cos \alpha$ and φ in the K^* in the $I = 0$ channel than in the individual reactions. It is difficult to do a subtraction with a scatter plot. In Fig. 37 we have divided the plot into bins, performed the subtraction, and entered the resulting number of events in each bin. The $\pi\omega\rho$ exchange model assumes no interference or absorption effects but the correlations indicate that something more elaborate than simple OME will be necessary to fully account for all the features of single pion production at 1585.

However it is quite remarkable that even though the K^* is produced in the $I = 1$ channel mainly through ω exchange and in the $I = 0$ channel mainly through π exchange, the momentum dependence of the cross sections for these different reactions is very similar. Figure 38 shows this behavior up to 3 GeV/c. Figure 39 shows the momentum dependence of the individual reactions involved in obtaining the $I = 0$ channel cross section.

V. CHARGE EXCHANGE ELASTIC SCATTERING

The observed charge exchange reaction is

$$K^+ d \rightarrow K^o pp \tag{19}$$

coming from the neutron reaction

$$K^+ n(p) \rightarrow K^o p(p) \tag{20}$$

We have no empirical Glauber correction available for elastic scattering. The cross section for (19) is included in Table VI. In what follows we will be concerned only with the differential cross section for the charge exchange reaction.

An important effect in the t distribution or production angular distribution for this reaction, much more important than in inelastic processes, is that of the Pauli exclusion principle particularly in the forward direction where $t \approx 0$. In inelastic reactions there is a much greater minimum $|t|$ and the effect becomes negligible. The general form for this correction factor, in charge exchange, is derivable[40] and the differential cross sections in (19) and (20) are related by

$$\left(\frac{d\sigma}{dt}\right)_d = \left(\frac{d\sigma}{dt}\right)_n \left[\frac{1 - H + R\left(1 - \frac{H}{3}\right)}{1 + R}\right] \tag{21}$$

where

$$R = \left(\frac{d\sigma}{dt}\right)_n^{\text{spin flip}} \Big/ \left(\frac{d\sigma}{dt}\right)_n^{\text{non spin flip}}$$

and H is a deuteron form factor given by

$$H = \frac{2(\alpha + \beta)\alpha\beta}{(\alpha - \beta)^2} \frac{1}{\sqrt{-t}} \left[\tan^{-1} \frac{\sqrt{-t}}{2\alpha} - 2 \tan^{-1} \frac{\sqrt{-t}}{\alpha + \beta} + \tan^{-1} \frac{\sqrt{-t}}{2\beta}\right]$$

where $\beta = 7\alpha$ and $\alpha = 45.5$ are the constants in the exponents in the Hulthén wave function for the deuteron.

The ratio R is a model-dependent number. A Regge pole model for charge exchange was developed several years ago by Rarita and Schwarzschild[41,42]

to account for $K^+n \rightarrow K^0p$ at 2.23 GeV/c and K^-p and π^-p charge exchange at higher momenta and also to account for π^-p charge exchange polarization. The model adds a lower lying ρ-type Regge trajectory, called ρ', to the ρ and A_2 trajectories usually associated with charge exchange. It is successful at the momenta it was designed to account for and it is natural to try it at lower momenta also.

Figure 40 shows the data, $(\frac{d\sigma}{dt})_d$, and two curves calculated from the model. The dashed curve is the model prediction with no modification of its parameters as presented by Rarita and Schwarzschild. The solid curve is the model prediction after some modificaton of these parameters, namely replacing the beam energy E by the less approximate form $E + \frac{t}{4m_\rho}$ and changing the values of the parameters D_o and D_1 in the ρ' spin flip residue function $D = D_o e^{D_1 t}$ from -264 to -135 mb and 2.95 to 2.3 $(GeV/c)^2$ respectively. These modifications were designed to achieve a better fit at the lower momenta at the cost, of course, of a somewhat poorer fit in the high momentum region above 2.2 GeV/c.

Figure 41 shows the charge exchange cross section for $|t| < 1$ $(GeV/c)^2$ for data at 2.23 and lower momenta. The dashed curve is the unmodified model and the solid curve is the result of modifying the parameters as above.

Figure 42 shows the differential cross section for this experiment in the K^+n c.m. The curves are Legendre polynomial fits to third order to $(\frac{d\sigma}{d\Omega})_n$ calculated from Eq. (21). Because the correction term is model dependent, the extremes $R = 0$ (no spin flip) and $R = \infty$ (all spin flip) and an average $R = 1$ were tried. The three cases are seen to be very close at 1585 MeV/c and so this fit does not afford a sensitive test of the Rarita-Schwarzschild model. The crosses in Fig. 41 are the data

points $(\frac{d\sigma}{d\Omega})_d$. The forward-most bin was omitted in the fits to prevent it from dominating the fits by virtue of the fact that the cross section goes to zero in the forward direction.

The intercept of the fit at $\cos\theta = 1$ is a measure of the absolute value squared of the non spin flip amplitude, $f(\theta)$, in the forward direction. The imaginary part of $f(0)$ can be found from the optical theorem and the (well measured) total cross sections for K^+p and K^+n. Listing the $KN \rightarrow KN$ reactions and their $I = 1$ and $I = 0$ s-channel amplitudes we have

$$\begin{aligned} K^+p &\rightarrow K^+p && A_1 \\ K^+n &\rightarrow K^+n && 1/2(A_1 + A_o) \\ K^+n &\rightarrow K^op && 1/2(A_1 - A_o) \quad . \end{aligned}$$

Thus

$$A_{\substack{CE \\ el.}} = A_{\substack{K^+p \\ el.}} - A_{\substack{K^+n \\ el.}}$$

and

$$\text{Im } A_{\substack{CE \\ el.}}(0) = \frac{k}{4\pi}\left(\sigma_{\substack{K^+p \\ total}} - \sigma_{\substack{K^+n \\ total}}\right) \quad .$$

Regge model predictions for this reaction assuming ρ and A_2 exchange call for the non spin flip amplitude in the forward direction to be mostly real.[42,43] We find

$$\left|\frac{\text{Re } f(0)}{\text{Im } f(0)}\right| = 8.4 \pm 1.4$$

in good agreement with the prediction.

ACKNOWLEDGMENTS

As is usually the case in high energy physics, far too many people made contributions to this experiment for them all to be individually acknowledged. The Bevatron staff, the bubble chamber crews, the computer center staff all were essential, of course. Special thanks for their efforts should go to the several generations of scanners and measurers and programmers of the Trilling-Goldhaber group spanned by this experiment.

I cannot satisfactorily express my gratitude to three individuals whose aid and encouragement were absolutely necessary for the successful completion of this work. To Drs. Charles Wohl, Allan Hirata, and Roger Bland go my deepest thanks.

I wish also to thank Drs. Donald Coyne and Jimmy MacNaughton for their encouragement and Dr. Chumin Fu for a number of interesting and illuminating discussions.

It was my privilege to know and work with Dr. Sulamith Goldhaber, though for much too short a time. It is a pleasure to acknowledge her influence and that of Professor Gerson Goldhaber on my research.

I would like to thank Dr. John Kadyk for many helpful discussions.

My advisor throughout this work has been Professor George Trilling. I would like to thank him for his interest and teaching and guidance over these ten years.

This work was supported by the U. S. Atomic Energy Commission.

Table I. Number of pictures in hydrogen and deuterium; number of events in each topology studied.

	Hydrogen				Deuterium			
Number of pictures	51,000				32,000			
Number of events	Total	Accepted	Rejected	Unresolved	Total	Accepted	Rejected	Unresolved
3 prongs	718	587	120	11	2668	2394	165	109
4 prongs	897	545	264	88	2090	1764	213	113
5 prongs	--	--	--	--	8	0	0	8
6 prongs	0	0	0	0	8	0	0	8
1 prong + "V"	--	--	--	--	518	383	117	18
2 prongs + "V"	962	798	137	27	1106	829	237	40

Table II. Distribution of rejected events in hydrogen and deuterium.

Reject type	Hydrogen			Deuterium			
	3 prong	4 prong	2 prong + "V"	3 prong	4 prong	1 prong + "V"	2 prong + "V"
False event	28	10	17	80	66	42	84
Not measurable	15	5	11	7	8	0	6
Non beam track	66	231	95	43	28	8	16
No fit	3	5	5	28	98	2	3
0 constraint	0	6	0	5	10	2	2
Outside fiducial volume	8	7	9	2	3	34	76
Outside decay fiducial volume	--	--	0	--	--	29	50

Table III. Hydrogen data:
number of accepted events in each reaction; cross sections.

Reaction	Event count	Corrected number of events	Cross section (mb)
$K^+p \to K^o p\pi^+$, $K^o \to \pi^+\pi^-$	766	789±40	
$\to K^o p\pi^+$, all K^o decays		2307±122	5.0±0.4
$K^+p \to K^+ p\pi^+\pi^-$	171	172±19	0.38±0.05
$\to K^o p\pi^+\pi^o$, $K^o \to \pi^+\pi^-$	52	52±10	
$\to K^o p\pi^+\pi^o$, all K^o decays		152±30	0.33±0.07
$\to K^o n\pi^+\pi^-$, $K^o \to \pi^+\pi^-$	13	13±5	
$\to K^o n\pi^+\pi^-$, all K^o decays		38±15	0.08±0.03
$K^+p \to K^+ p\pi^+\pi^-\pi^o$	4	$4^{+4.5}_{-2.5}$	$0.009^{+0.010}_{-0.005}$
$\to K^o p\pi^+\pi^+\pi^-$	1	3^{+7}_{-2}	$0.006^{+0.015}_{-0.004}$
$K^+ \to \pi^+\pi^+\pi^-$	587	590±34	
$\pi^+p \to \pi^+ p\pi^+\pi^-$	284		
$\to \pi^+ p\pi^+\pi^-\pi^o$	48		
$\to \pi^+ n\pi^+\pi^+\pi^-$	4		
$pp \to \pi^+\pi^- pp$	1		

Table IVa. Deuterium data: 3 and 4 prong accepted events by reaction, including ambiguities.

Reaction	Number of accepted events
$K^+d \to K^+\pi^-pp$	707
$\to K^+\pi^-pp\pi^o$	73
$\to K^+\pi^+\pi^-pn$	141
$\to \pi^+\pi^-ppK^o$	89
$\pi^+d \to \pi^+\pi^-pp$	842
$\to \pi^+\pi^-pp\pi^o$	517
$\to \pi^+\pi^+\pi^-pn$	522
$K^+d \to K^+\pi^-pp$ or $K^+\pi^-pp\pi^o$	7
$\to K^+\pi^-pp$ or $K^+\pi^-pp\pi^o$ or $\pi^+d \to \pi^+\pi^-pp$	2
$\to K^+\pi^-pp$ or $K^+\pi^-pp\pi^o$ or $\pi^+d \to \pi^+\pi^-pp$ or $\pi^+\pi^-pp\pi^o$	9
$\to K^+\pi^-pp$ or $K^+\pi^-pp\pi^o$ or $\pi^+d \to \pi^+\pi^-pp\pi^o$	2
$\to K^+\pi^-pp$ or $\pi^+d \to \pi^+\pi^-pp$	442
$\to K^+\pi^-pp$ or $\pi^+d \to \pi^+\pi^-pp$ or $\pi^+\pi^-pp\pi^o$	135
$\to K^+\pi^-pp$ or $\pi^+d \to \pi^+\pi^-pp$ or $pd \to p\pi^-pp$	1
$\to K^+\pi^-pp$ or $\pi^+d \to \pi^+\pi^-pp\pi^o$	28
$\to K^+\pi^-pp\pi^o$ or $\pi^+d \to \pi^+\pi^-pp$	1
$\to K^+\pi^-pp\pi^o$ or $\pi^+d \to \pi^+\pi^-pp$ or $\pi^+\pi^-pp\pi^o$	1
$\to K^+\pi^-pp\pi^o$ or $\pi^+d \to \pi^+\pi^-pp\pi^o$	9
$\to K^+\pi^-pp\pi^o$ (two configurations)	1
$\to K^+\pi^-pp\pi^o$ or $\pi^+\pi^-ppK^o$	1
$\to \pi^+\pi^-ppK^o$ or $\pi^+d \to \pi^+\pi^-pp$	1
$\to \pi^+\pi^-ppK^o$ or $\pi^+d \to \pi^+\pi^-pp$ or $\pi^+\pi^-pp\pi^o$	2
$\to \pi^+\pi^-ppK^o$ or $\pi^+d \to \pi^+\pi^-pp\pi^o$	113
$\to \pi^+\pi^-ppK^o$ or $\pi^+d \to \pi^+\pi^+\pi^-pn$	1
$\to K^+\pi^+\pi^-pn$ or $\pi^+d \to \pi^+\pi^-pp$ or $\pi^+\pi^+\pi^-pn$	1
$\to K^+\pi^+\pi^-pn$ or $\pi^+d \to \pi^+\pi^+\pi^-pn$	40
$\to K^+\pi^+\pi^-pn$ or $\pi^+d \to \pi^+\pi^-pp\pi^o$	4
$\pi^+d \to \pi^+\pi^-pp$ or $\pi^+\pi^-pp\pi^o$	76
$\to \pi^+\pi^-pp\pi^o$ or $\pi^+\pi^+\pi^-pn$	2
$pd \to p\pi^-pp$	21
$K^+d \to K^+\pi^+\pi^-d$	4
$\to \pi^+\pi^+\pi^-dK^o$	3

Table IVb. Deuterium data:
accepted 1 and 2 prong vee events by reaction; taus.

Reaction	Number of events ($K^o \to \pi^+\pi^-$)	Corrected number of events
$K^+d \to K^opp$	245	823
$\to K^opp\pi^o$	241	777
$\to K^o\pi^+pn$	566	1847
$\to K^opp(\pi^o\pi^o)$	10	32
$\to K^o\pi^+p(n\pi^o)$	48	153
$\to K^o\pi^+\pi^+(nn)$	11	35
$\to K^o\pi^+d$	12	42
$\to K^o\pi^+d\pi^o$	9	29
$\to K^o_2pp$ candidates	8 (K^opp vertex fit, no K^o_1 fit)	
Background K^o_1's	11	
$\Lambda \to p\pi^-$	51	
$K^+ \to \pi^+\pi^+\pi^-$	372	

Table Va. Effects of the beam window cut.

Reaction	Total	In window	Out window	In/Out
$K^+d \rightarrow K^+\pi^-pp$[a]	744	566	178	3.18
$K^+d \rightarrow K^+\pi^-pp$[a] or $\pi^+d \rightarrow \pi^+\pi^-pp$[a]	589	348	241	1.44
$\pi^+d \rightarrow \pi^+\pi^-pp$[a]	924	186	738	0.252
Taus and K_1^o events	1514	1142	372	3.07
"Unambiguous" 1 constraint K fits	303	194	109	1.78
"Unambiguous" 1 constraint π fits	1027	264	763	0.346

[a]Includes 1 constraint ambiguities.

Table Vb. 12 misidentified taus in the $\pi^+d \rightarrow \pi^+\pi^+\pi^-pn$ events.

Event	$m(\pi^+\pi^+\pi^-)$ (MeV)	Spectator	Spectator momentum (MeV/c)	Target momentum (MeV/c)
1.	540.4	p	0.5	92.6
2.	741.0	n	65.6	153.9
3.	490.3	p	0.3	83.4
4.	493.0	p	0.4	81.7
5.	494.8	p	0.1	101.1
6.	453.4	p	0.1	68.1
7.	489.6	p	4.2	84.1
8.	653.6	n	87.5	121.4
9.	532.1	p	0.1	135.2
10.	492.6	p	0.1	82.3
11.	496.4	p	0.3	82.3
12.	492.8	p	0.5	87.5
13.	684.4	n	89.1	132.2
14.	489.4	p	2.6	80.1
15.	498.9	p	0.7	83.4
16.	482.3	p	0.0	106.3
17.	493.4	p	0.5	83.7
18.	700.6	n	146.5	146.7
19.	495.8	p	0.0	87.9

Table VI. Deuterium cross sections.

Reaction	σ (mb)	Comments
$K^+d \rightarrow KNN \rightarrow [K^+pn]$	14.88±0.87	
$\rightarrow K^opp$	2.57±0.21	
$\rightarrow KNN\pi \rightarrow [K^+nn\pi^+]$	1.23±0.19	Obtained by interpolating hydrogen data and using empirical shielding correction. Used to obtain σ_c.
$\rightarrow K^opn\pi^+$	5.88±0.39	
$\rightarrow K^+pp\pi^-$	3.76±0.26	Obtained through use of beam window.
$\rightarrow [K^+pn\pi^o]$	3.01±0.33	Obtained by subtraction of other σ's from σ(KNNπ).
$\rightarrow K^opp\pi^o$	2.42±0.20	
$\rightarrow KNN\pi\pi \rightarrow K^onn\pi^+\pi^+$	0.11±0.04	Missing mass.
$\rightarrow K^+pn\pi^+\pi^-$	0.52±0.09	Beam window $\frac{in}{out}$ K and π ratios.
$\rightarrow K^opp\pi^+\pi^-$	0.27±0.05	Rescanned for "V"'s.
$\rightarrow [K^+nn\pi^+\pi^o]$		
$\rightarrow K^opn\pi^+\pi^o$	0.48±0.07	Missing mass.
$\rightarrow K^+pp\pi^-\pi^o$	0.37±0.07	Beam window $\frac{in}{out}$ K and π ratios.
$\rightarrow [K^+pn\pi^o\pi^o]$		
$\rightarrow K^opp\pi^o\pi^o$	0.10±0.04	Missing mass.
$K^+d \rightarrow KNN$	17.55±0.84	
$\rightarrow KNN\pi$	16.30±0.76	
$\rightarrow KNN\pi\pi$	2.20±0.36	
($KNN\pi\pi$ observed)	1.86±0.15	
$K^o\pi^+p(n)$	4.37±0.32	Components of $K^opn\pi^+$
$K^o\pi^+n(p)$	1.39±0.14	
$K^o\pi^+d$	0.13±0.04	
$K^+\pi^op(n)$	1.73±0.27	Components of $K^+pn\pi^o$. Obtained $\sigma(K^*\pi^op) = 1.97\pm0.23$ by interpolating hydrogen data. Used to obtain $\sigma(I = 0)$. $\sigma(K^+\pi^on(p))$ contains $\sigma(K^+\pi^od)$.
$K^+\pi^on(p)$	1.28±0.42	
$K^+\pi^od$		
$K^+\pi^+\pi^-p(n)$	0.35±0.07	Components of $K^+pn\pi^+\pi^-$
$K^+\pi^+\pi^-n(p)$	0.16±0.05	
$K^+\pi^+\pi^-d$	0.01±0.01	

Table VII. K^+n cross sections for single and double pion production reactions; cross section for single pion production in the $I = 0$ channel.

Reaction	σ (mb)	Comments
$K^+n \rightarrow K^o\pi^+n$	1.58±0.16	
$\rightarrow [K^+\pi^on]$	1.46±0.50	Obtained by scaling $\sigma(K^+\pi^on(p))$ by empirical shielding correction.
$\rightarrow K^+\pi^-p$	4.29±0.53	
$\rightarrow K^o\pi^op$	2.76±0.36	
$\rightarrow K^+\pi^+\pi^-n$	0.18±0.06	
$\rightarrow K^o\pi^+\pi^-p$	0.31±0.07	
$\rightarrow K^o\pi^+\pi^on$		Missing mass events. Cannot separate n(p) from p(n).
$\rightarrow K^+\pi^-\pi^op$	0.42±0.09	
$\rightarrow [K^+\pi^o\pi^on]$		
$\rightarrow K^o\pi^o\pi^op$	0.11±0.05	
$\sigma_{KN\pi}(I = 0) =$	11.70±1.79	

Table VIII. Resonance cross sections.

Reaction	$\sigma(K\Delta)$	$\sigma(K^*N)$	$\sigma(K^*-\Delta$ Int.)	σ(bkgrnd.)	φ(deg.)	χ^2/d.o.f.
$K^+p \rightarrow K^o\pi^+p$	2.05±0.34	2.15±0.35	0.55±0.30	0.25±0.30	29±9	16/16
$K^+d \rightarrow K^o\pi^+p(n)$	1.80±0.40	1.07±0.30	0.62±0.28	0.88±0.29	14±10	24.3/14
$K^+d \rightarrow K^o\pi^+n(p)$	0.20±0.04	0.69±0.34	0.01±0.31	0.50±0.32	77±30	2.7/4
$K^+d \rightarrow K^+\pi^-p(p)$	0.20±0.04	2.44±0.40	0.15±0.23	0.98±0.26	49±14	46/32
$K^+d \rightarrow K^o\pi^op(p)$	0.40±0.09	1.16±0.31	0.16±0.32	0.71±0.47	8±26	7.1/11

Table IX. Resonance cross sections in K^+n reactions; cross section for K^* production in the $I = 0$ channel.

Reaction	σ (mb)	Reaction	σ (mb)
$K^+n \rightarrow K^{*+}n$ $\hookrightarrow K^o\pi^+$	0.79±0.40	$K^+n \rightarrow K^o\Delta^+$ $\hookrightarrow \pi^+n$	0.23±0.05
$\rightarrow K^{*o}p$ $\hookrightarrow K^+\pi^-$	2.78±0.54	$\rightarrow K^+\Delta^o$ $\hookrightarrow \pi^-p$	0.23±0.05
$\rightarrow K^{*o}p$ $\hookrightarrow K^o\pi^o$	1.32±0.37	$\rightarrow K^o\Delta^+$ $\hookrightarrow \pi^op$	0.46±0.11

$$\sigma_{I=0}(K^*) = 7.49\pm2.09$$

Table X. K^* and Δ density matrix elements for the reaction $K^+p \rightarrow K^{*0}\Delta^{++} \rightarrow K^+p\pi^+\pi^-$.

	K^*			Δ		
Momentum (GeV/c)	ρ_{00}	$\rho_{1,-1}$	Re ρ_{10}	ρ_{33}	Re $\rho_{3,-1}$	Re ρ_{31}
1.367	0.23±0.10	-0.14±0.10	-0.01±0.06	0.12±0.08	0.17±0.06	0.04±0.07
1.585	0.43±0.06	-0.01±0.05	-0.06±0.04	0.23±0.04	-0.04±0.04	0.02±0.05
1.96[a]	≈ 0.8			≈ 0.12		
3.0[b]	0.76±0.05	-0.03±0.03	-0.13±0.02	0.01±0.04	-0.035±0.035	0.07±0.02
Predictions for pion exchange	1	0	0	0	0	0

a. We give approximate values deduced from angular distributions given in Ref. 34.

b. Reference 35.

Table XI. Density matrix elements for K^* production in K^+n reactions.

-t interval $(GeV/c)^2$		$K^+n \to K^{*o}p$, $K^{*o} \to K^+\pi^-$	$K^+n \to K^{*o}p$, $K^{*o} \to K^o\pi^o$	$K^+n \to K^{*+}n$, $K^{*+} \to K^o\pi^+$	OME predictions: Pseudoscalar exchange	OME predictions: Unnatural parity with $J \geq 1$	OME predictions: Natural parity exchange
From	To						
			ρ_{00}				
All		0.51±0.04	0.56±0.08	0.44±0.09	1	--	0
0	0.2	0.57±0.05	0.72±0.11	0.78±0.15			
0.2	0.4	0.46±0.07	0.37±0.13	0.51±0.17			
0.4	1.4	0.41±0.07	0.49±0.17	0.15±0.12			
			$\rho_{1,-1}$				
All		0.06±0.03	-0.02±0.06	0.10±0.08	0	--	--
0	0.2	0.07±0.04	0.09±0.08	-0.05±0.10			
0.2	0.4	0.01±0.06	-0.12±0.10	-0.11±0.14			
0.4	1.4	0.09±0.06	-0.09±0.13	0.39±0.12			
			Re ρ_{10}				
All		-0.15±0.02	-0.12±0.05	-0.15±0.06	0	--	0
0	0.2	-0.14±0.03	-0.14±0.06	-0.38±0.10			
0.2	0.4	-0.21±0.04	-0.19±0.08	0.11±0.15			
0.4	1.4	-0.11±0.04	0.01±0.10	-0.09±0.07			

Table XII

Ratio	Prediction	Experimental result 1)	Experimental result 2)
$\frac{\sigma(K^+p \rightarrow K^{*+}p)}{\sigma(K^+n \rightarrow K^{*+}n)}$	$\frac{2}{1}$	2.7±0.54	2.1±0.45
$\frac{\sigma(K^+n \rightarrow K^{*o}p)}{\sigma(K^+p \rightarrow K^{*+}p)}$	$\frac{1.5}{1}$	1.3±0.27	1.6±0.34
$\frac{\sigma_o(KN \rightarrow K^*N)}{\sigma_1(KN \rightarrow K^*N)}$	$\frac{3}{1}$	2.3±0.70	2.9±0.87

Experimental result 1) was calculated using only the hydrogen data for $\sigma(K^+p \rightarrow K^{*+}p)$. Experimental result 2) used the average of the hydrogen data and the deuterium data for this cross section.

APPENDIX A

The Method of Shmushkevich

The ispin relations (1) and (2) are special cases of a general observation due to I. Shmushkevich which seems at first glance to be so obvious as to be trivial but which provides an amazingly simple method of obtaining relative rates in cases, like the deuterium data in this experiment, where Clebsch-Gordan procedures are much more involved and susceptible to error.

The observation is that since the strong interactions conserve ispin, if the initial state is unpolarized in ispin space, the final state will also be unpolarized in I space. That means that within each final state multiplet all I_z states will be equally populated. In the case of K^+d interactions, the initial state is to be considered as K^+d and K^od equally populated. For pion production the final state will contain equal numbers of K^+'s and K^o's, equal numbers of protons and neutrons, and equal numbers of π^+'s, π^-'s and π^o's. If we write out all possible reactions for single pion production and relate their cross sections according to these requirements we have

$$
\begin{aligned}
K^+d &\rightarrow K^o pn\pi^+ && \sigma_1 \\
&\rightarrow K^+ nn\pi^+ && \sigma_2 \\
&\rightarrow K^+ pp\pi^- && \sigma_3 \\
&\rightarrow K^o pp\pi^o && \sigma_4 \\
&\rightarrow K^+ pn\pi^o && \sigma_5 \\
K^od &\rightarrow K^o pn\pi^o && \sigma_6 \\
&\rightarrow K^+ nn\pi^o && \sigma_7 \\
&\rightarrow K^o nn\pi^+ && \sigma_8 \\
&\rightarrow K^o pp\pi^- && \sigma_9 \\
&\rightarrow K^+ pn\pi^- && \sigma_{10}
\end{aligned}
$$

Charge symmetry requires that

$$\sigma_1 = \sigma_{10}$$
$$\sigma_2 = \sigma_9$$
$$\sigma_3 = \sigma_8$$
$$\sigma_4 = \sigma_7$$
$$\sigma_5 = \sigma_6$$

and this guarantees that the final state doublets, K^+ and K^o and p and n, are equally populated. For the triplet π^+, π^-, π^o it is required that

$$\sigma_1 + \sigma_2 + \sigma_8 = \sigma_3 + \sigma_9 + \sigma_{10} = \sigma_4 + \sigma_5 + \sigma_6 + \sigma_7$$

which because of charge symmetry we can rewrite as

$$\sigma_1 + \sigma_2 + \sigma_3 = 2(\sigma_4 + \sigma_5) \quad .$$

But $\sigma_1 + \sigma_2 + \sigma_3 = \sigma_c$ and $\sigma_4 + \sigma_5 = \sigma_o$.

Hence $\sigma_c = 2\sigma_o$.

It is apparent that we did not need to write down the K^od reactions or even the K^+d reactions for that matter. Because the initial state is a doublet, the doublets in the final state will pair up according to charge symmetry and any information about relative rates within the set of states from one member of the initial state doublet can come only from the triplet in the final state. The number of π^+'s overall is equal to the number of charged pions in either set and the same is true of course for the π^-'s. The number of π^o's overall is twice the number in either set. Thus we could write $\sigma_c = 2\sigma_o$ immediately.

For double pion production,

$$\text{no. of } \pi^+\text{'s} = \text{no. of } \pi^-\text{'s} = 2\sigma_{cc} + \sigma_{co}$$
$$\text{no. of } \pi^o\text{'s} = 4\sigma_{oo} + 2\sigma_{co} \quad .$$

Then $2\sigma_{cc} + \sigma_{co} = 4\sigma_{oo} + 2\sigma_{co}$

or $2\sigma_{cc} = 4\sigma_{oo} + \sigma_{co}$.

For triple pion production,

$$\text{no. of } \pi^{+}\text{'s} = \text{no. of } \pi^{-}\text{'s} = 3\sigma_{ccc} + 2\sigma_{cco} + \sigma_{coo}$$

$$\text{no. of } \pi^{o}\text{'s} = 6\sigma_{ooo} + 4\sigma_{coo} + 2\sigma_{cco} \ .$$

Then $3\sigma_{ccc} + 2\sigma_{cco} + \sigma_{coo} = 6\sigma_{ooo} + 4\sigma_{coo} + 2\sigma_{cco}$

or $\sigma_{ccc} = 2\sigma_{ooo} + \sigma_{coo}$

with no information about σ_{cco} which simply reflects the fact that any rate for a state containing $\pi^{+}\pi^{-}\pi^{o}$ will satisfy the equal population requirement.

APPENDIX B

The πρω Exchange Model

$K^+N \to K^*N$ reactions can be listed with their s and t channel amplitudes as follows:

Reaction	s channel	t channel
$K^+p \to K^{*+}p$	A_1	$(a_1 - a_0)/2$
$K^+n \to K^{*+}n$	$(A_1 + A_0)/2$	$-(a_1 + a_0)/2$
$K^+n \to K^{*o}p$	$(A_1 - A_0)/2$	a_1

The s channel amplitudes in terms of the t channel amplitudes are

$$A_0 = -(a_0 + 3a_1)/2$$
$$A_1 = -(a_0 - a_1)/2 \ .$$

We now assume that the dominant processes are exchange of low mass $I = 0$ and $I = 1$ mesons, in particular η and ω and π and ρ. Then

$$A_0 \approx -[(\eta + \omega) + 3(\pi + \rho)]/2 \qquad (B1)$$
$$A_1 \approx -[(\eta + \omega) - (\pi + \rho)]/2 \ . \qquad (B2)$$

The angular distributions seen in this experiment indicate both pseudoscalar and vector exchange. If one assumes further that only one meson of each kind is involved, the possible pairs are $\eta\omega$, $\pi\rho$, $\eta\rho$, and $\pi\omega$. Equations (B1) and (B2) then make certain predictions for each pair. For $\eta\omega$, $A_0 = A_1$ and the angular distributions for the K^* in the $I = 1$ channel and in the $I = 0$ channel should be the same. Clearly they are not (Figs. 24, 26, 27, and 35). The same observations apply to the $\pi\rho$ pair which would give $A_0 = -3A_1$. For $\eta\rho$, there would be much more vector exchange in A_0 than in A_1. The experimental observation is just the opposite; there is much more pseudoscalar exchange in A_0 than in A_1. Thus the last pair, $\pi\omega$, which accounts for this, is the candidate.

If they were the only exchanged particles however, A_0 and A_1 would have the same amount of vector exchange and thus a_1 would have only pseudoscalar exchange. But as remarked in the text we do see some vector exchange in K^{*o} production. Assuming some ρ exchange will account for this observation. This suggests a possible minimal set of exchanges, π, ω, ρ such that

$$A_0 \approx -\,[\omega + 3(\pi + \rho)]/2 \quad , \quad a_0 \approx \omega$$
$$A_1 \approx -\,[\omega - (\pi + \rho)]/2 \quad , \quad a_1 \approx \pi + \rho \ .$$

The fact that the $I = 0$ channel K^* looks like almost pure pion exchange further suggests that

$$\rho \approx -\frac{\omega}{3} \ .$$

Use of one more experimental observation leads to predictions from this model for the relative rates for various reactions observed in this experiment. Consider

$$\frac{\sigma(K^+p \to K^{*+}p)}{\sigma(K^+n \to K^{*+}n)} = \left|\frac{a_1 - a_0}{a_1 + a_0}\right|^2 = \left|\frac{\pi + \rho - \omega}{\pi + \rho + \omega}\right|^2 = \frac{\left|\pi - \frac{4}{3}\omega\right|^2}{\left|\pi + \frac{2}{3}\omega\right|^2} \ .$$

If one assumes no interference between vector and pseudoscalar exchange processes then

$$\frac{\sigma(K^+p \to K^{*+}p)}{\sigma(K^+n \to K^{*+}n)} = \frac{\pi^2 + \frac{16}{9}\omega^2}{\pi^2 + \frac{4}{9}\omega^2} \ .$$

Experimentally we have $\sim 2{:}1$ for this ratio (if we average the deuterium and hydrogen data to get $\sigma(K^+p \to K^{*o}p)$).

Then

$$\frac{\pi^2 + \frac{16}{9}\omega^2}{\pi^2 + \frac{4}{9}\omega^2} = \frac{2}{1} \ \to \ \omega^2 = \frac{9}{8}\pi^+ \quad \text{and} \quad \rho^2 = \frac{1}{8}\pi^2 \ .$$

Putting this into the model results in the following predictions:

$$\frac{\sigma(K^+n \to K^{*o}p)}{\sigma(K^+p \to K^{*+}p)} = \frac{|a_1|^2}{\left|\frac{a_1 - a_0}{2}\right|^2} = \frac{|\pi + \rho|^2}{\frac{1}{4}|\pi + \rho - \omega|^2} = 4\,\frac{|\pi - \frac{\omega}{3}|^2}{|\pi - \frac{4}{3}\omega|^2}$$

$$= 4\,\frac{(\pi^2 + \frac{\omega^2}{9})}{(\pi^2 + \frac{16}{9}\omega^2)} = 1.5$$

and

$$\frac{\sigma_0(KN \to K^*N)}{\sigma_1(KN \to K^*N)} = \left|\frac{A_0}{A_1}\right|^2 = \left|\frac{a_0 + 3a_1}{a_0 - a_1}\right|^2 = \left|\frac{\omega + 3(\pi + \rho)}{\omega - (\pi + \rho)}\right|^2$$

$$= \left|\frac{3\pi}{\frac{4}{3}\omega - \pi}\right|^2 = \frac{9\pi^2}{\frac{16}{9}\omega^2 + \pi^2} = \frac{3}{1} \quad .$$

Table XII lists these predictions and the experimental results computed two ways, 1) using only the hydrogen data for $K^+p \to K^{*+}p$ and 2) averaging the hydrogen and the deuterium data for this cross section.

In Fig. 38, the hydrogen results are plotted vs beam momentum and compared with $\sigma_0(KN \to K^*N)$. Averaging with the deuterium results will lower the 1585 MeV/c point from 3.2±0.4 to 2.54±0.37 but will also lower the point at 1365 MeV/c and preserve the general shape of the curve.

FOOTNOTES AND REFERENCES

1. V. Cook, D. Keefe, L. T. Kerth, P. G. Murphy, W. A. Wenzel, and T. F. Zipf, in Proceedings of the 1962 International Conference on High-Energy Physics at CERN, p. 364.

2. J. Fisk, H. K. Ticho, D. H. Stork, W. Chinowsky, G. Goldhaber, S. Goldhaber, and T. F. Stubbs, in Proceedings of the 1962 International Conference on High-Energy Physics at CERN, p. 358.

3. R. L. Cool, G. Giacomelli, T. F. Kycia, B. A. Leontic, K. K. Li, A. Lundby, and J. Teiger, Phys. Rev. Letters 17, 102 (1966). R. L. Cool, G. Giacomelli, T. F. Kycia, B. A. Leontic, K. K. Li, A. Lundby, J. Teiger, and C. Wilkin, Phys. Rev. D1, 1887 (1970).

4. D. V. Bugg, R. S. Gilmore, K. M. Knight, D. C. Salter, G. H. Stafford, E. J. N. Wilson, J. D. Davies, J. D. Dowell, P. M. Hattersley, R. J. Homer, A. W. O'Dell, A. A. Carter, R. J. Tapper, and K. F. Riley, Phys. Rev. 168, 1466 (1968).

5. R. W. Bland, M. G. Bowler, J. L. Brown, G. Goldhaber, S. Goldhaber, V. H. Seeger, and G. H. Trilling, Phys. Rev. Letters 18, 1077 (1967).

6. R. W. Bland, Single Pion Production in the K^+p Channel from 860 to 1360 MeV/c (Ph.D. Thesis), UCRL-18131 (1968), unpublished.

7. R. W. Bland, M. G. Bowler, J. L. Brown, J. A. Kadyk, G. Goldhaber, S. Goldhaber, V. H. Seeger, and G. H. Trilling, Nuclear Physics B13, 595 (1969).

8. R. W. Bland, M. G. Bowler, J. L. Brown, G. Goldhaber, S. Goldhaber, J. A. Kadyk, V. H. Seeger, and G. H. Trilling, Nuclear Physics B18, 537 (1970).

9. R. W. Bland, G. Goldhaber, and G. H. Trilling, Physics Letters 29B, 618 (1969).

B. H. Hall, R. W. Bland, G. Goldhaber, and G. H. Trilling, UCRL-19231 (1969).

B. H. Hall, R. W. Bland, G. Goldhaber, and G. H. Trilling, UCRL-19787 (1970).

G. Goldhaber, The Search for Z^*'s, in Hyperon Resonances - 70, ed. by E. C. Fowler (Moore Publishing Co., Durham, North Carolina, 1970).

10. A. A. Hirata, C. G. Wohl, R. W. Bland, G. Goldhaber, B. H. Hall, J. A. Kadyk, V. H. Seeger, and G. H. Trilling, Contribution to the XIVth International Conference on High-Energy Physics, Vienna, August 28-September 6, 1968, UCRL-18322 (1968).

11. A. A. Hirata, C. G. Wohl, G. Goldhaber, and G. H. Trilling, Phys. Rev. Letters 21, 1485 (1968); Errata, Phys. Rev. Letters 21, 1728 (1968).

12. A. A. Hirata, K^+d Interactions from 865 to 1365 MeV/c (Ph.D. Thesis), UCRL-20248 (1970), unpublished.

13. R. B. Bell, R. W. Bland, M. G. Bowler, J. L. Brown, R. P. Ely, S.-Y. Fung, G. Goldhaber, A. A. Hirata, J. A. Kadyk, J. Louie, J. S. Sahouria, V. H. Seeger, W. M. Smart, and G. H. Trilling, in Proceedings of the XIIth International Conference on High-Energy Physics, Dubna, August 5-15, 1964, Vol. 2, p. 546; UCRL-11527 (1964).

14. P. Daronian, A. Daudin, M. A. Jabiol, C. Lewin, C. Kochowski, B. Ghidini, S. Mongelli, and V. Picciarelli, Nuovo Cimento 41A, 503 (1966).

15. S. Dagan, Z. M. Ma, J. W. Chapman, L. R. Fortney, and E. C. Fowler, Phys. Rev. 161, 1384 (1967).

16. As measured and "swum" to the chamber entrance--not as fitted in the event.

17. T. C. Bacon, W. J. Fickinger, D. G. Hill, H. W. K. Hopkins, D. K. Robinson, and E. O. Salant, Phys. Rev. 157, 1263 (1967) give the

value 6.6±0.3 mb at 1.68 BeV/c for $\pi^+ n \rightarrow \pi^+ \pi^- p$ after applying a shielding correction. Their value for $\pi^+ d \rightarrow \pi^+ \pi^- pp$ would then be approximately 10% lower, about 6 mb.

18. N. Barash-Schmidt, A. Barbaro-Galtieri, G. Conforto, L. R. Price, M. Roos, A. H. Rosenfeld, P. Söding, and C. G. Wohl, Review of Particle Properties, Revs. Mod. Phys. 41, 109 (1969), UCRL-8030.

19. Densities were determined by measuring the stopping length of a muon from the two body decay of a pion at rest, $\pi^+ \rightarrow N^+ + \nu$, J. L. Brown, Trilling-Goldhaber Technical Note TN-29 (1964), unpublished.

20. Equations (1) and (2) are independent of the relative importance of the various isospin amplitudes involved in these reactions. They can be laboriously derived in the usual manner using Clebsch-Gordan coefficients but are derived almost instantly using the remarkably simple and elegant method of Shmushkevich. See

a) I. Shmushkevich, Dokl. Akad. Nauk SSSR 103, 235 (1955);

b) N. Dushin and I. Shmushkevich, Dokl. Akad. Nauk SSSR 106, 801 (1956) [translation: Soviet Phys.-Doklady 1, 94 (1956)];

c) G. Pinski, A. J. Macfarlane, and E. C. G. Sudarshan, Phys. Rev. 140B, 1045 (1965);

d) C. G. Wohl, Isospin Analysis of Single Pion Production in K^+N Interactions, Trilling-Goldhaber Group Physics Note TG-160 (1968), unpublished;

e) C. G. Wohl, Linear Relations Between Cross Section or Decay Rates from Isospin Conservation, Trilling-Goldhaber Group Physics Note TG-165 (1969), unpublished;

f) The method is outlined with examples in Appendix A of this thesis.

21. L. R. Price, N. Barash-Schmidt, O. Benary, R. W. Bland, A. H. Rosenfeld, C. G. Wohl, A Compilation of K^+N Reactions, UCRL-20000, p. 27 (1969).

22. W. Slater, D. H. Stork, H. K. Ticho, W. Lee, W. Chinowsky, G. Goldhaber, S. Goldhaber, and T O'Halloran, Phys. Rev. Letters 7, 378 (1961).

23. I. Butterworth, J. L. Brown, G. Goldhaber, S. Goldhaber, A. A. Hirata, J. A. Kadyk, B. M. Schwarzschild, and G. H. Trilling, Phys. Rev. Letters 15, 734 (1965) and unpublished data of the same authors.

24. J. D. Jackson, Nuovo Cimento 34, 1644 (1964).

25. In discussing final states of the form $A + B^* \rightarrow \begin{matrix} A + C + D \\ \hookrightarrow C + D \end{matrix}$ capital letters are used to denote the orbital A-B^* angular momentum state; lower case letters are used to denote the orbital C-D angular momentum state.

26. In his thesis[6] and in a later report,[8] Bland discusses the nature of the background required for such interference.

27. P. Eberhard and M. Pripstein, Phys. Rev. Letters 10, 351 (1963).

28. L. Stodolski and J. J. Sakurai, Phys. Rev. Letters 11, 90 (1963). Details of its application here are to be found in Bland's thesis[6] and in a later summary.[8]

29. J. D. Jackson and H. Pilkuhn, Nuovo Cimento 33, 906 (1964) and 34, 1841E (1964).

30. S. Goldhaber, W. Chinowsky, G. Goldhaber, and T. O'Halloran, Phys. Rev. 142, 913 (1966).

31. A. Bettini, M. Cresti, S. Limenthal, L. Perruzzo, R. Santangelo, D. Locke, D. J. Crennell, W. T. Davies, and P. B. Jones, Phys. Letters 16, 83 (1965); G. B. Chadwick, D. J. Crennell, W. T. Davies, M. Derrick, J. H. Mulvey, P. B. Jones, D. Radojicic, C. A. Wilkinson, A. Bettini, M. Cresti, S. Limenthal, L. Perruzzo, and R. Santangelo, Phys. Letters 6, 309 (1963).

32. S. Goldhaber, J. L. Brown, I. Butterworth, G. Goldhaber, A. A. Hirata, J. A. Kadyk, and G. H. Trilling, Phys. Rev. Letters 15, 737 (1965).

33. G. Goldhaber, W. Chinowsky, S. Goldhaber, W. Lee, and T. O'Halloran, Phys. Letters 6, 62 (1963).

34. W. Chinowsky, G. Goldhaber, S. Goldhaber, W. Lee, and T. O'Halloran, Phys. Rev. Letters 9, 330 (1962).

35. M. Ferro-Luzzi, R. George, Y. Goldschmidt-Clermont, V. P. Henri, B. Jongejans, D. W. G. Leith, G. R. Lynch, F. Muller, and J.-M. Perreau, Nuovo Cimento 39, 417 (1965).

36. N. Schmitz, Proceedings of the 1965 Easter School for Physicists, CERN 65-24, Vol. I.

37. C. Fu, private communication.

38. C. Fu, Resonance Productions in K^+p Interactions at 4.6 GeV/c and 9 GeV/c (Ph.D. Thesis), UCRL-19809 (1970), unpublished.

39. A recent paper by Slater, Rotation of the Symmetry Axis in K-π Scattering, UCLA Preprint (1970), examines this effect (in $K^{*o}\Delta^{++}$ production) in terms of a rotation in the production plane as suggested by Donohue and Högassen in calculations based on the absorption model of Gottfried and Jackson.

40. W. Lee, Charge-Exchange Scattering of Positive K Mesons on Deuterons (Ph.D. Thesis), UCRL-9691 (1961), unpublished.

41. B. M. Schwarzschild, K^+n Charge Exchange and the ρ' Regge Trajectory (Ph.D. Thesis), UCRL-17572 (1967).

42. W. Rarita and B. M. Schwarzschild, Phys. Rev. 162, 1378 (1967).

43. R. J. N. Phillips and W. Rarita, Phys. Rev. 139, B1336 (1965).

44. G. Lynch, Review of the KN and $\bar{K}N$ Total Cross Sections Below 3.5 GeV/c, in Hyperon Resonances - 70, ed. by E. C. Fowler (Moore Publishing Co., Durham, North Carolina, 1970).

45. T. Bowen, P. K. Caldwell, F. Ned Dikmen, E. W. Jenkins, R. M. Kalbach, D. V. Peterson, and A. E. Pifer, in Hyperon Resonances - 70, ed. by E. C. Fowler (Moore Publishing Co., Durham, North Carolina, 1970), p. 3.

46. T. A. Filippas, V. P. Henri, B. Jongejans, M. Krammer, J.-M. Perreau, B. Focardi, A. Minguzzi-Ranzi, L. Monari, G. Saltini, P. Serra, E. Barralet, E. Huffer, and F. Muller, Nuovo Cimento 51A, 1053 (1967).

FIGURE CAPTIONS

Fig. 1. The K25 beam layout.

Fig. 2. Horizontal vs vertical beam track coordinates at the entrance to the chamber.

Fig. 3. Azimuthal angle vs dip angle of beam tracks at chamber entrance.

Fig. 4. Beam track momentum distributions at entrance to chamber; total and in and out of the "window" defined by X, Z, φ, and λ cutoffs.

Fig. 5. $\pi^+ d \rightarrow \pi^+\pi^+\pi^- np$ fits vs the target nucleon momentum.

Fig. 6. Cross sections for single pion final states in $K^+ d$ reactions as a function of beam momentum; also the charge exchange cross section and the observed double pion cross section.

Fig. 7. The $K^+ d$ total cross section as a function of beam momentum (from Cool et al.,[3] Bugg et al.,[4] and Bowen et al.[45]), the KNN, KNNπ, and KNN$\pi\pi$ cross sections and the breakdown of the KNN cross section into $K^o pp$ and $K^+ pn$ cross sections. The $K^+ d \rightarrow K^o pp$ cross sections at low momentum are from Slater et al.[22] The points at 2.26 GeV/c are from Butterworth et al.[23]

Fig. 8. Proton momentum vs neutron momentum in $K^+ d \rightarrow K^o \pi^+ pn$.

Fig. 9. σ's for $K^+ p \rightarrow K^o \pi^+ p$, $K^+ d \rightarrow K^o \pi^+ p(n)$, $K^+ d \rightarrow K^o \pi^+ n(p)$, and $K^+ d \rightarrow K^o \pi^+ d$ as a function of beam momentum.

Fig. 10. The total $K^+ N$ $I = 0$ cross section, $\sigma_o(KN)$ and $\sigma_o(KN\pi)$ as a function of beam momentum. For a discussion of the unfolding of the total $I = 0$ cross section, see Ref. 44.

Fig. 11. Dalitz plots for $K^+ p \rightarrow K^o \pi^+ p$ and $K^+ p(n) \rightarrow K^o \pi^+ p(n)$.

Fig. 12. Dalitz plots for $K^+ n(p) \rightarrow K^+ \pi^- pp$, $K^+ n(p) \rightarrow K^o \pi^o pp$, and $K^+ n(p) \rightarrow K^o \pi^+ n(p)$.

Fig. 13. Definition of $\lambda_{K\pi}$, the pion decay angle in the $K\pi$ c.m. with respect to the direction of the outgoing nucleon.

Fig. 14. Triangle plot for the reaction $K^+p \to K^+p\pi^+\pi^-$ at 1585 MeV/c.

Fig. 15. Mass distributions for the reaction $K^+p \to K^+p\pi^+\pi^-$; the solid curve is the result of the fit described in the text, and the dashed curve is the component attributed to $K^*\Delta$ production alone.

Fig. 16. $\sigma(K^+p \to K\Delta)$ as a function of beam momentum. The curves are the predictions of the Stodolski-Sakurai ρ exchange model with M1 coupling, (a) with $(g^2_{K^+\rho^+K^o}/4\pi)(g^2_{p\rho^+\Delta^{++}}/4\pi) = 450$, and (b) with the product of the squares of the coupling constants = 90. The data at low momenta are from Filippas et al.[46] The data at 1455 MeV/c are from Bettini et al. and Chadwick et al.[31] The data at 1.96 GeV/c are from S. Goldhaber et al.[30]

Fig. 17. Differential cross sections for $K^+p \to K^o\Delta^{++}$ at the five momenta of the K25 experiment. The transformation from cos θ to t is approximate, assuming the experimental Δ-peak mass values, 1.464 $(GeV)^2$ at 1.585 GeV/c. The curves are the predictions of the M1 ρ exchange model.

Fig. 18. Coefficients in the Legendre expansion of the $K\Delta$ production angular distribution, $d\sigma/d\Omega \propto 1 + \sum_{\ell=1} A_\ell P_\ell(\cos\theta)$. The low momentum points are from Ref. 46. The point at 1.455 GeV/c is from Ref. 31.

Fig. 19. Variation of the $K\Delta$ Legendre coefficients with $M^2_{N\pi}$.

Fig. 20. Coordinate system used in describing the Δ decay. The decay angles refer to the direction of the decay nucleon. Here

$$\hat{n} = \frac{\vec{p}_{K\text{-in}} \times \vec{p}_{K\text{-out}}}{|\vec{p}_{K\text{-in}} \times \vec{p}_{K\text{-out}}|} \quad .$$

Fig. 21. Distributions in cos γ for Δ^{++} decay. With the assumption of overall parity conservation, the distributions have been folded about cos $\gamma = 0$. The curves show the predictions of the magnetic dipole model, $W(\cos\gamma) \propto 1 + 3\cos^2\gamma$.

Fig. 22. Distributions in δ for Δ^{++} decay. The magnetic dipole model predicts isotropy as shown by the solid lines. Background interference effects are seen at the two lower momenta. The distributions above the K^* threshold are shown in $\delta_{\text{mod } \pi}$.

Fig. 23. Density matrix elements for the Δ produced in the reaction $K^+p \to K^o\Delta^{++}$. The magnetic dipole model predicts $\rho_{33} = 0.375$, $\text{Re } \rho_{3,-1} = 0.218$ and $\text{Re } \rho_{3,1} = 0$.

Fig. 24. Differential cross sections for $K^+p \to K^{*+}p$. The data at 1.96 GeV/c are from S. Goldhaber et al.[30] The data at 1.455 GeV/c are from Bettini et al. and Chadwick et al.[31]

Fig. 25. Normalized Legendre coefficients for the K^* production angular distribution as a function of beam momentum; $d\sigma/d\Omega \propto 1 + \sum_{\ell=1} A_\ell P_\ell(\cos\theta)$. The data at 1.96 GeV/c are from S. Goldhaber et al.[30] The data at 1.455 GeV/c come from Bettini et al. and Chadwick et al.[31]

Fig. 26. Density matrix elements for K^* decay in the reaction $K^+p \to K^{*+}p$, $K^{*+} \to K^o\pi^+$, as a function of beam momentum. Here $|t|$ is in $(\text{GeV/c})^2$. The data from other experiments come from S. Goldhaber et al.[30] and Bettini et al. and Chadwick et al.[31]

Fig. 27. The K^* decay angular distributions for the reaction $K^+p \to K^{*+}p$, $K^{*+} \to K^o\pi^+$. The curves correspond to the density matrix elements given in Fig. 26.

Fig. 28. Production angular distributions for $K^+p \to K^{*o}\Delta^{++}$. The data at 1.96 GeV/c for this reaction come from G. Goldhaber et al.[33]

Fig. 29. $M^2_{K\pi}$ distributions for $K^+n(p)$ reactions. The curves are the results of the Dalitz plot fitting program described in the text.

Fig. 30. $M^2_{N\pi}$ distributions for $K^+n(p)$ reactions. The curves are the results of the Dalitz plot fitting program described in the text.

Fig. 31. Production and decay angular distributions for K^*'s produced in K^+n reactions at 1585 MeV/c.

Fig. 32. Exchange diagrams for K^+p and K^+n reactions observed in this experiment. The lowest mass exchange particles allowed are indicated.

Fig. 33. Correlation plots in K^* decay at 1585 MeV/c, $\cos\alpha$ vs φ. The distributions in φ have been folded assuming parity conservation in decay and are shown in $\varphi_{\text{mod } \pi}$.

Fig. 34. Correlation plots in K^* decay at 1585 MeV/c, $\cos\alpha$ vs φ. The distributions in φ have been folded in accordance with overall parity conservation which corresponds to the transformation $\varphi \rightarrow -\varphi$.

Fig. 35. Production and decay angular distributions for the K^* produced in the $I = 0$ channel. The distributions of the component reactions are shown scaled as described in the text.

Fig. 36. The differential cross section $d\sigma/dt$ for the K^* produced in the $I = 0$ channel and its density matrix elements as a function of $|t|$.

Fig. 37. Correlation plot for the decay of the K^* produced in the $I = 0$ channel, $\cos\alpha$ vs φ. The φ distribution has been folded according to overall parity conservation, $\varphi \rightarrow -\varphi$.

Fig. 38. $\sigma_{K^*}(I = 1$ channel) and $\sigma_{K^*}(I = 0$ channel) as functions of beam momentum.

Fig. 39. Cross sections for the individual reactions involved in obtaining $\sigma_{K^*}(I = 0$ channel) as functions of beam momentum.

Fig. 40. $d\sigma/dt$ for the reaction $K^+d \rightarrow K^0p(p)$. The dashed curve is the prediction of the unmodified Rarita-Schwarzschild model; the solid curve is the prediction of the model modified as described in the text.

Fig. 41. The cross section for the reaction $K^+d \rightarrow K^0p(p)$ as a function of beam momentum. The dashed curve is the prediction of the unmodified Rarita-Schwarzschild model; the solid curve is the result of the model modified as described in the text.

Fig. 42. The differential cross section for the reaction $K^+d \rightarrow K^0p(p)$ at 1585 MeV/c. The curves are the Legendre polynomial fits to third order to Eq. (21) with R set equal to 0 (no spin flip), ∞ (all spin flip) and 1 (equal amounts of spin flip and nonspin flip). The crosses are the data points, the diamonds are the points with $R = 1$. The extremes $R = 0$ and $R = \infty$ are the small dashes above and below the diamonds. These variations are distinguishable from the data only well above $\cos\theta = 0$. The forwardmost bin was omitted in the fits as described in the text. All charge exchange fits were tried also with a spectator momentum cutoff at 300 MeV/c. This cutoff eliminated 16.7% of the data but no visible difference in the (normalized) fits was detected.

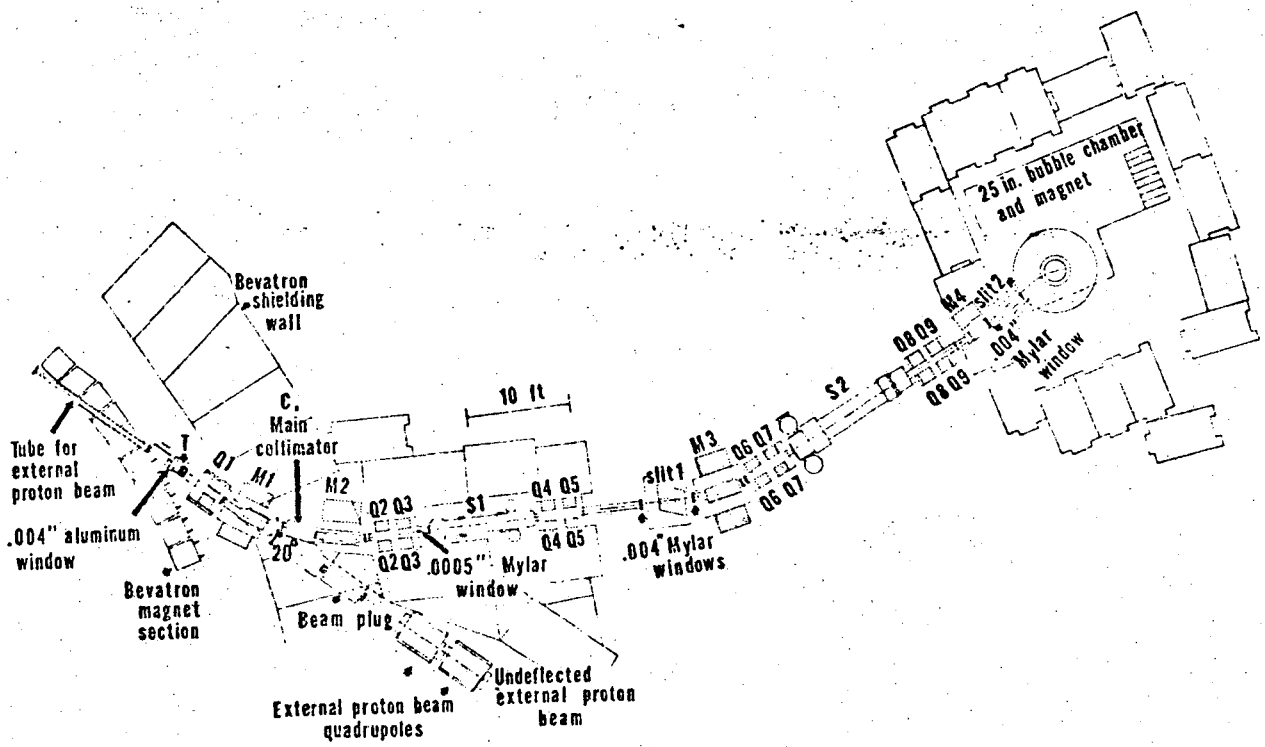
25 in. bubble chamber and magnet
Bevatron shielding wall
Tube for external proton beam
.004" aluminum window
Bevatron magnet section
C. Main collimator
Q1
M1
M2
20°
10 ft
Q2 Q3
S1
Q4 Q5
.0005" Mylar window
Beam plug
External proton beam quadrupoles
Undeflected external proton beam
slit1
M3
Q6 Q7
.004" Mylar windows
S2
Q8 Q9
M4
slit2
.004" Mylar window
MUB-3362

Fig. 1

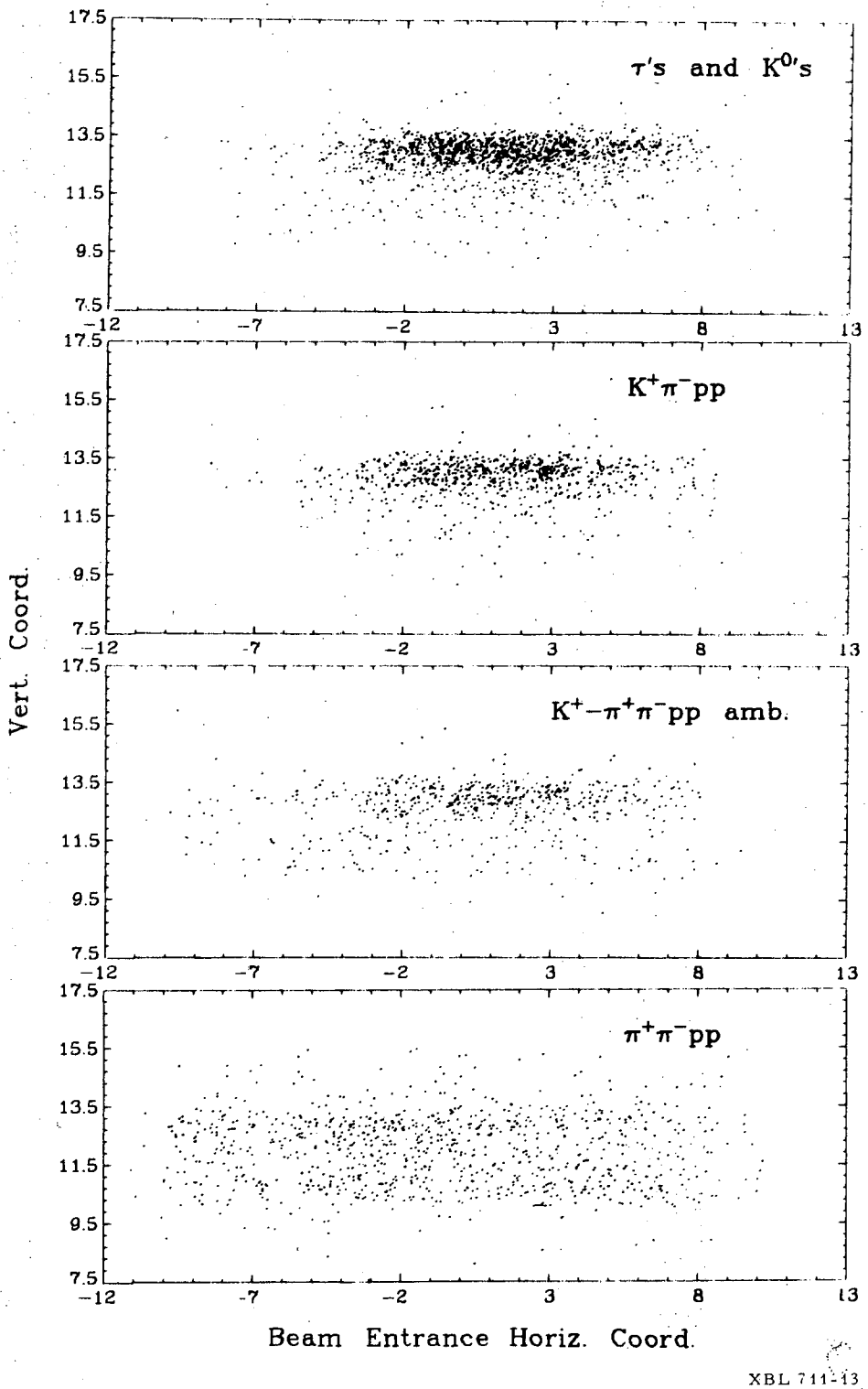
τ's and K⁰'s
K⁺π⁻pp
K⁺−π⁺π⁻pp amb.
π⁺π⁻pp
Vert. Coord.
Beam Entrance Horiz. Coord.
17.5
15.5
13.5
11.5
9.5
7.5
−12
−7
−2
3
8
13
XBL 711-13

Fig. 2

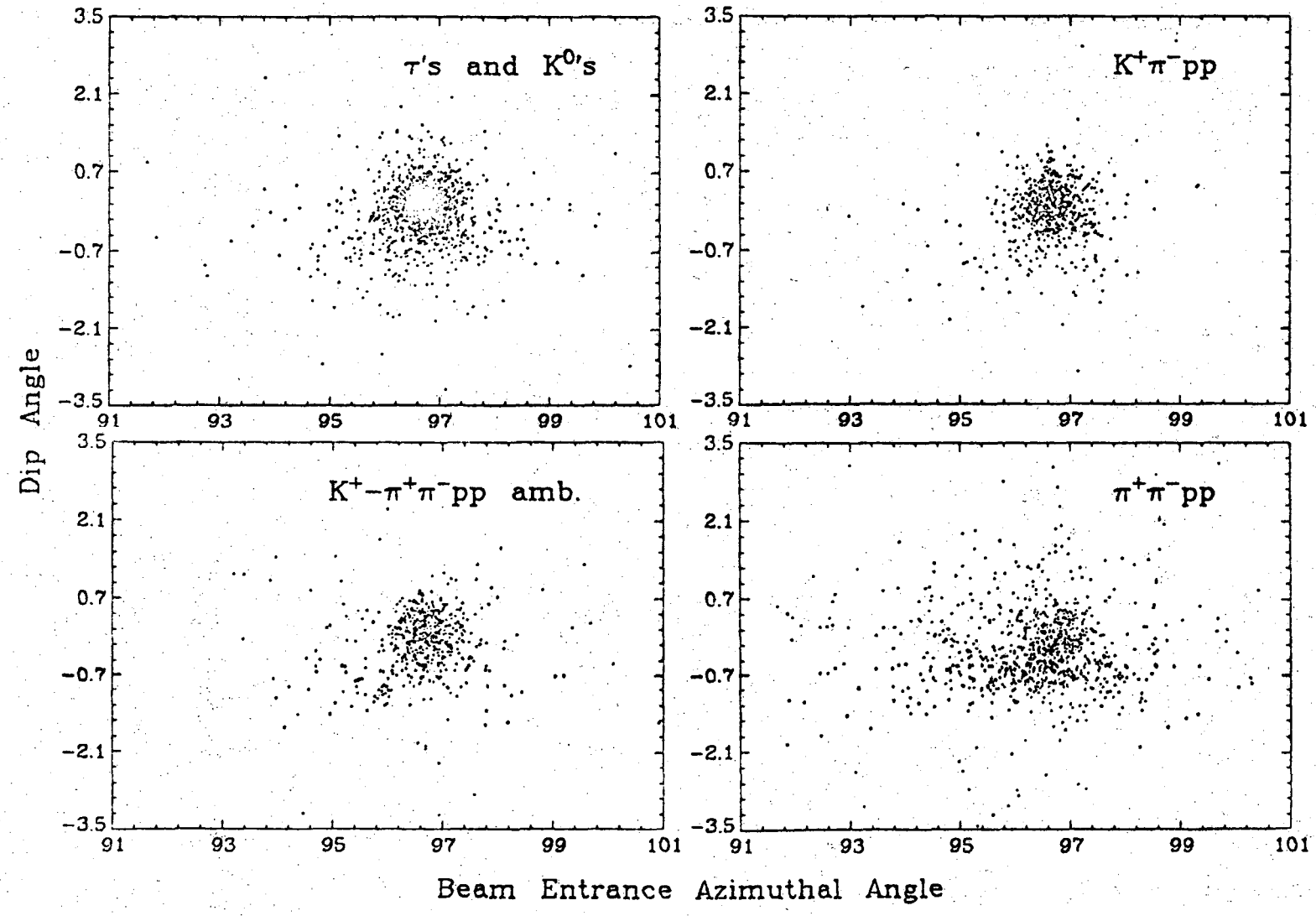

XBL 711-9

Fig. 3

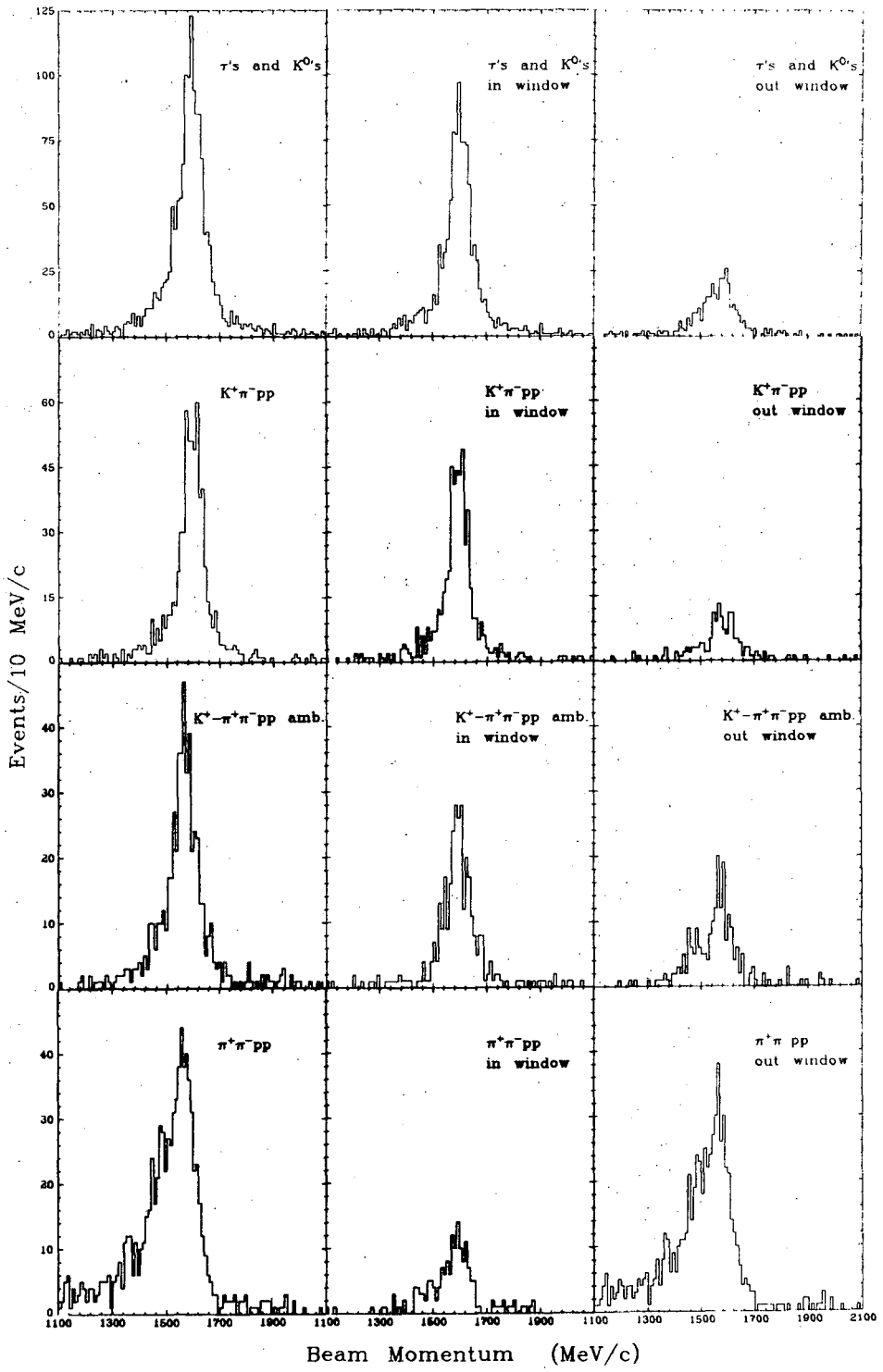
τ's and K⁰'s
τ's and K⁰'s in window
τ's and K⁰'s out window
K⁺π⁻pp
K⁺π⁻pp in window
K⁺π⁻pp out window
K⁺−π⁺π⁻pp amb.
K⁺−π⁺π⁻pp amb. in window
K⁺−π⁺π⁻pp amb. out window
π⁺π⁻pp
π⁺π⁻pp in window
π⁺π pp out window
Events/10 MeV/c
Beam Momentum (MeV/c)
XBL 713-574

Fig. 4

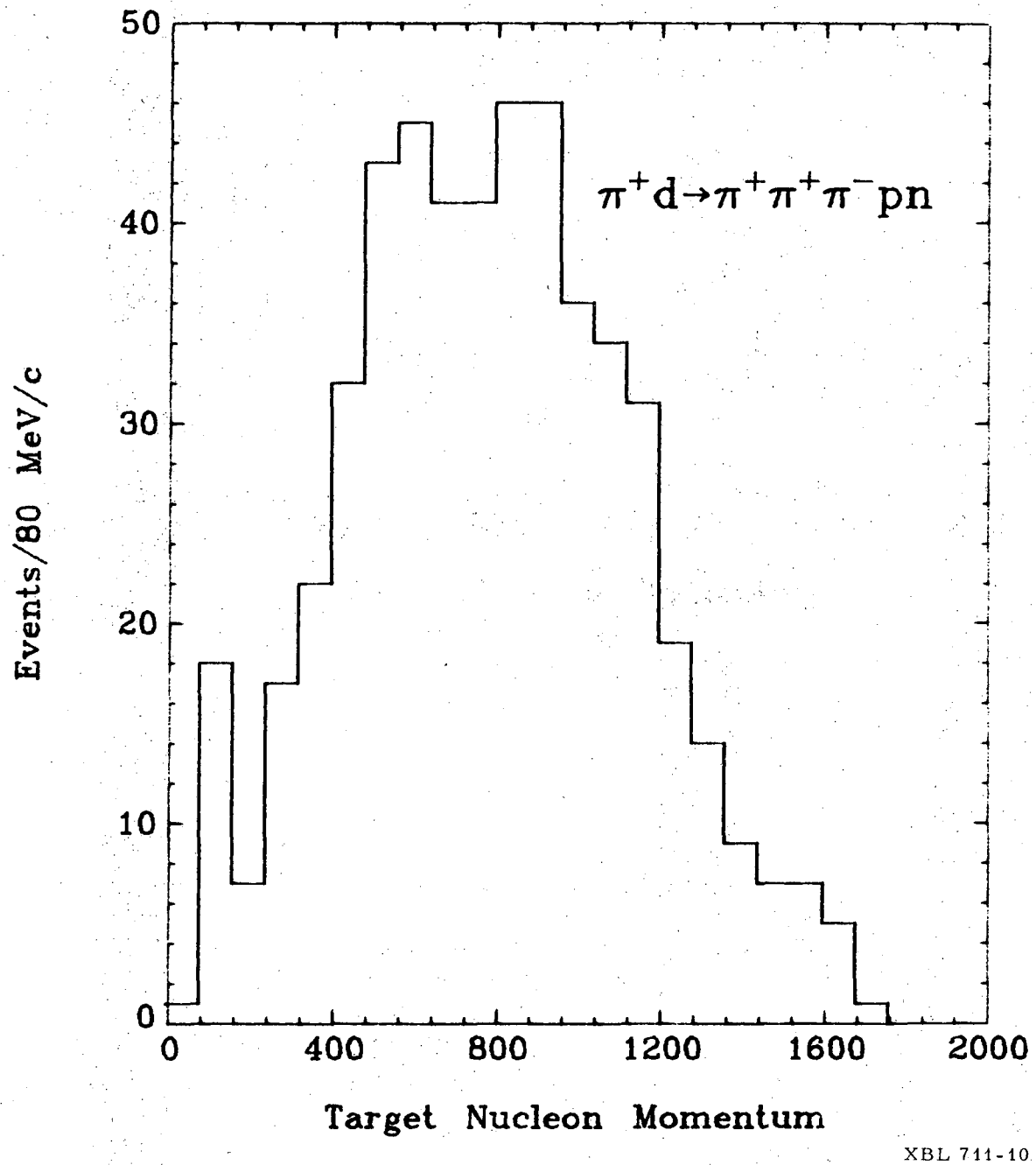
50
40
30
20
10
0
0
400
800
1200
1600
2000
Events/80 MeV/c
Target Nucleon Momentum
$\pi^+ d \rightarrow \pi^+ \pi^+ \pi^- pn$
XBL 711-10

Fig. 5

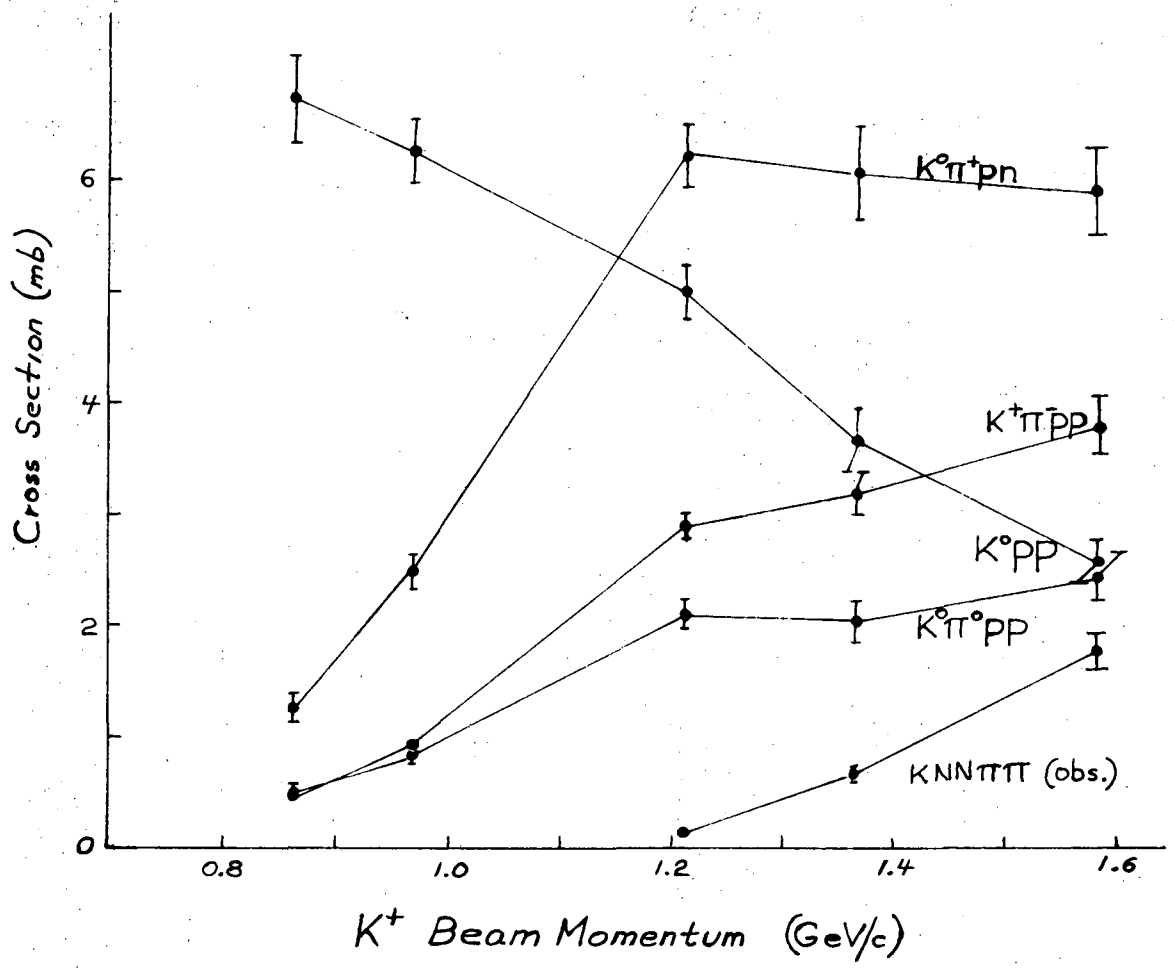

XBL 712-298

Fig. 6

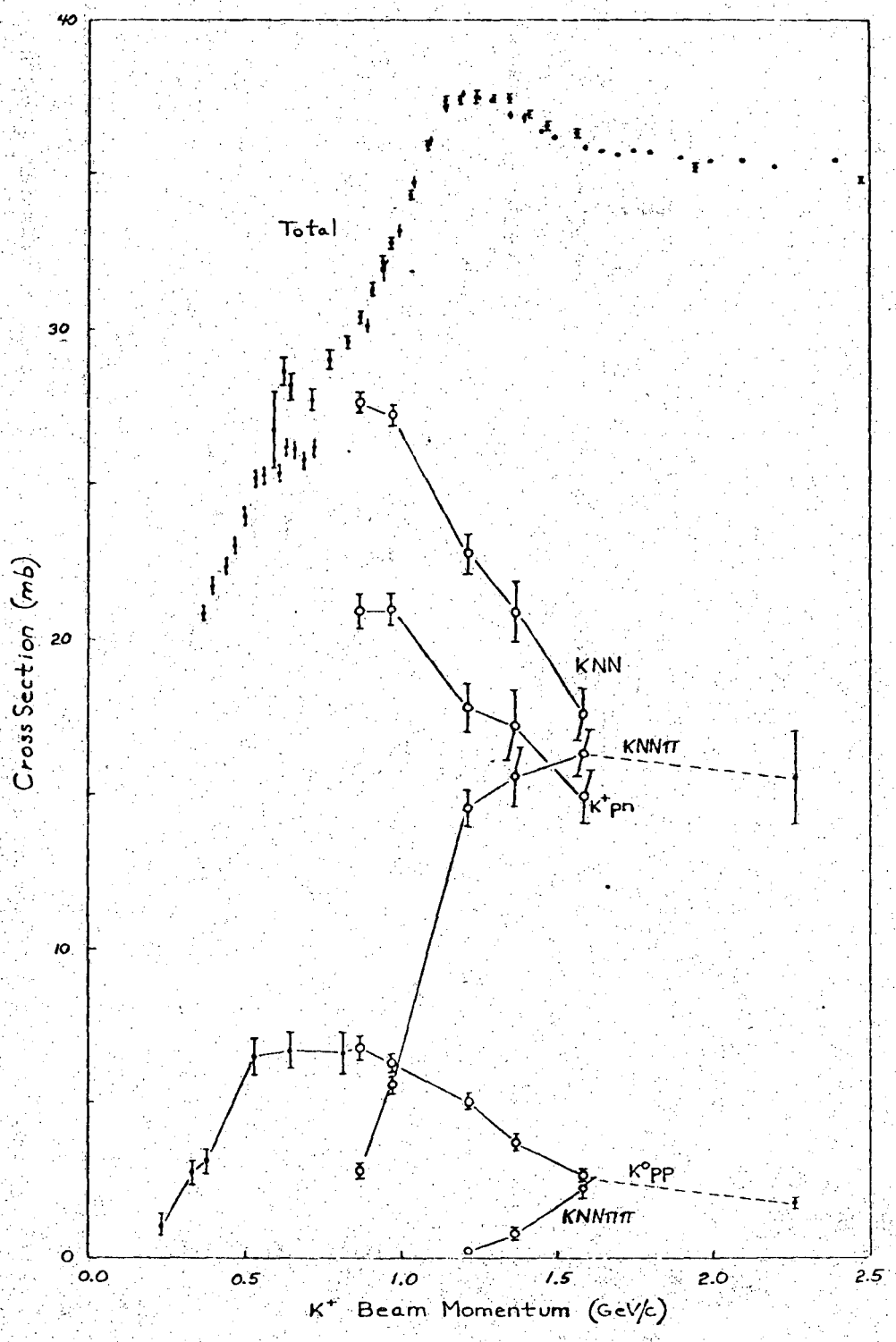

XBL 713-367

Fig. 7

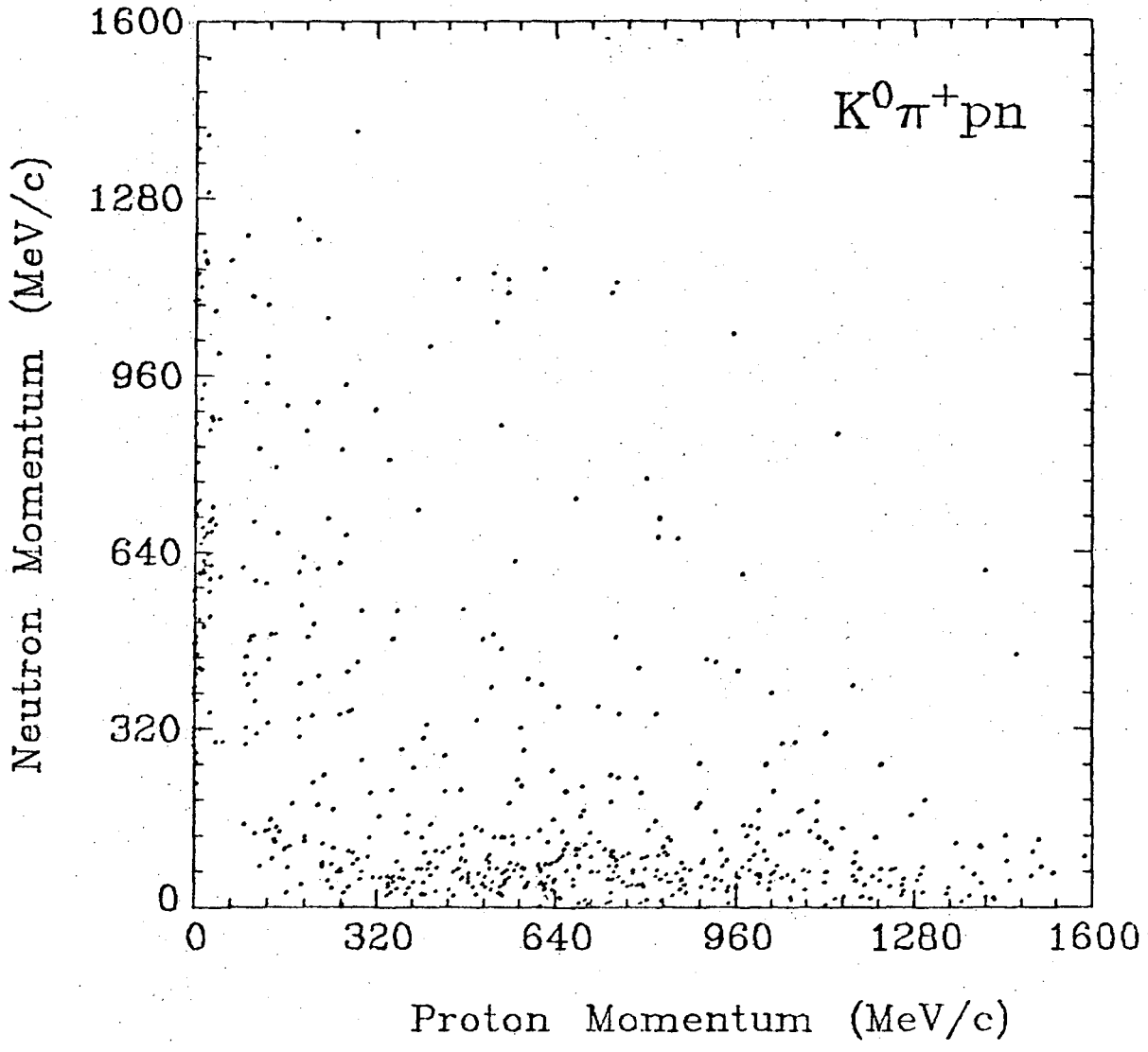
1600
1280
960
640
320
0
Neutron Momentum (MeV/c)
$K^0\pi^+pn$
0
320
640
960
1280
1600
Proton Momentum (MeV/c)
XBL 711-12

Fig. 8

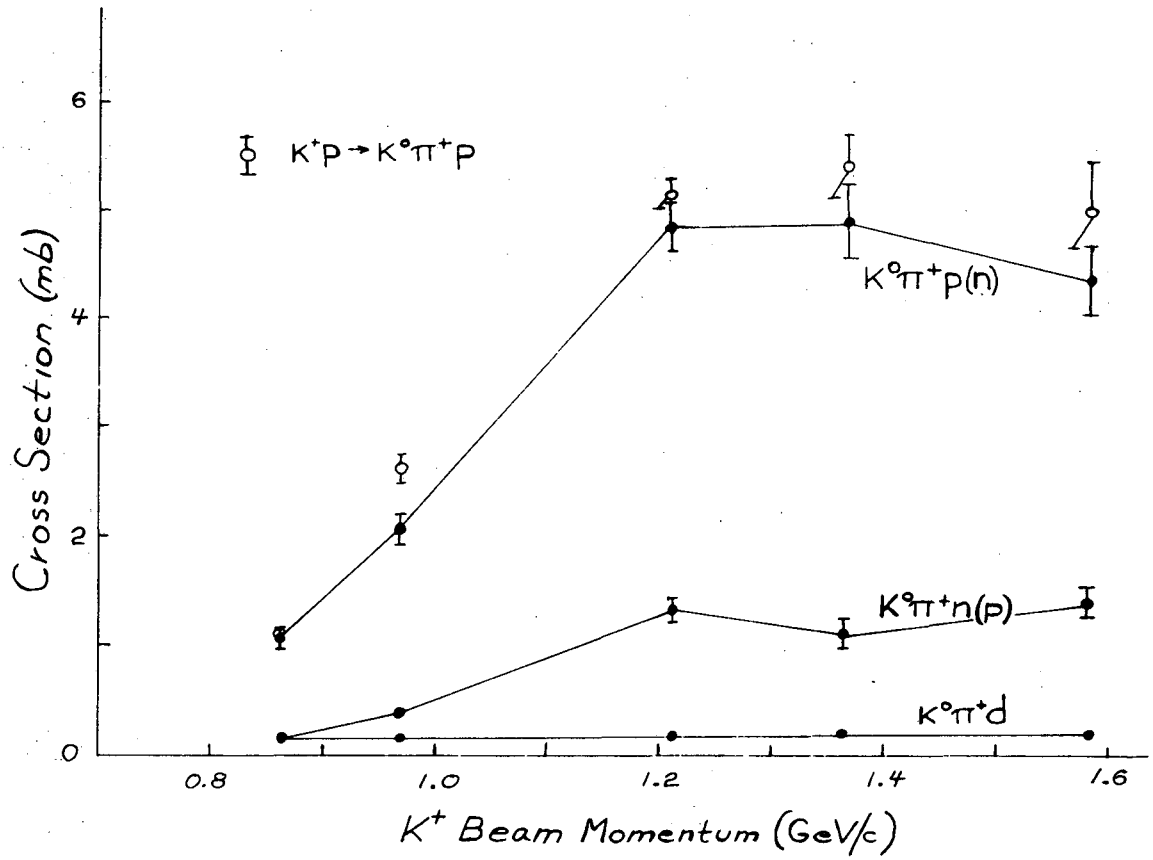

XBL 712-301

Fig. 9

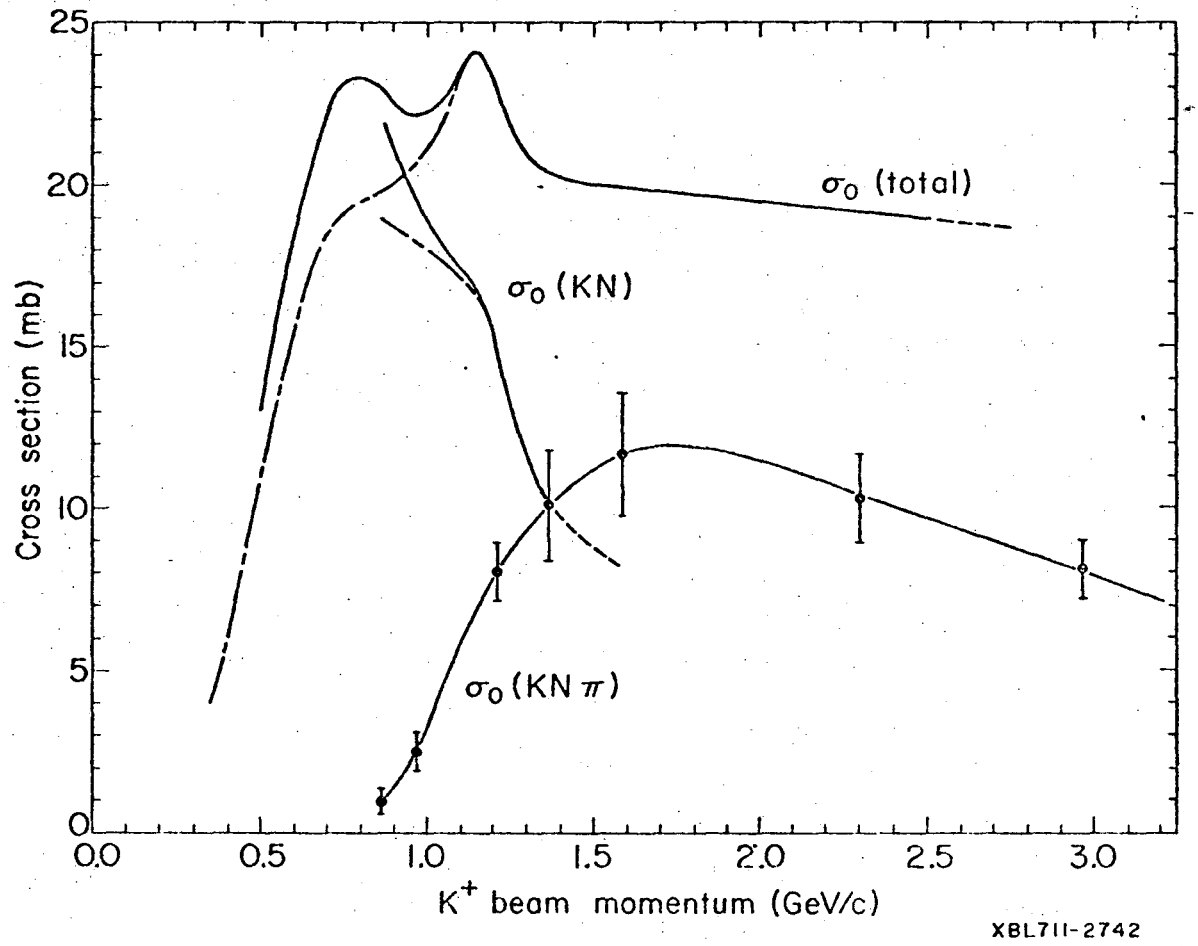
25
20
15
10
5
0
Cross section (mb)
σ_0 (total)
σ_0 (KN)
σ_0 (KN π)
0.0
0.5
1.0
1.5
2.0
2.5
3.0
K^+ beam momentum (GeV/c)
XBL711-2742

Fig. 10

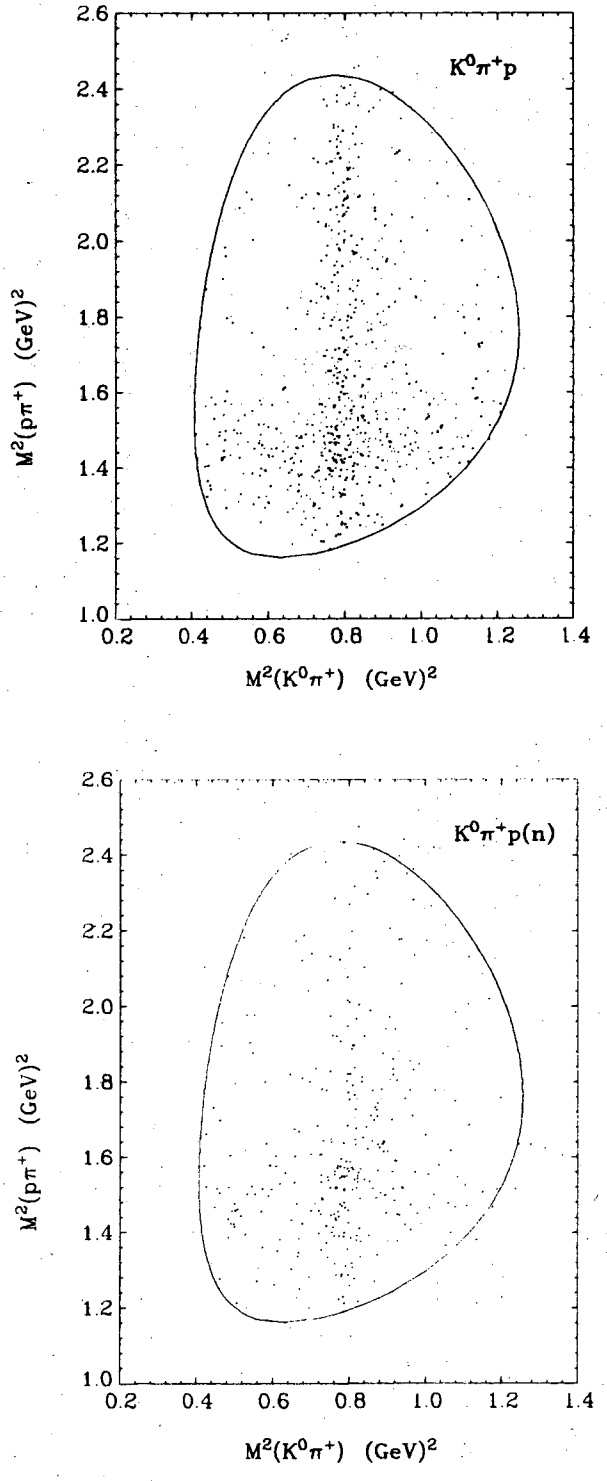
$K^0\pi^+p$
$K^0\pi^+p(n)$
$M^2(p\pi^+)$ (GeV)^2
$M^2(K^0\pi^+)$ (GeV)^2
2.6
2.4
2.2
2.0
1.8
1.6
1.4
1.2
1.0
0.2
0.4
0.6
0.8
1.0
1.2
1.4
XBL 711-1

Fig. 11

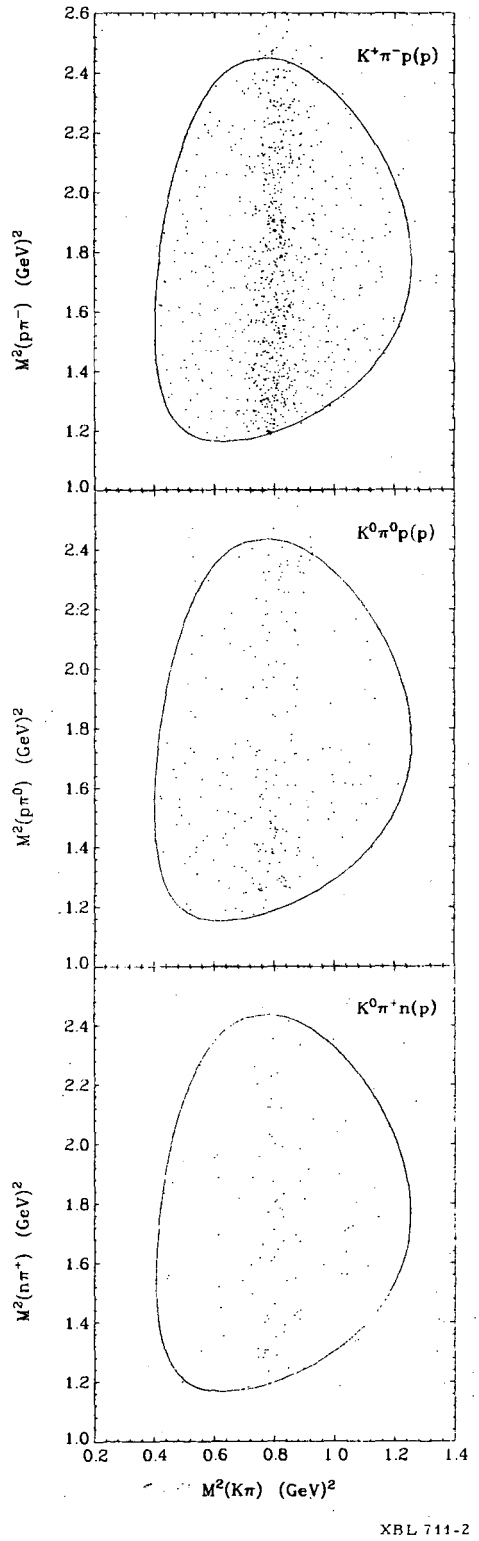
$K^+\pi^-p(p)$
$K^0\pi^0p(p)$
$K^0\pi^+n(p)$
$M^2(p\pi^-)$ (GeV)^2
$M^2(p\pi^0)$ (GeV)^2
$M^2(n\pi^+)$ (GeV)^2
$M^2(K\pi)$ (GeV)^2
2.6
2.4
2.2
2.0
1.8
1.6
1.4
1.2
1.0
0.2
0.4
0.6
0.8
1.0
1.2
1.4
XBL 711-2

Fig. 12

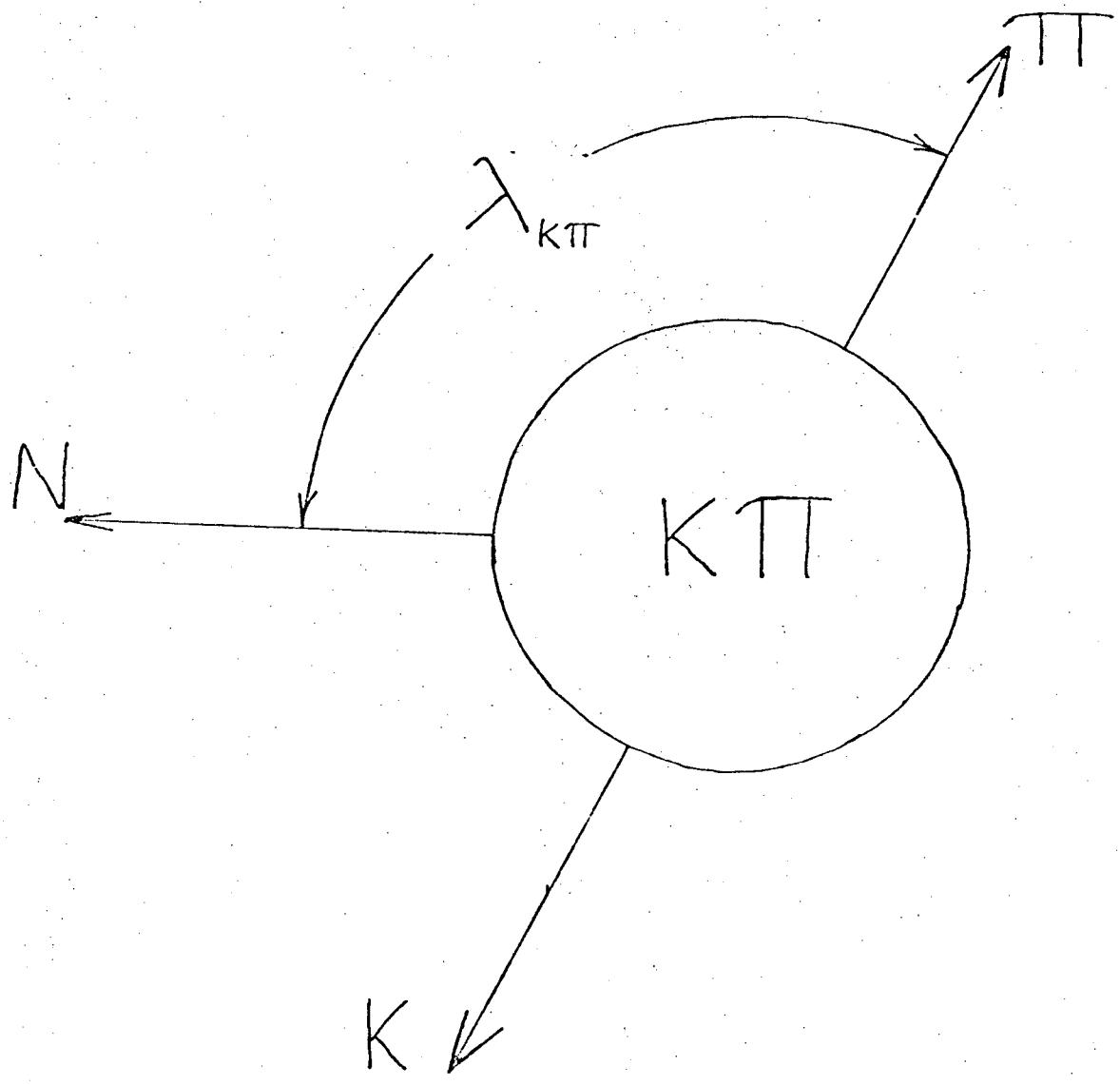

XBL 712-300

Fig. 13

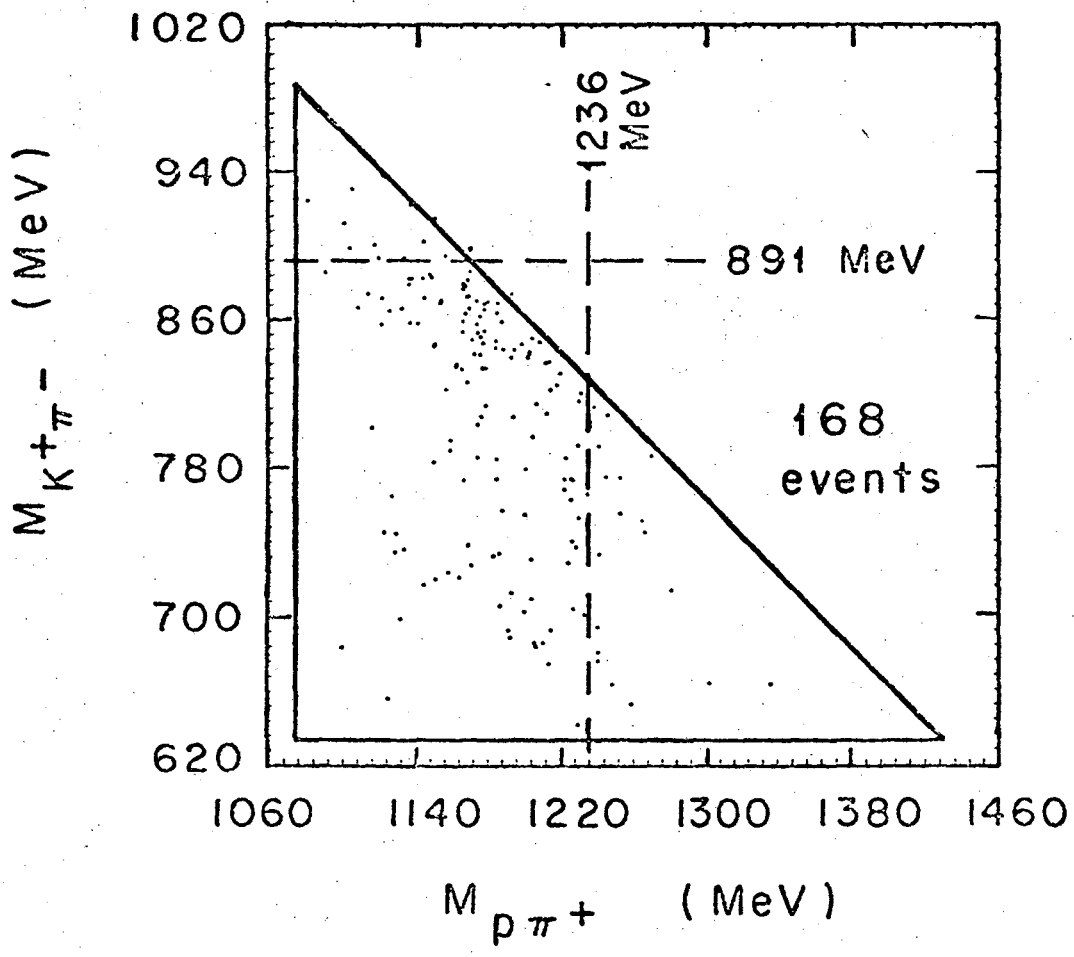

XBL696-2946

Fig. 14

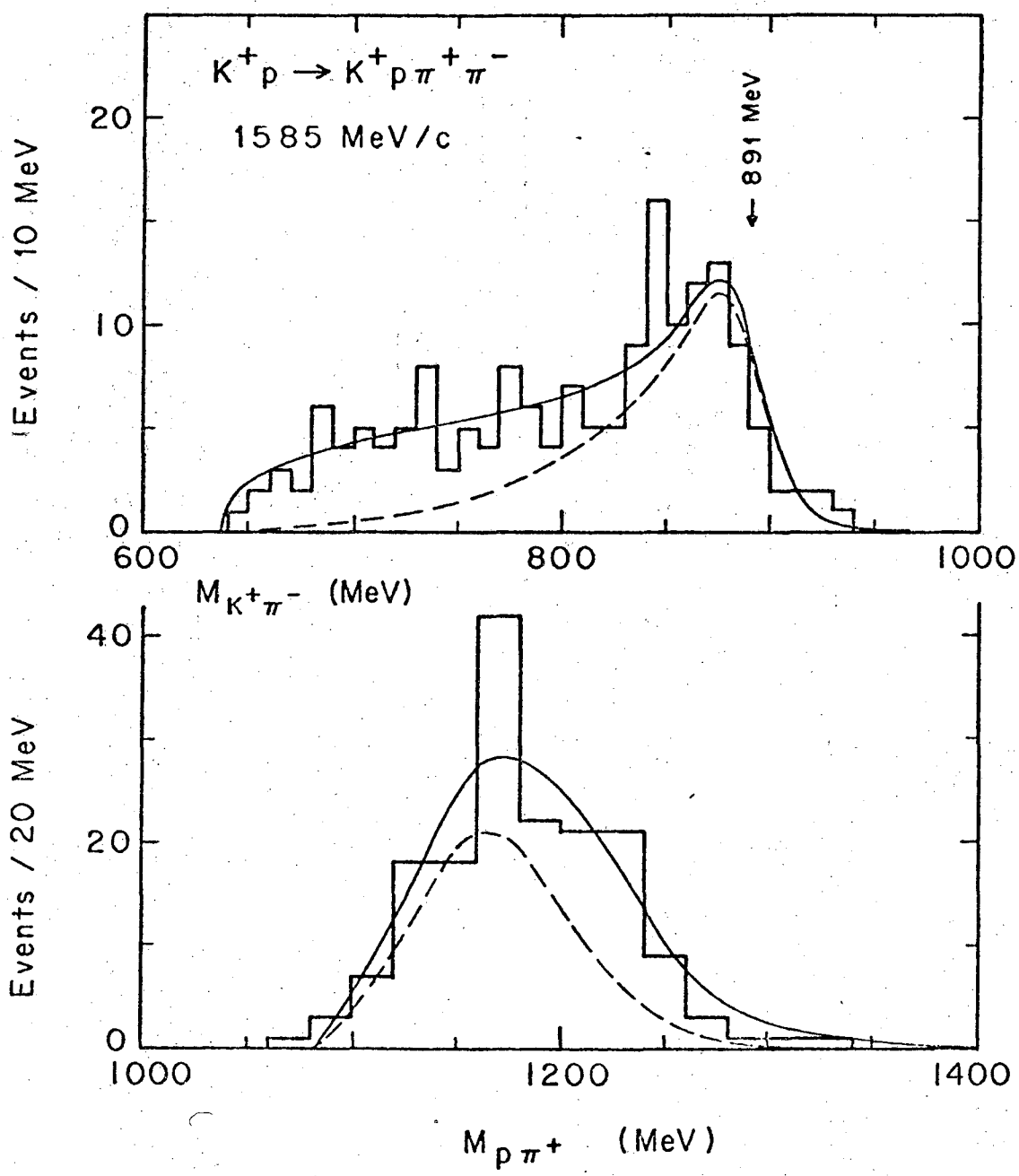

XBL696-2971

Fig. 15

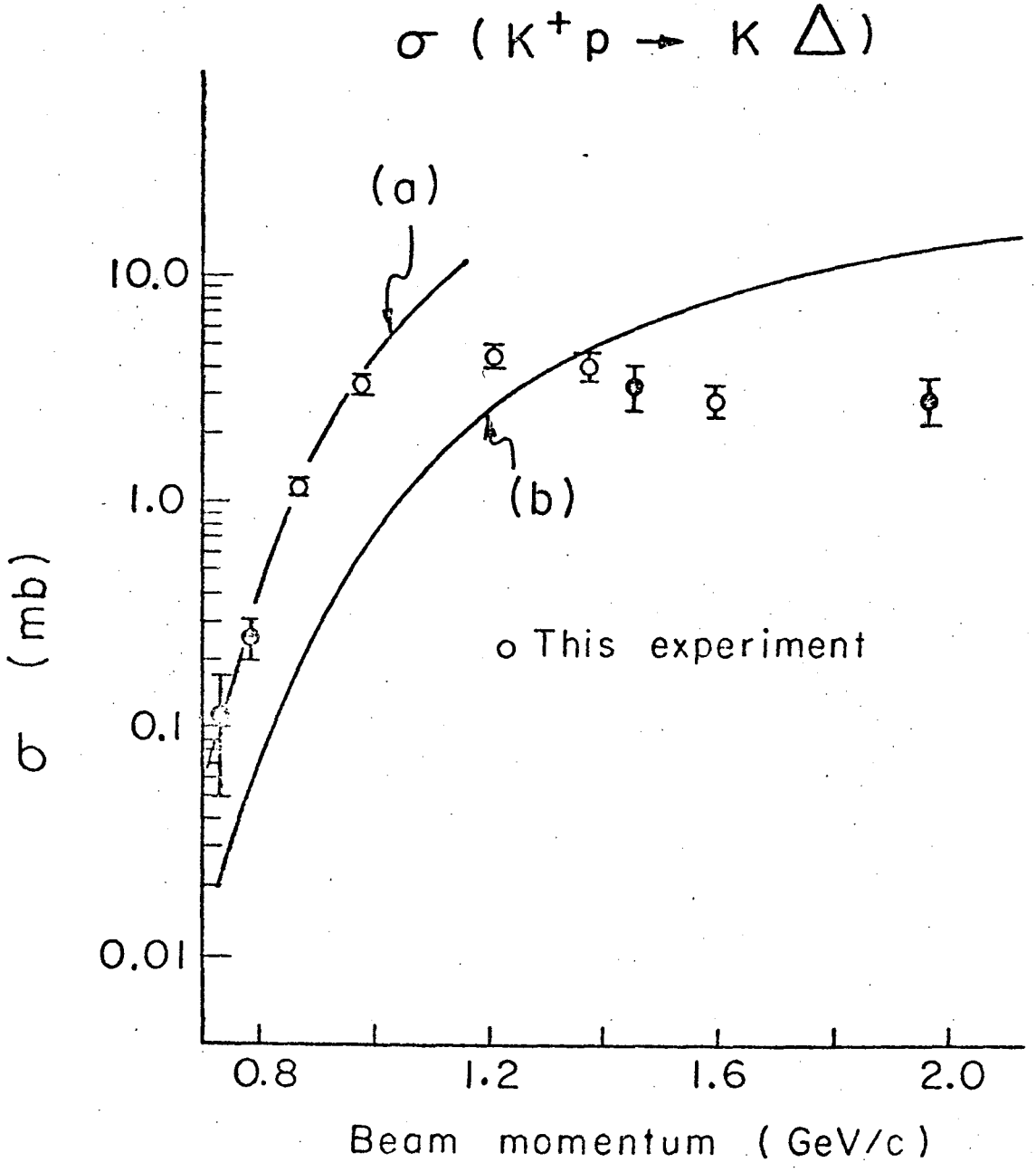
σ (K⁺p → K Δ)
(a)
(b)
10.0
1.0
0.1
0.01
σ (mb)
o This experiment
0.8
1.2
1.6
2.0
Beam momentum (GeV/c)
XBL6910-3897

Fig. 16

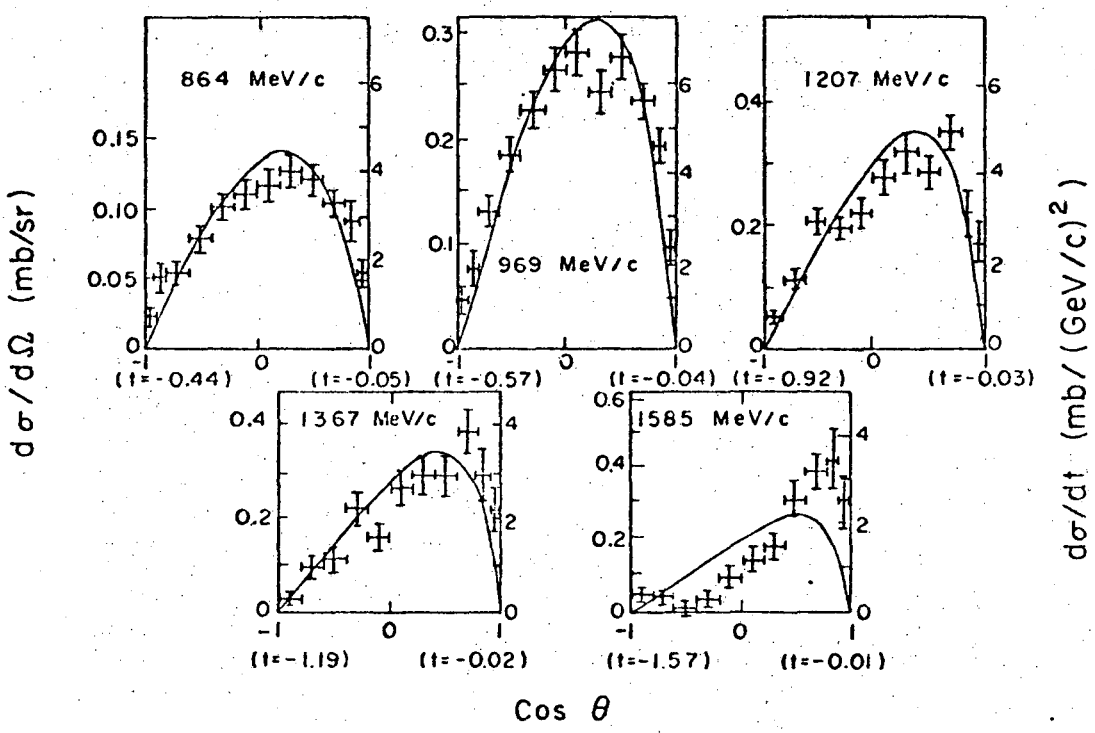
dσ/dΩ (mb/sr)
dσ/dt (mb/(GeV/c)²)
Cos θ
864 MeV/c
969 MeV/c
1207 MeV/c
1367 MeV/c
1585 MeV/c
(t=-0.44)
(t=-0.05)
(t=-0.57)
(t=-0.04)
(t=-0.92)
(t=-0.03)
(t=-1.19)
(t=-0.02)
(t=-1.57)
(t=-0.01)
XBL6910-3886

Fig. 17

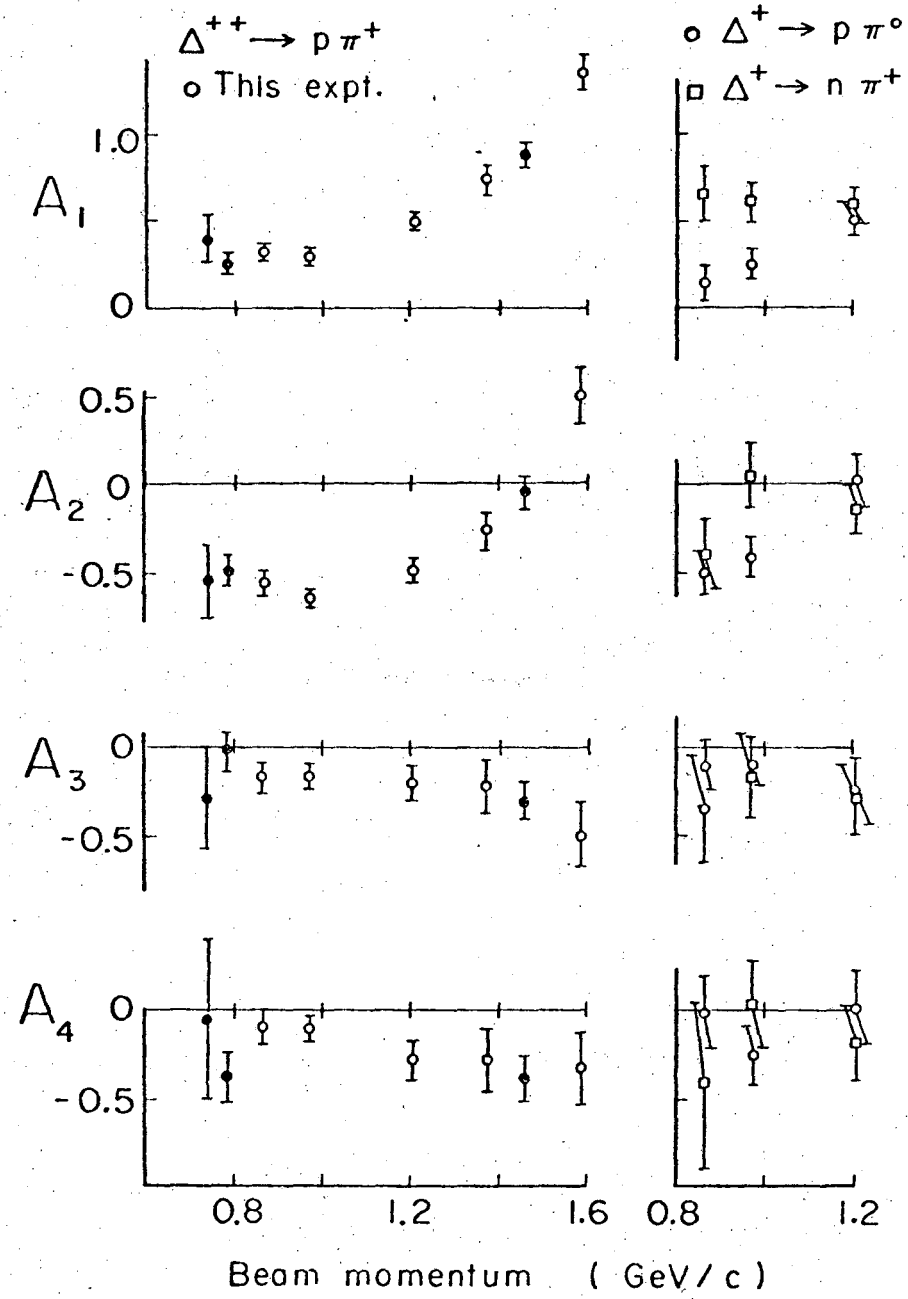

XBL6910-3887

Fig. 18

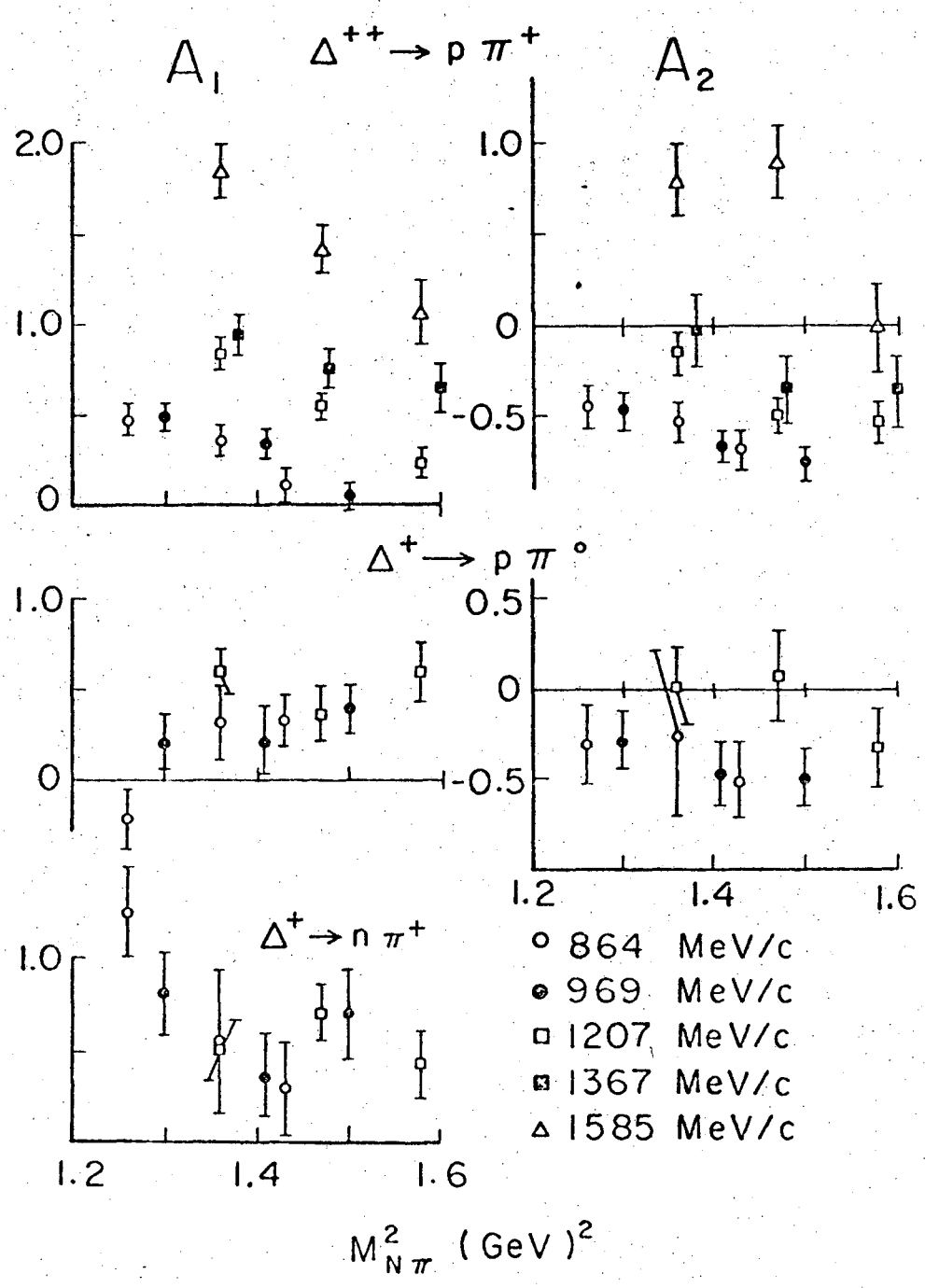
A1
Δ++ → p π+
A2
2.0
1.0
0
1.0
0
-0.5
Δ+ → p π °
1.0
0
0.5
0
-0.5
1.2
1.4
1.6
Δ+ → n π+
1.0
1.2
1.4
1.6
○ 864 MeV/c
◉ 969 MeV/c
□ 1207 MeV/c
▣ 1367 MeV/c
△ 1585 MeV/c
M²Nπ (GeV)²
XBL6910-3888

Fig. 19

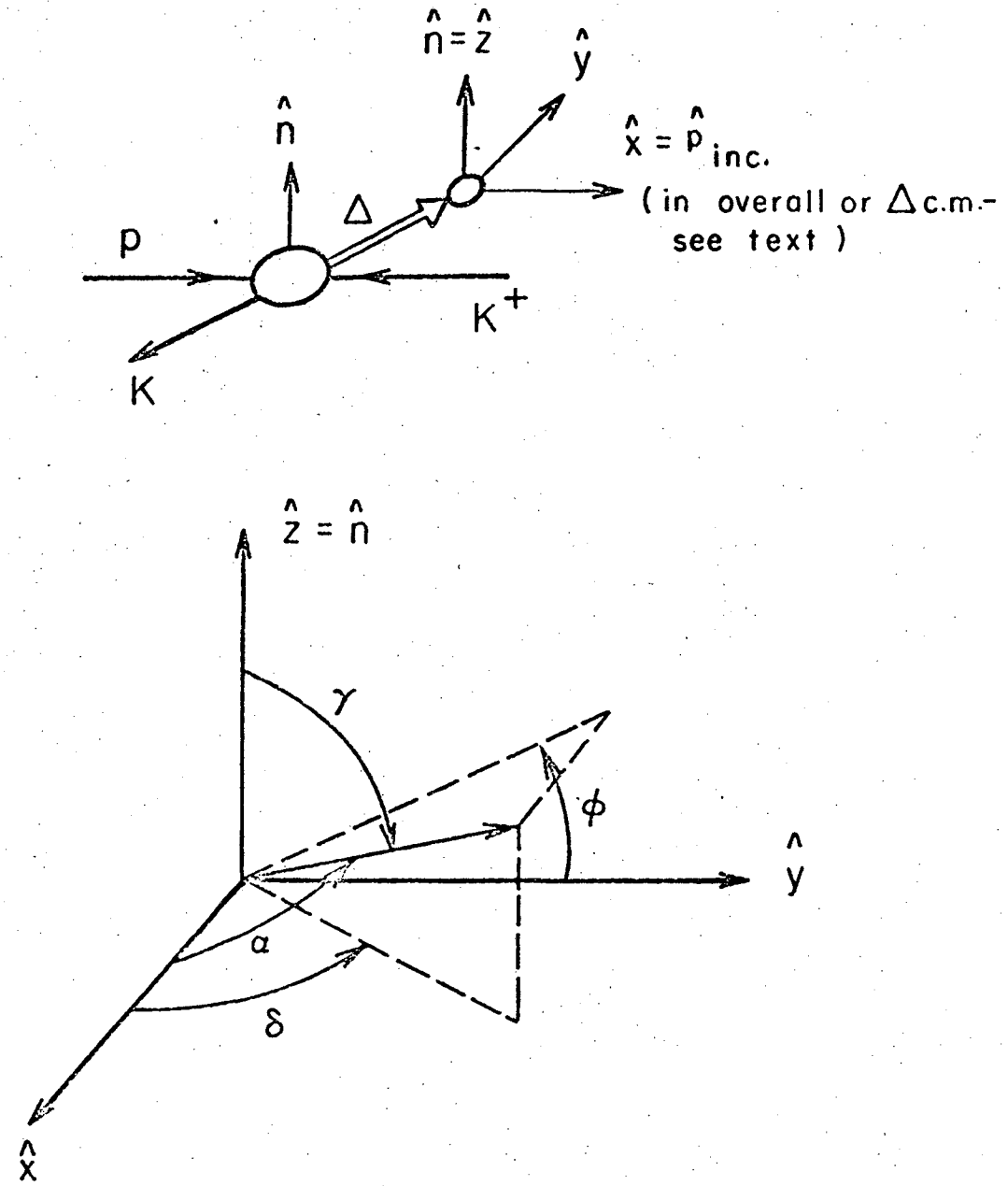
n̂ = ẑ
ŷ
n̂
x̂ = p̂ inc.
(in overall or Δ c.m.-
see text)
Δ
p
K+
K
ẑ = n̂
γ
φ
ŷ
α
δ
x̂
XBL6910-3889

Fig. 20

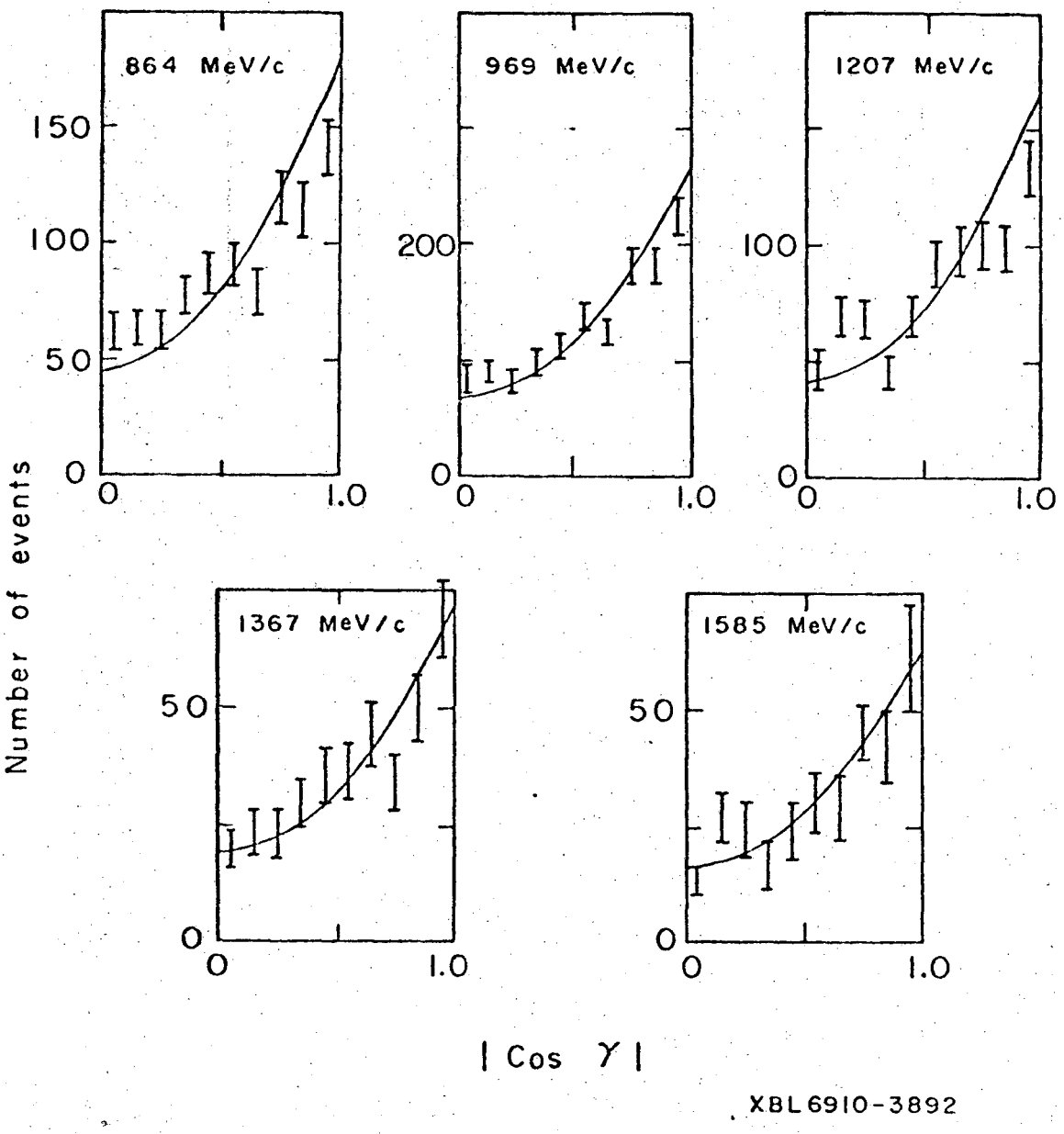
864 MeV/c
969 MeV/c
1207 MeV/c
1367 MeV/c
1585 MeV/c
Number of events
| Cos γ |
XBL6910-3892

Fig. 21

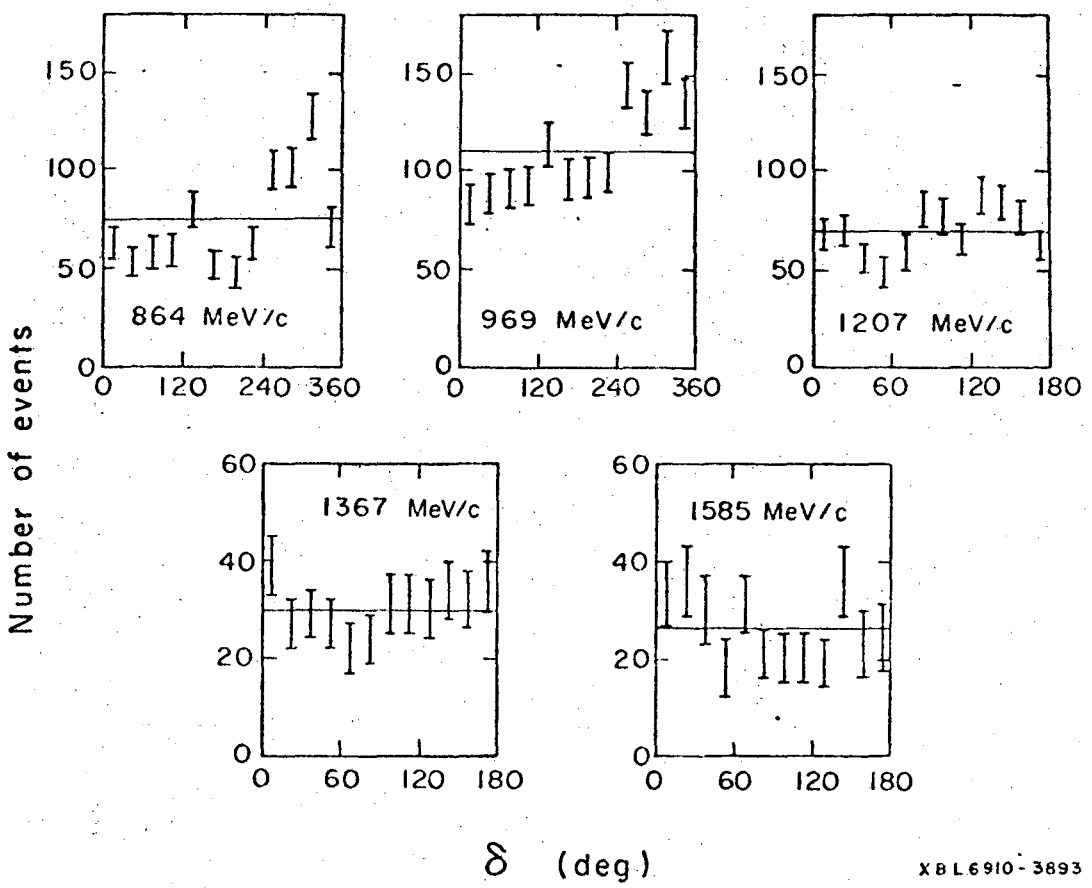
Number of events
150
100
50
0
0 120 240 360
864 MeV/c
969 MeV/c
1207 MeV/c
0 60 120 180
60
40
20
0
1367 MeV/c
1585 MeV/c
δ (deg)
XBL6910-3893

Fig. 22

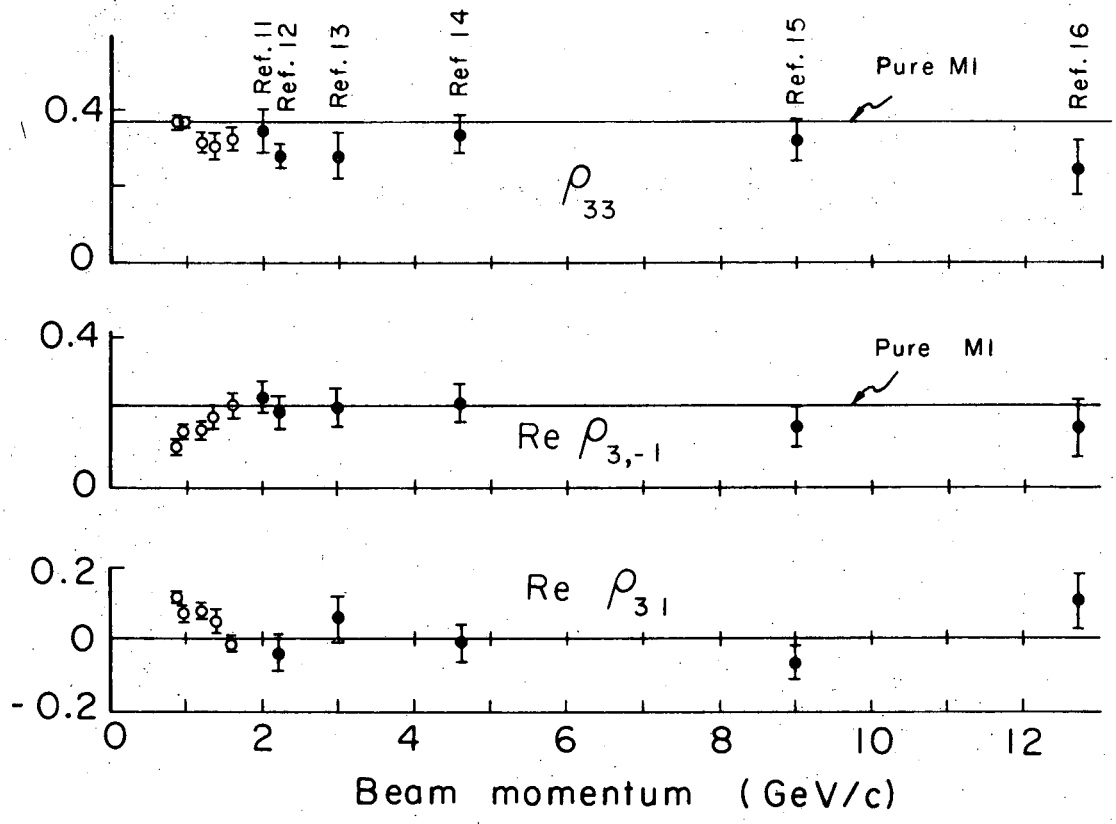
Ref. 11
Ref. 12
Ref. 13
Ref 14
Ref. 15
Pure MI
Ref. 16
0.4
0
ρ_{33}
0.4
Pure MI
0
Re $\rho_{3,-1}$
0.2
0
-0.2
Re ρ_{31}
0
2
4
6
8
10
12
Beam momentum (GeV/c)
XBL6910-3891

Fig. 23

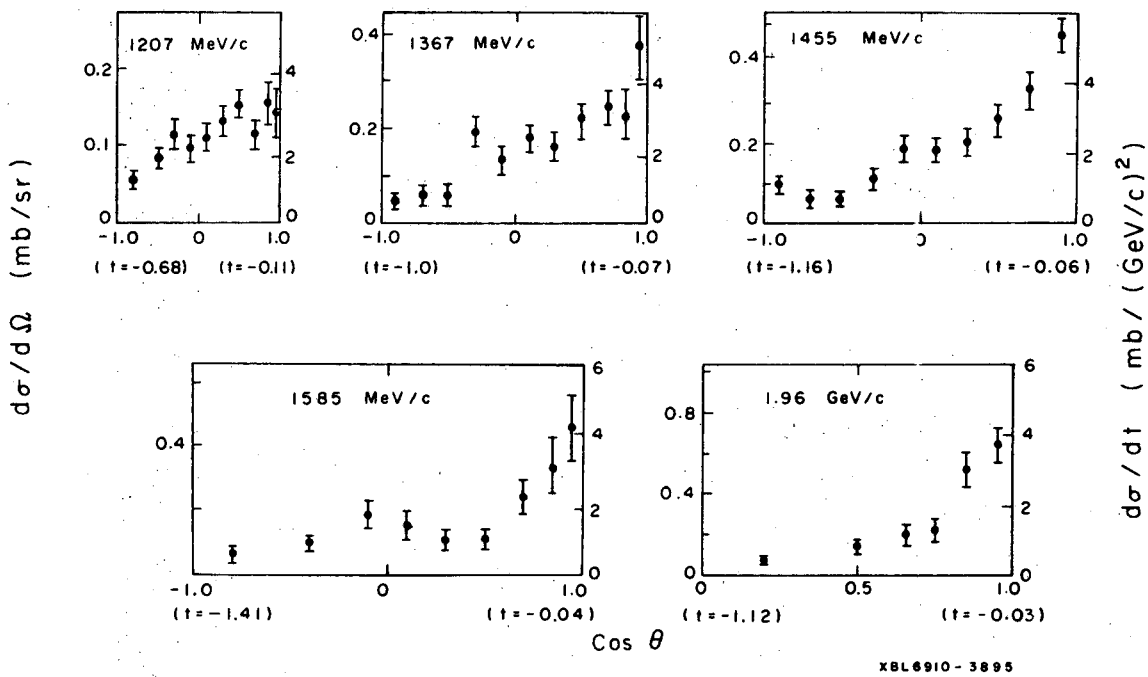
1207 MeV/c
1367 MeV/c
1455 MeV/c
1585 MeV/c
1.96 GeV/c
(t=-0.68)
(t=-0.11)
(t=-1.0)
(t=-0.07)
(t=-1.16)
(t=-0.06)
(t=-1.41)
(t=-0.04)
(t=-1.12)
(t=-0.03)
dσ/dΩ (mb/sr)
dσ/dt (mb/(GeV/c)²)
Cos θ
XBL6910-3895

Fig. 24

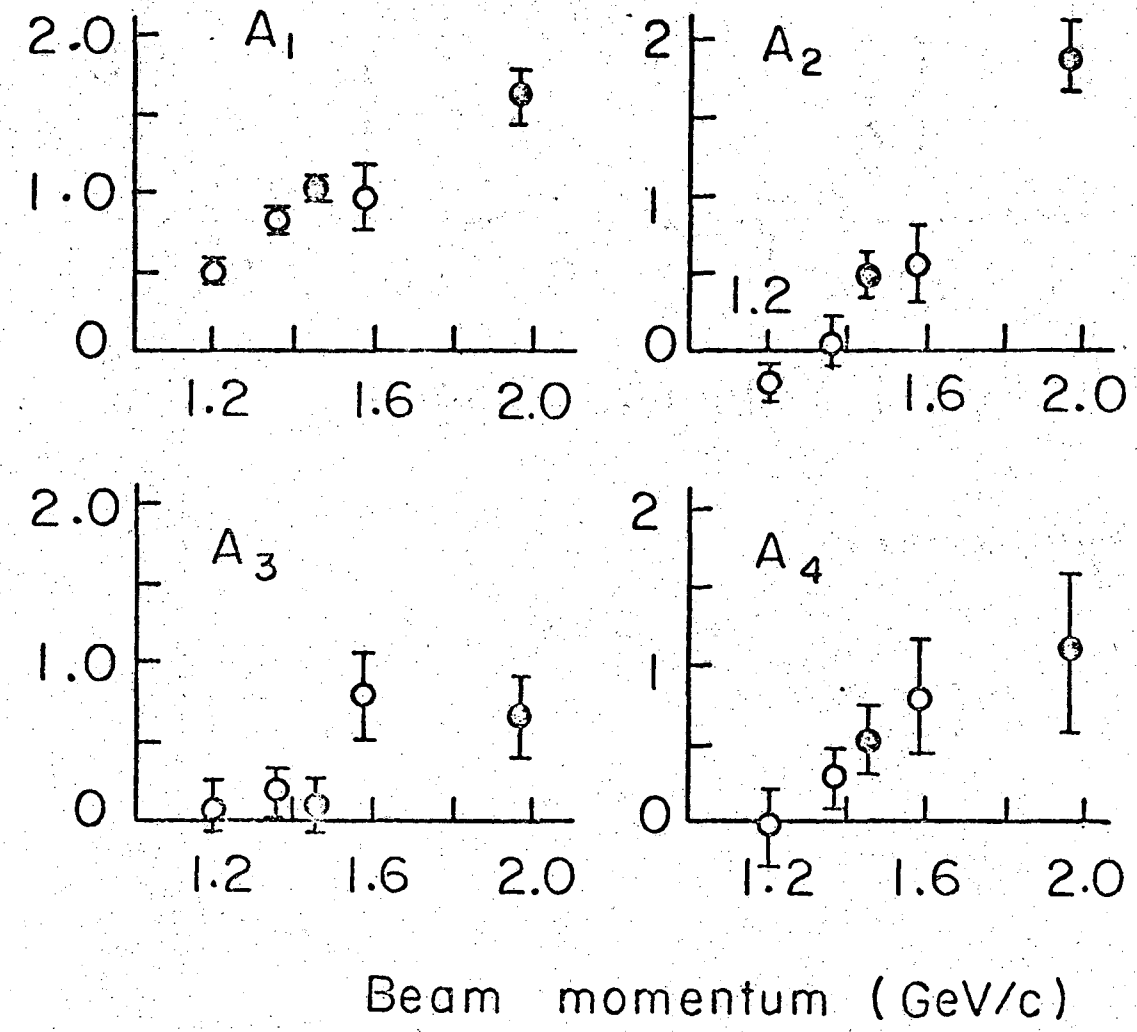

XBL6910-3898

Fig. 25

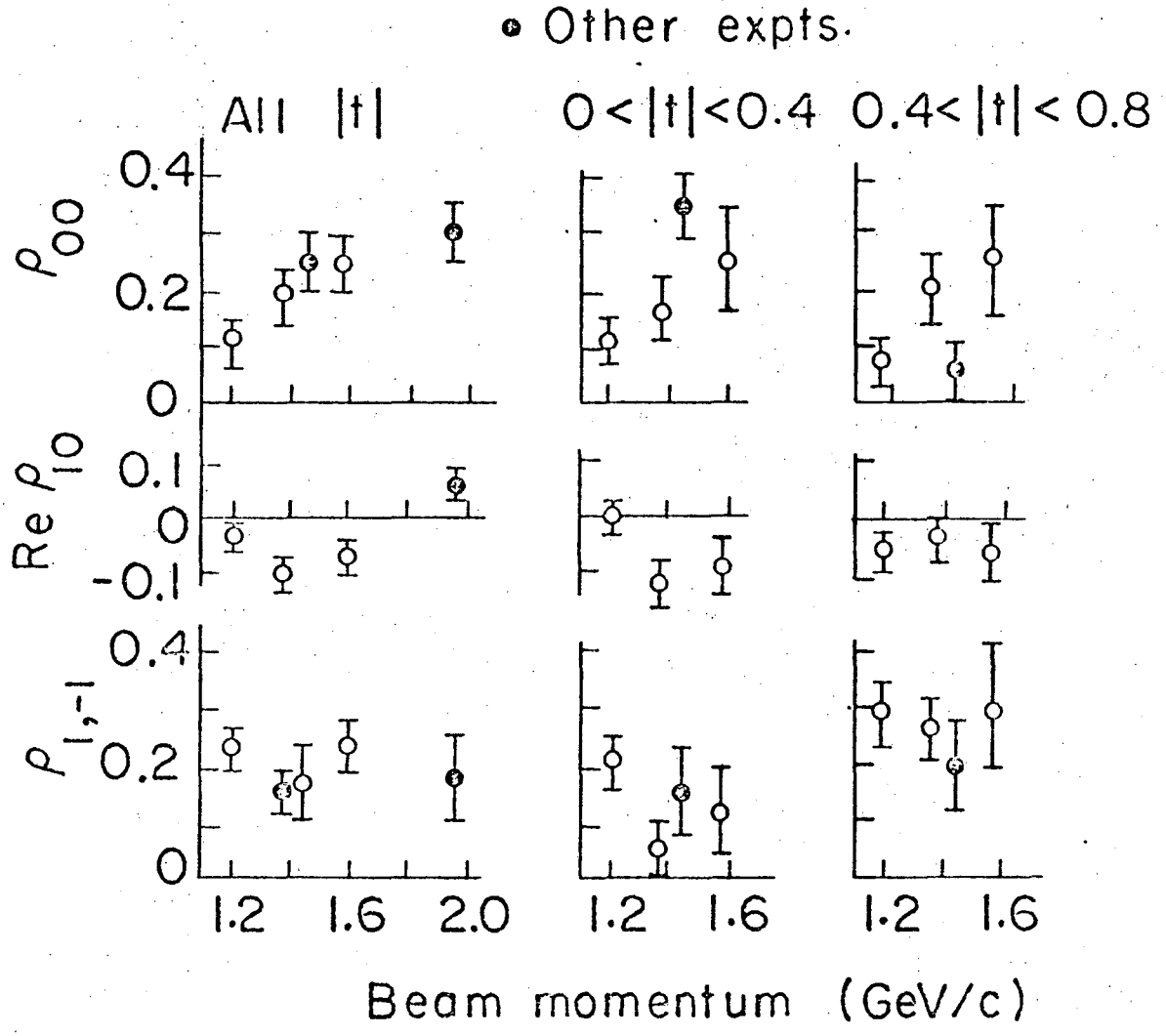

XBL6911-3899

Fig. 26

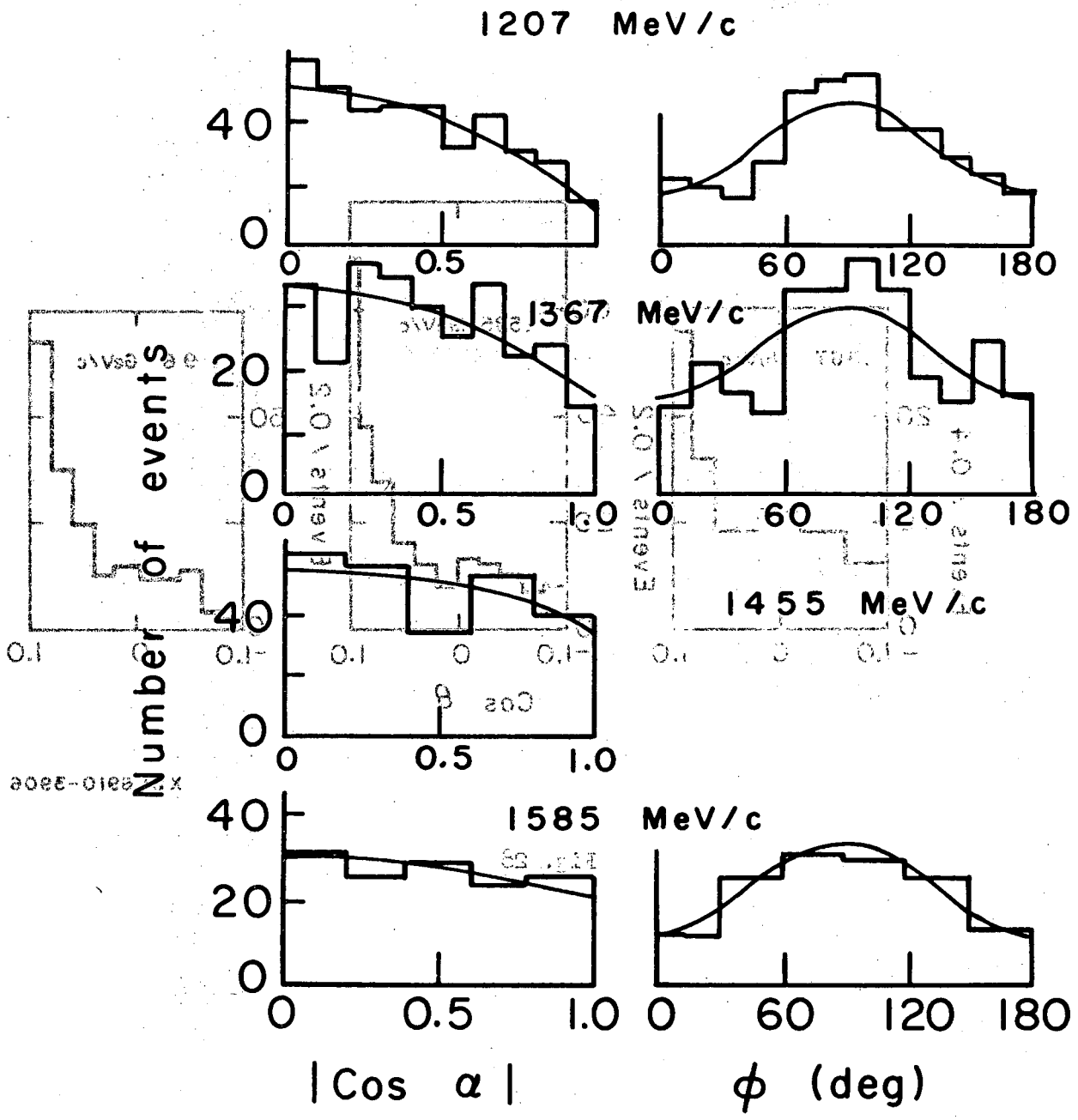
1207 MeV/c
1367 MeV/c
1455 MeV/c
1585 MeV/c
Number of events
|Cos α|
φ (deg)
XBL6910-3900

Fig. 27

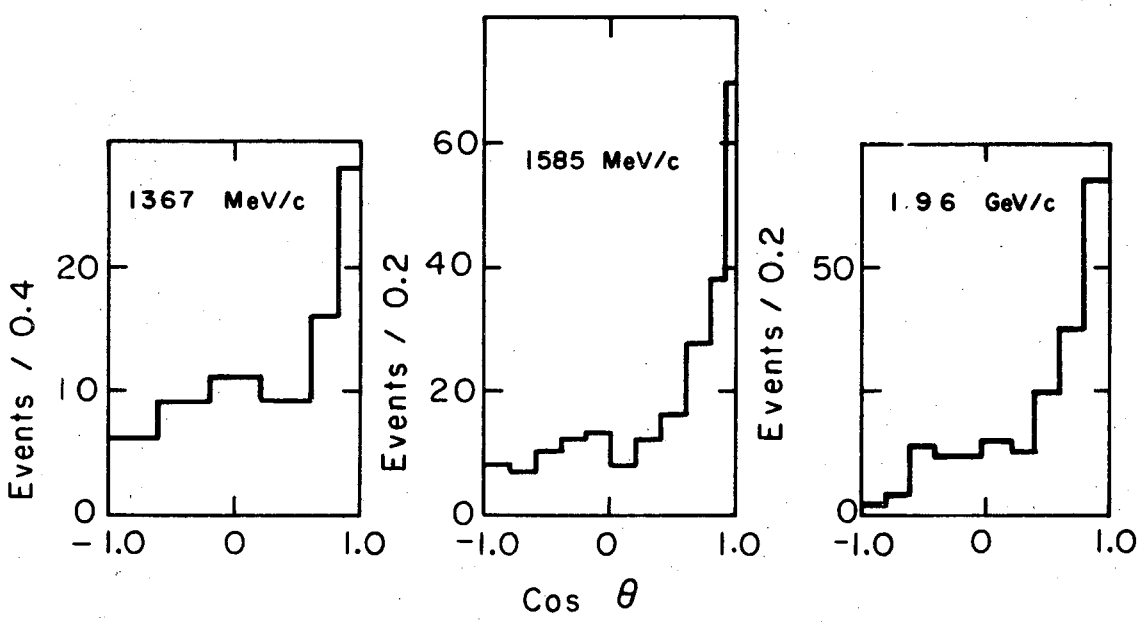
1367 MeV/c
1585 MeV/c
1.96 GeV/c
Events / 0.4
Events / 0.2
Events / 0.2
Cos θ
XBL6910-3906

Fig. 28

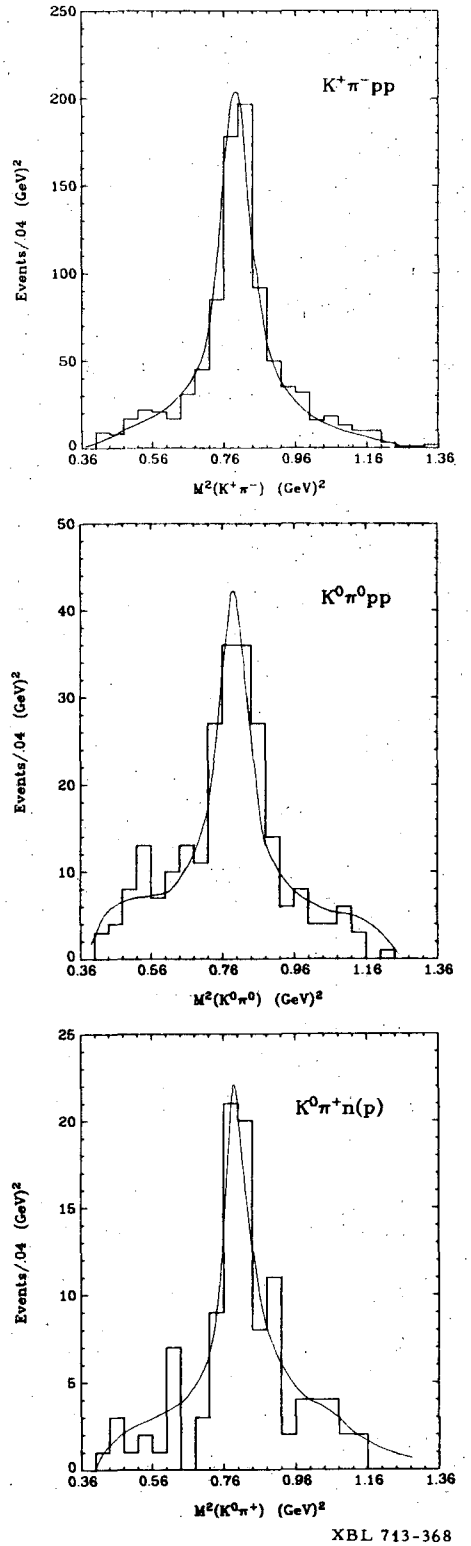
$K^+\pi^-pp$
$K^0\pi^0pp$
$K^0\pi^+n(p)$
Events/.04 (GeV)^2
$M^2(K^+\pi^-)$ (GeV)^2
$M^2(K^0\pi^0)$ (GeV)^2
$M^2(K^0\pi^+)$ (GeV)^2
0.36
0.56
0.76
0.96
1.16
1.36
XBL 713-368

Fig. 29

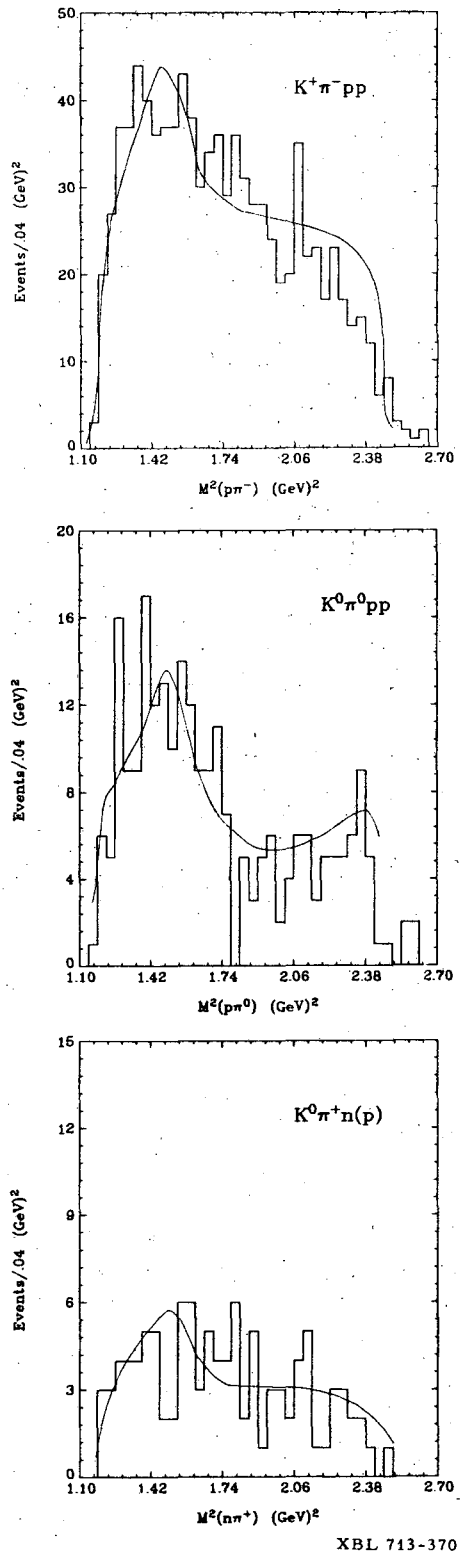
$K^+\pi^-pp$
Events/.04 (GeV)²
$M^2(p\pi^-)$ (GeV)²
$K^0\pi^0pp$
Events/.04 (GeV)²
$M^2(p\pi^0)$ (GeV)²
$K^0\pi^+n(p)$
Events/.04 (GeV)²
$M^2(n\pi^+)$ (GeV)²
1.10
1.42
1.74
2.06
2.38
2.70
XBL 713-370

Fig. 30

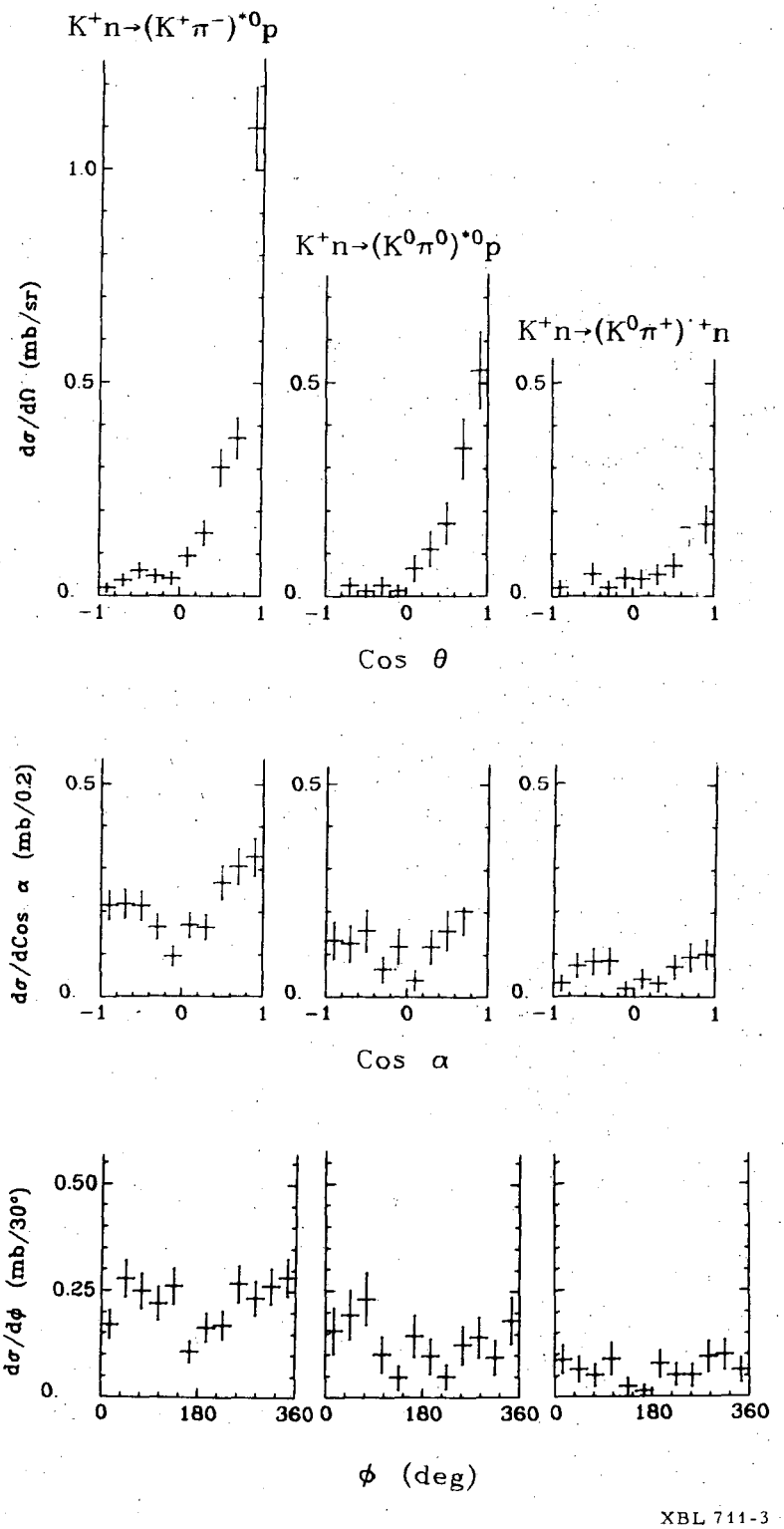
$K^+n\to(K^+\pi^-)^{*0}p$
$K^+n\to(K^0\pi^0)^{*0}p$
$K^+n\to(K^0\pi^+)^{*+}n$
$d\sigma/d\Omega$ (mb/sr)
Cos θ
$d\sigma/d\text{Cos }\alpha$ (mb/0.2)
Cos α
$d\sigma/d\phi$ (mb/30°)
ϕ (deg)
XBL 711-3

Fig. 31

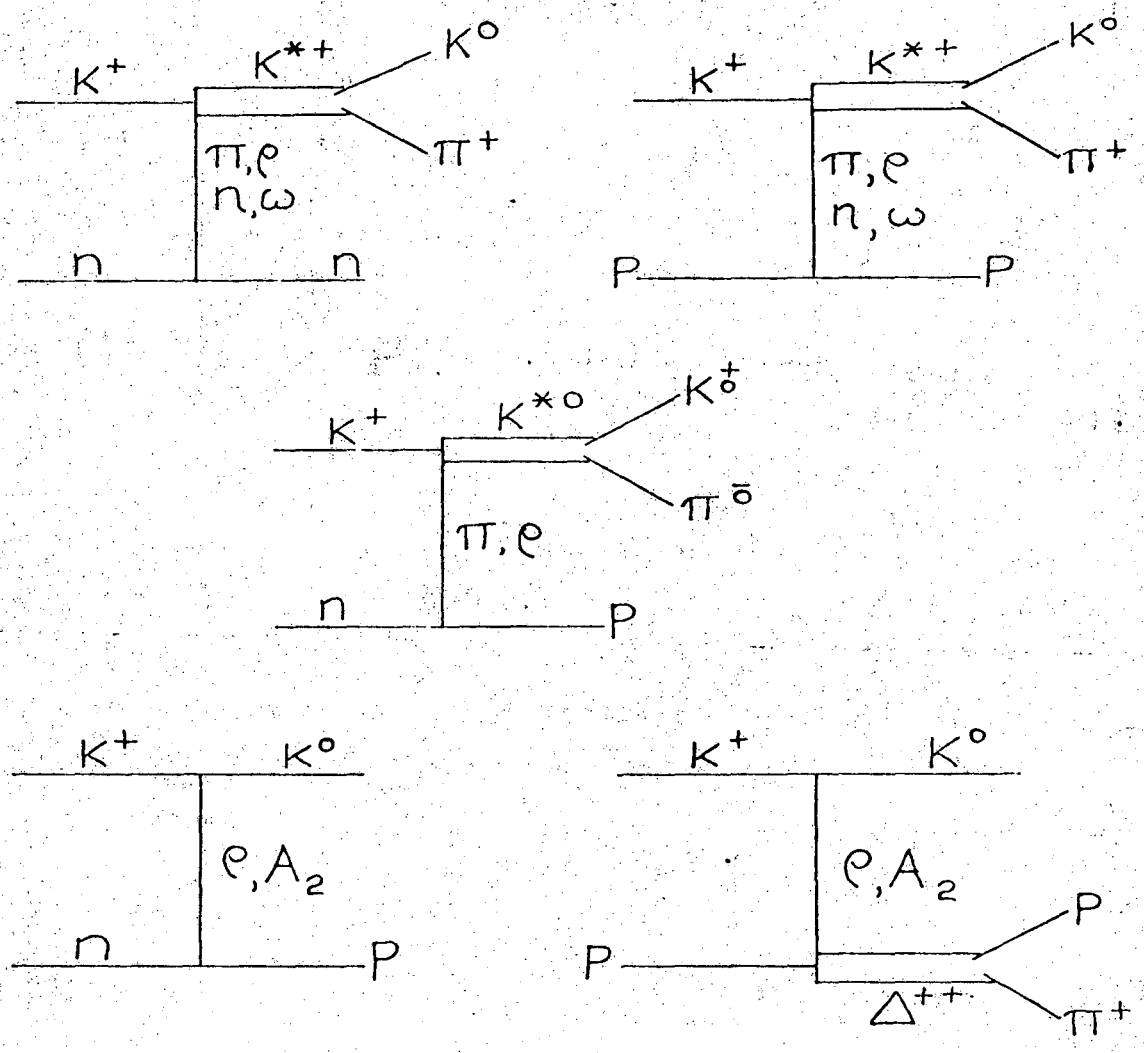

XBL 713-365

Fig. 32

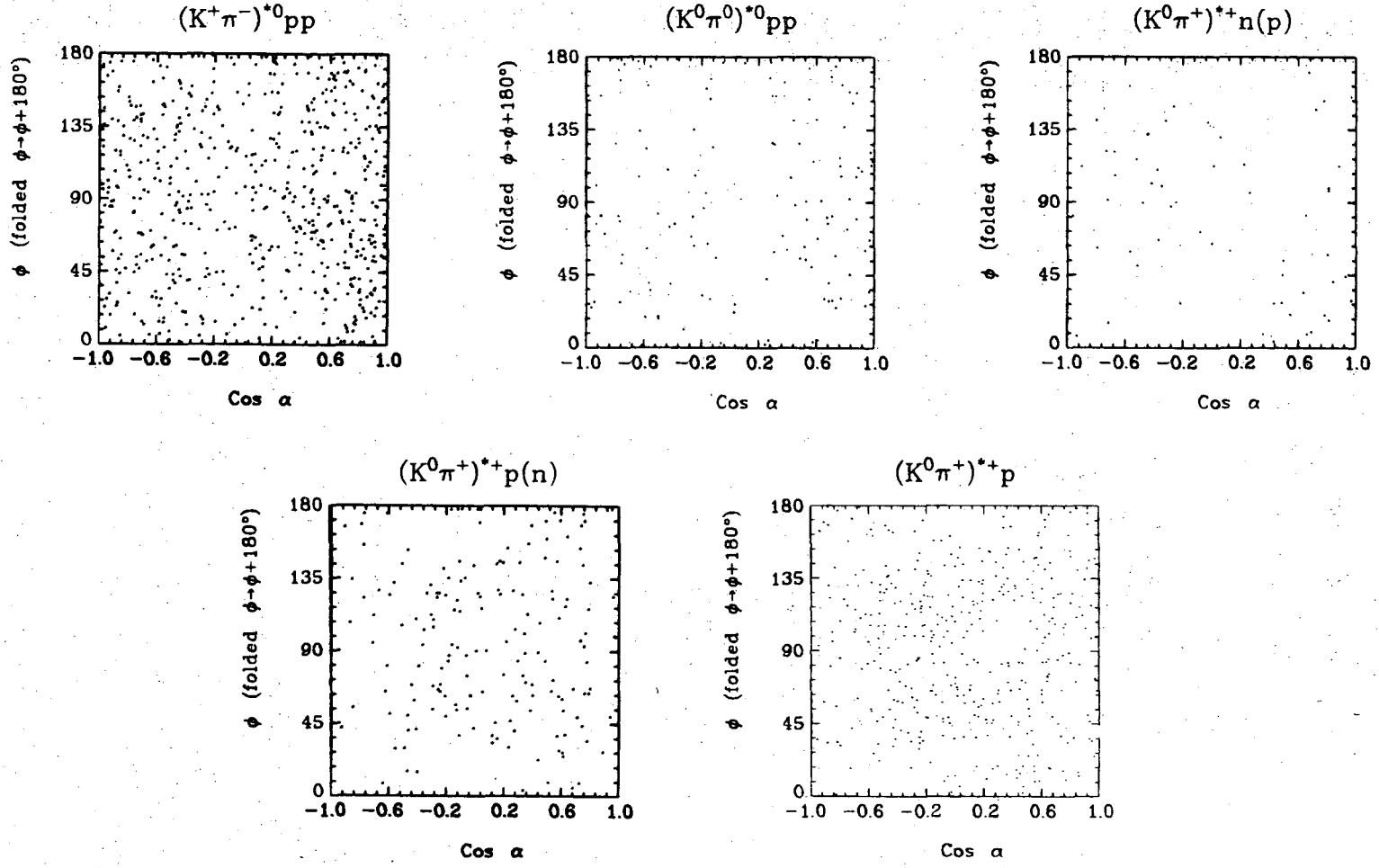

XBL 711-5

Fig. 33

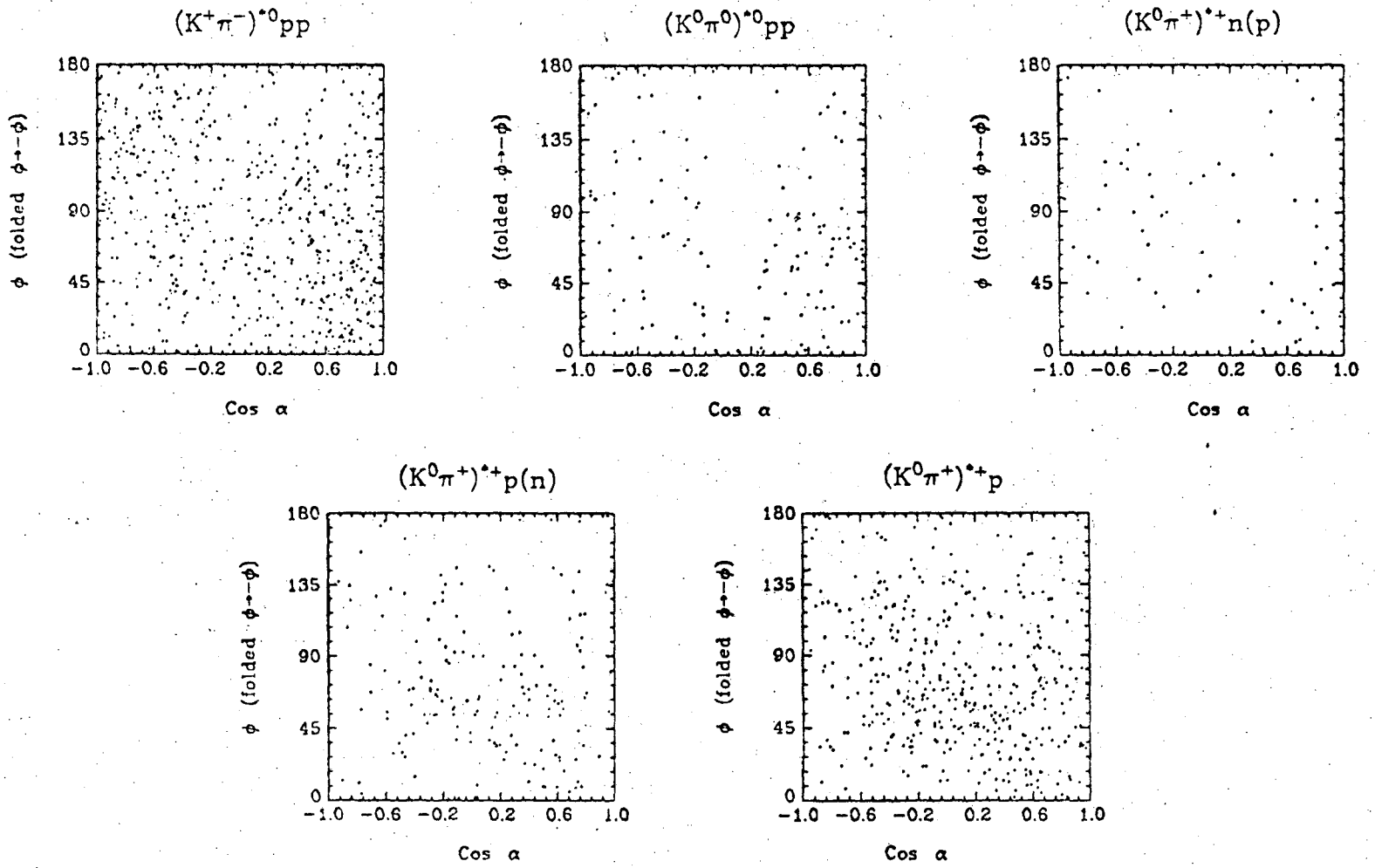

Fig. 34

XBL 711-4

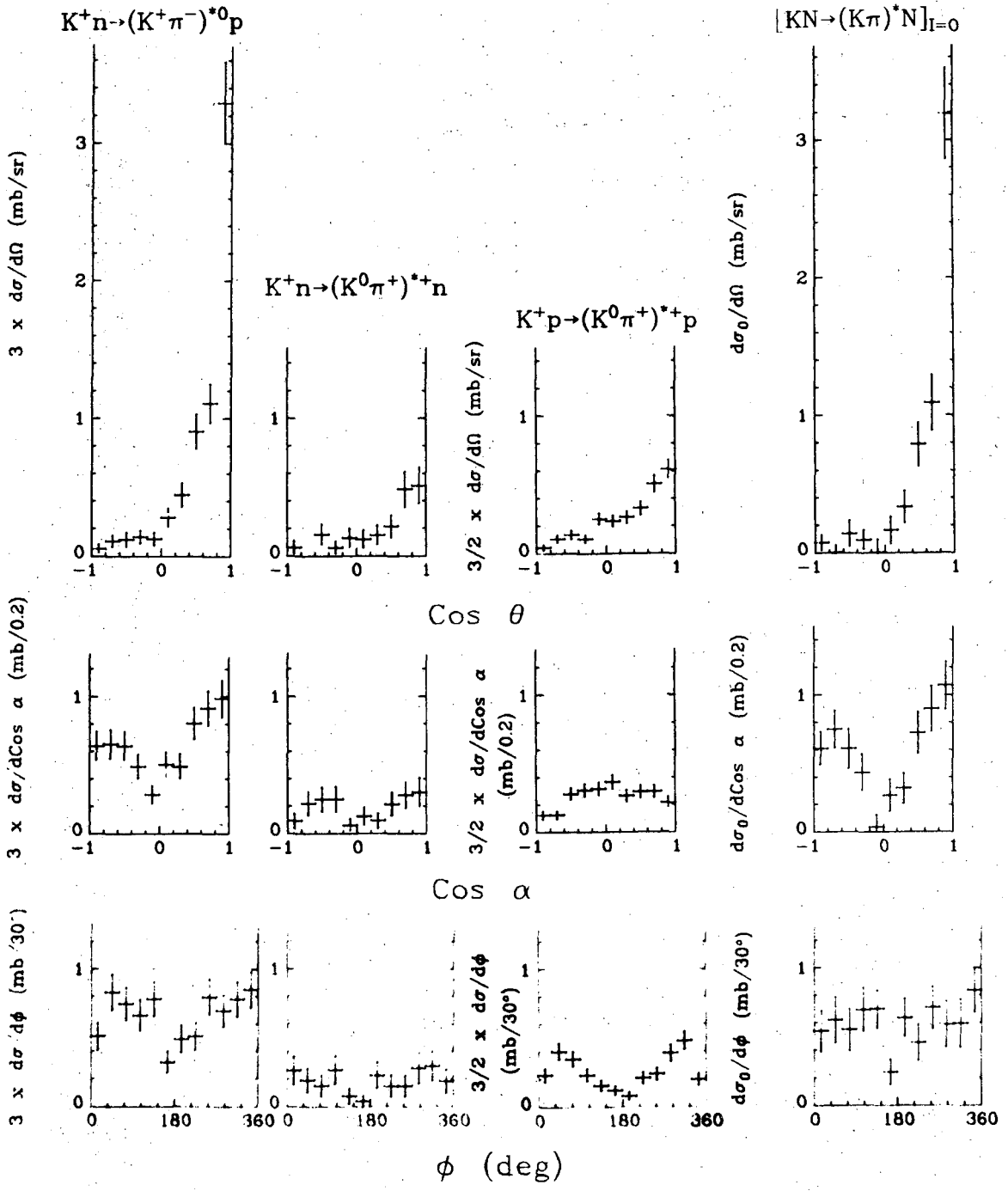

XBL 711-6

Fig. 35

$(KN \to K^*N)_{I=0}$

1585 MeV/c

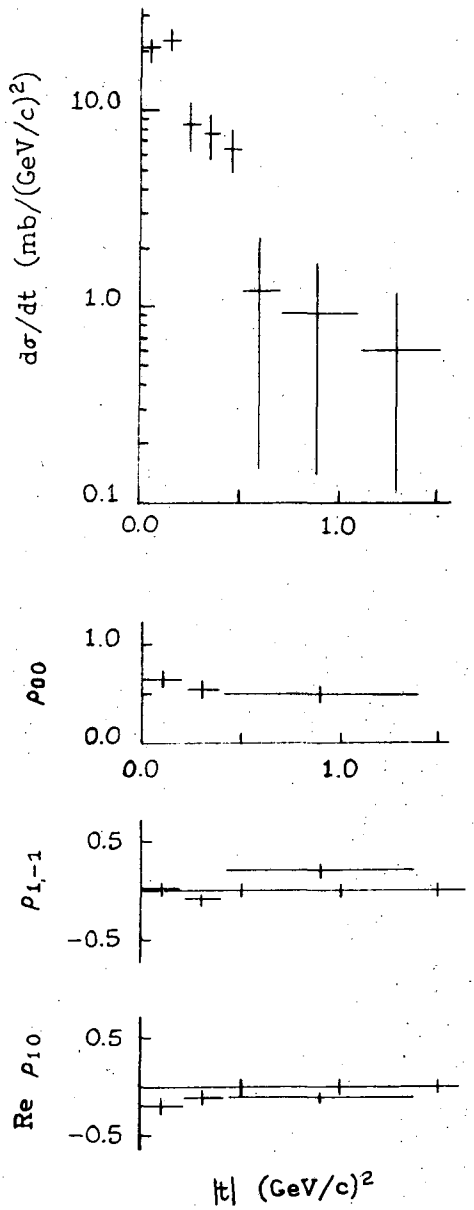

XBL 713-366

Fig. 36

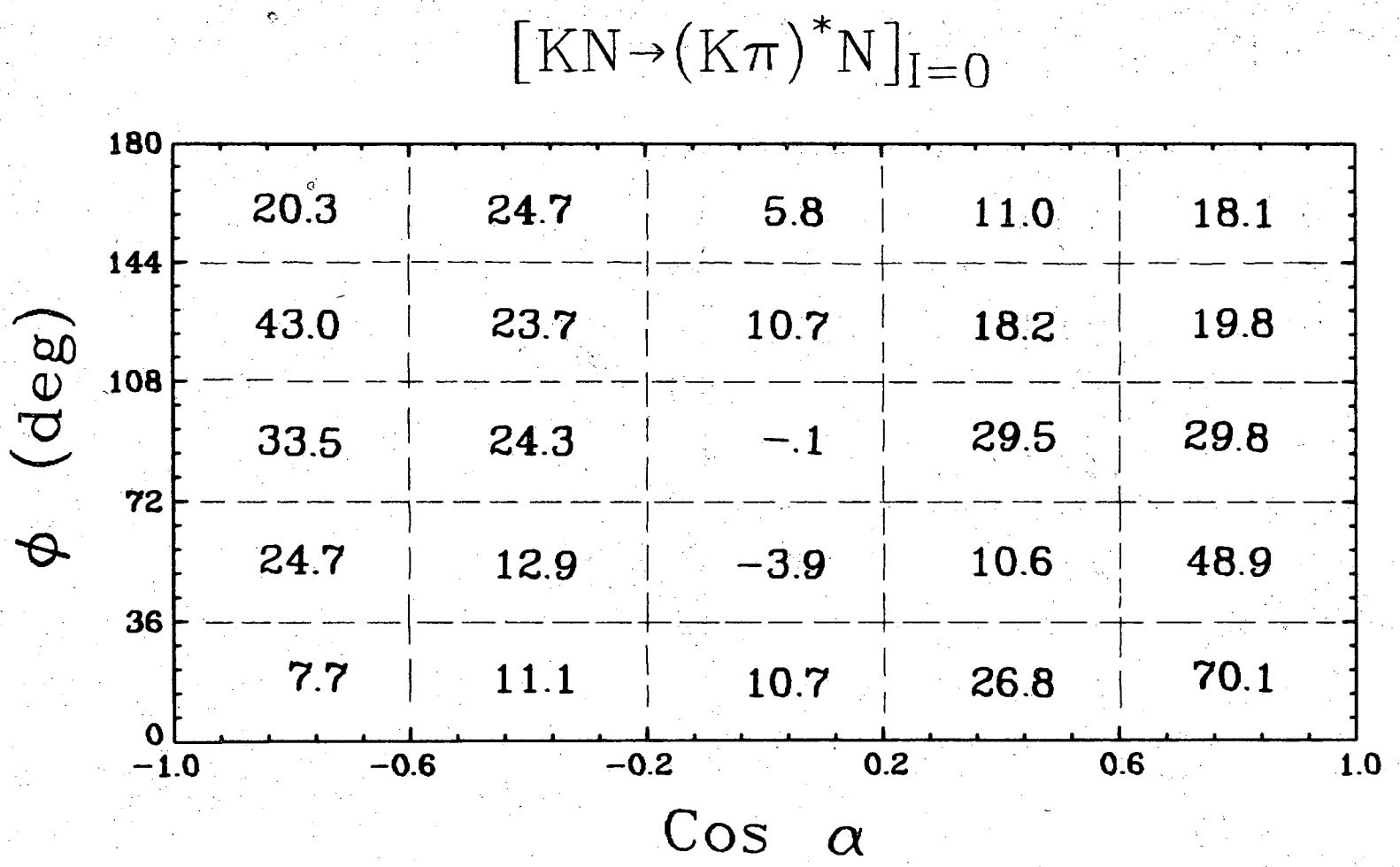
$[KN \to (K\pi)^* N]_{I=0}$
180
144
108
72
36
0
φ (deg)
20.3
24.7
5.8
11.0
18.1
43.0
23.7
10.7
18.2
19.8
33.5
24.3
−.1
29.5
29.8
24.7
12.9
−3.9
10.6
48.9
7.7
11.1
10.7
26.8
70.1
−1.0
−0.6
−0.2
0.2
0.6
1.0
Cos α
XBL 711-11

Fig. 37

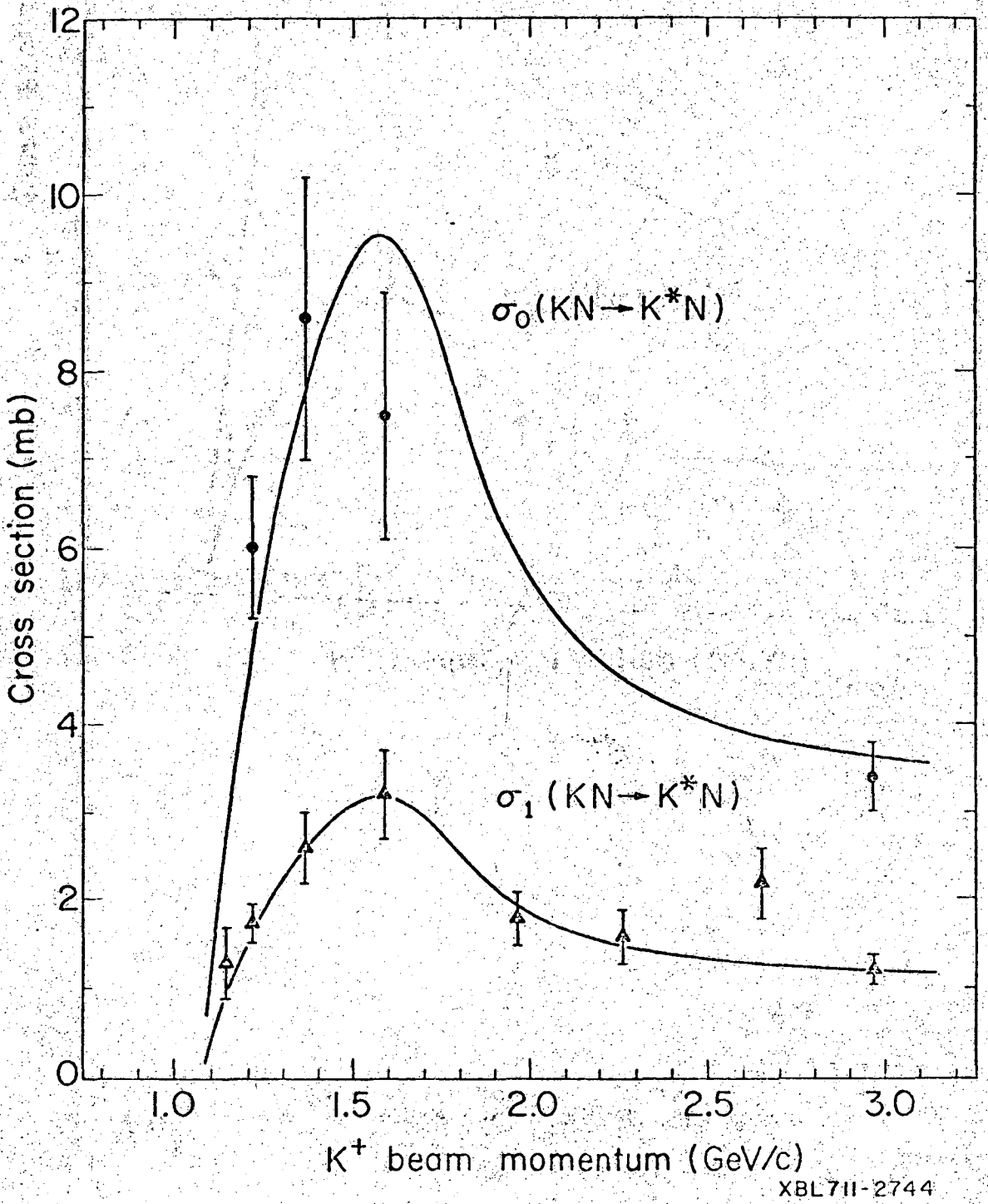
12
10
8
6
4
2
0
Cross section (mb)
$\sigma_0(KN \rightarrow K^*N)$
$\sigma_1(KN \rightarrow K^*N)$
1.0
1.5
2.0
2.5
3.0
K^+ beam momentum (GeV/c)
XBL711-2744

Fig. 38

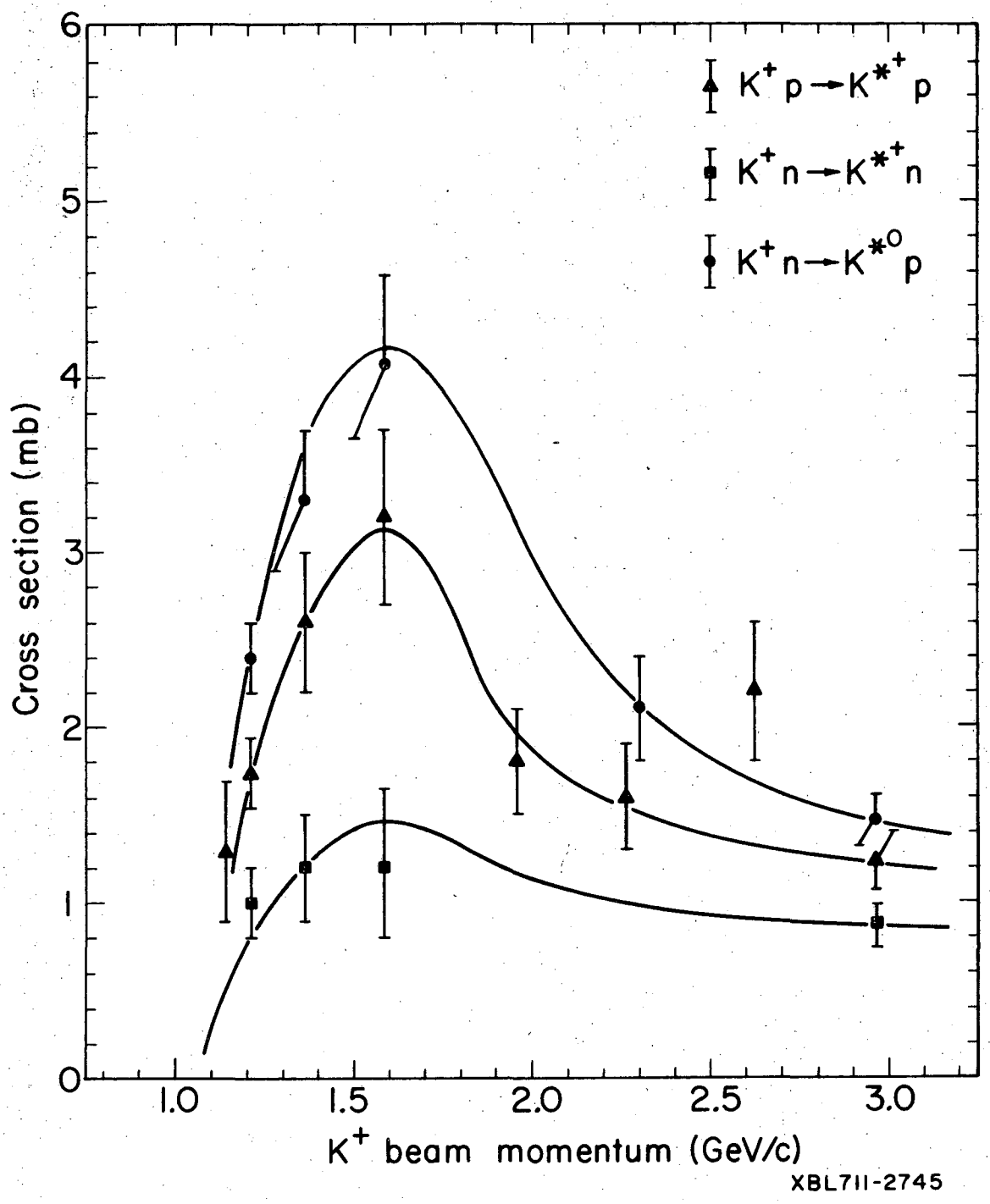
$K^+p \rightarrow K^{*+}p$
$K^+n \rightarrow K^{*+}n$
$K^+n \rightarrow K^{*0}p$
Cross section (mb)
K^+ beam momentum (GeV/c)
0
1
2
3
4
5
6
1.0
1.5
2.0
2.5
3.0
XBL711-2745

Fig. 39

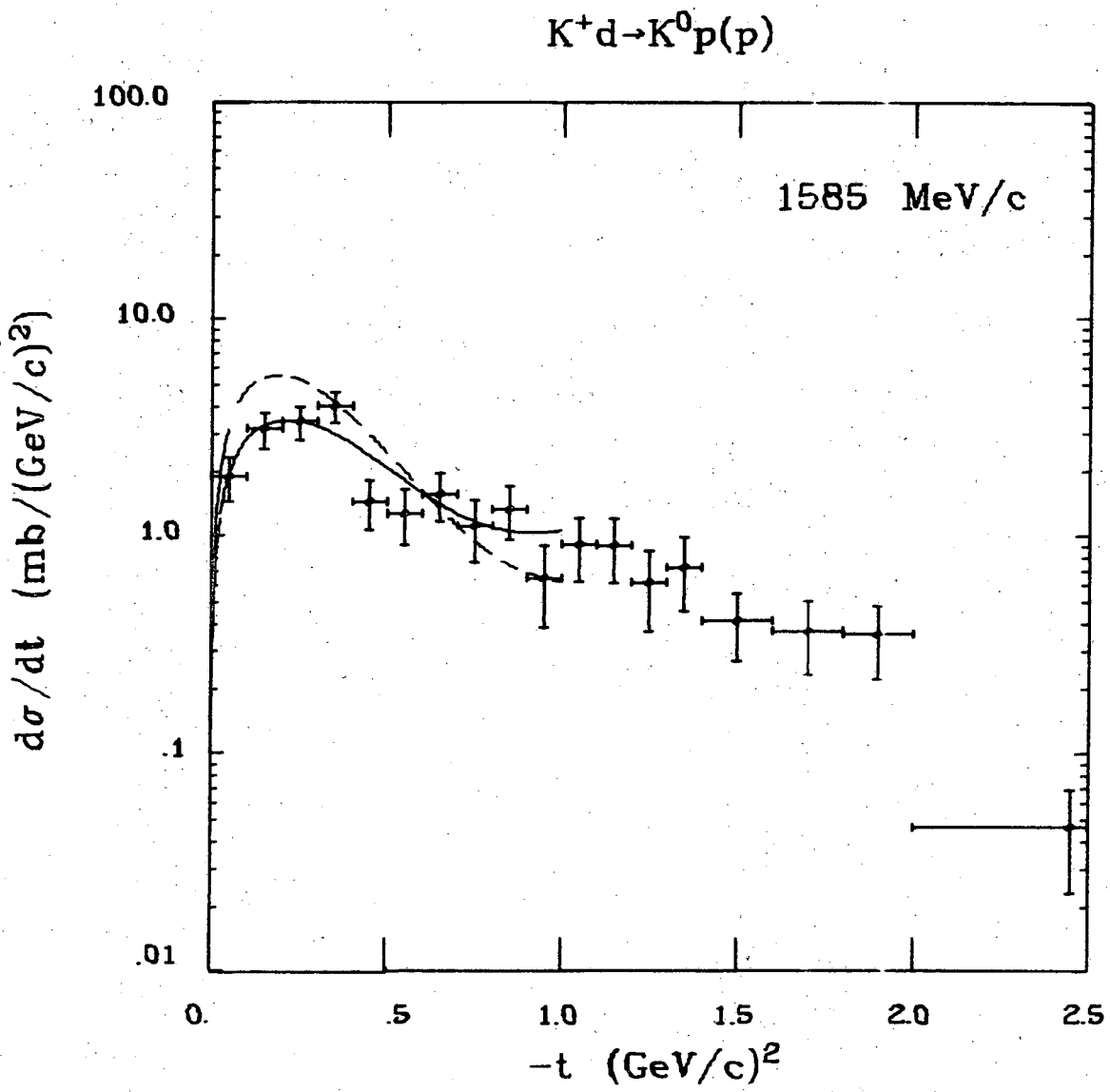
$K^+d \rightarrow K^0p(p)$
1585 MeV/c
100.0
10.0
1.0
.1
.01
$d\sigma/dt$ (mb/(GeV/c)^2)
0.
.5
1.0
1.5
2.0
2.5
$-t$ (GeV/c)^2
XBL 711-8

Fig. 40

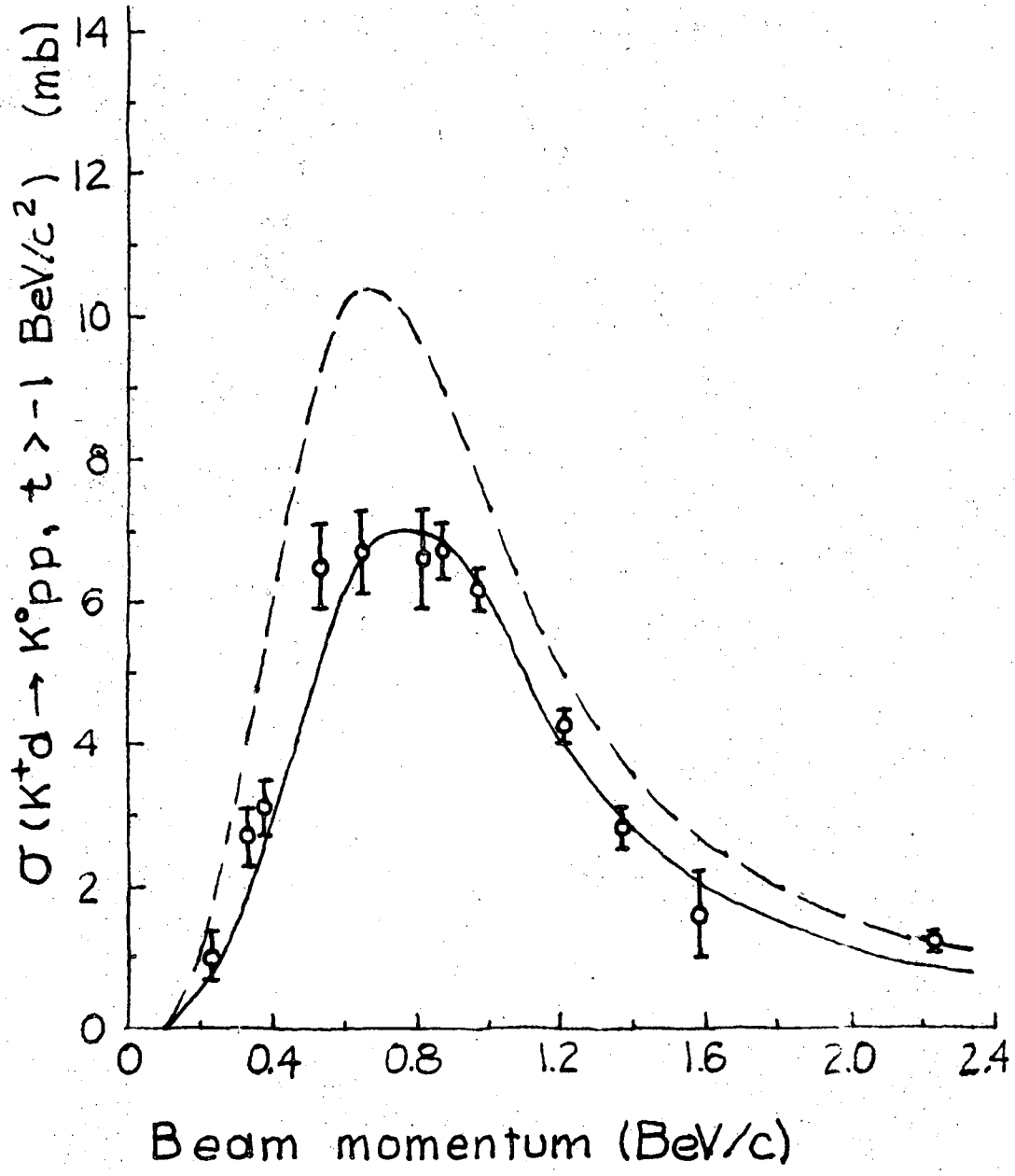

XBL 688-5658

Fig. 41

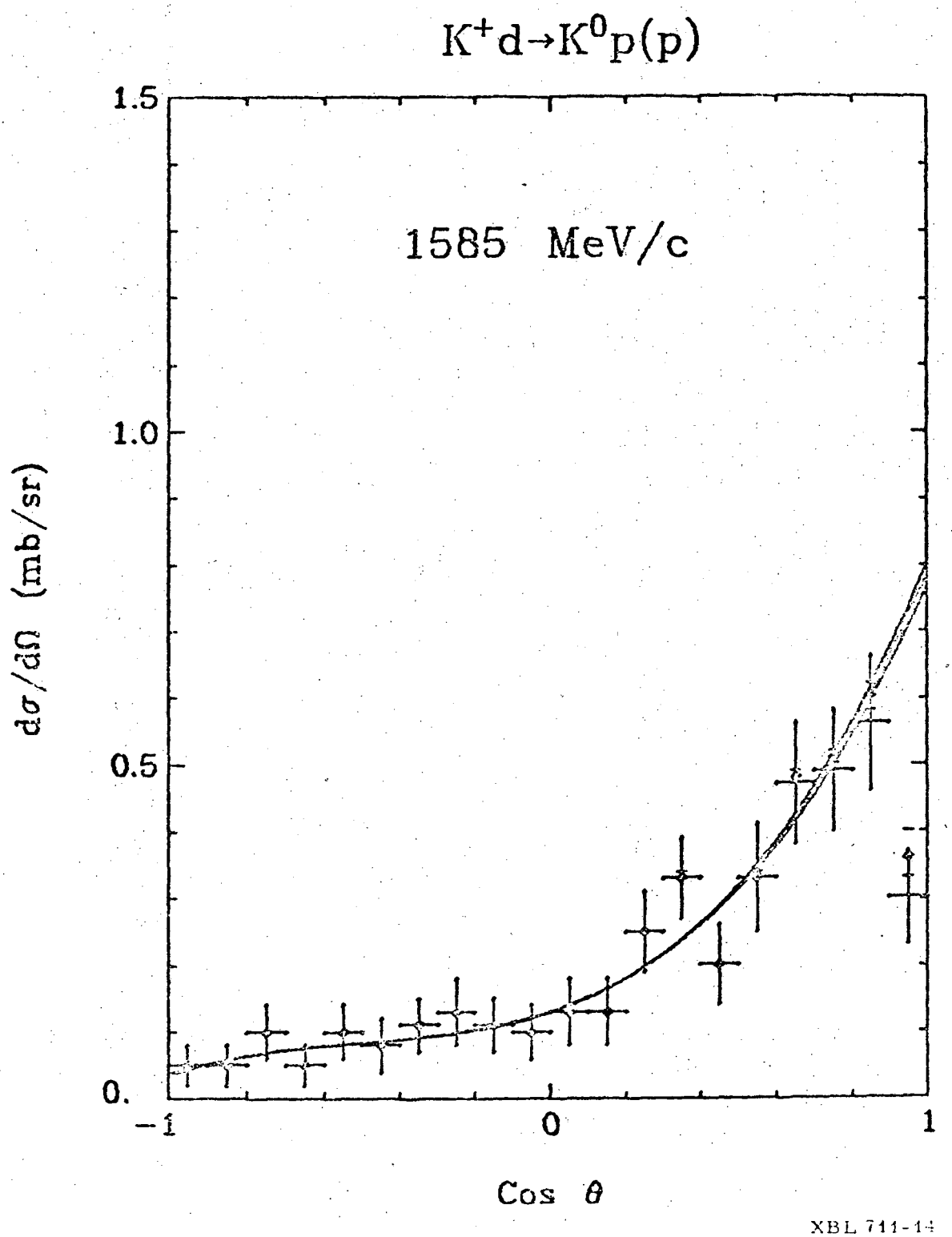
$K^+d \rightarrow K^0p(p)$
1585 MeV/c
1.5
1.0
0.5
0.
−1
0
1
$d\sigma/d\Omega$ (mb/sr)
Cos θ
XBL 711-14

Fig. 42

TECHNICAL INFORMATION DIVISION
LAWRENCE RADIATION LABORATORY
UNIVERSITY OF CALIFORNIA
BERKELEY, CALIFORNIA 94720